JAC: Jena's Atomic Calculator

— Manual, compendium & theoretical background —

http://www.atomic-theory.uni-jena.de/

Stephan Fritzsche

Helmholtz-Institut Jena &

Theoretisch-Physikalisches Institut, Friedrich-Schiller-Universität Jena, Fröbelstieg 3, D-07743 Jena, Germany

(Email: s.fritzsche@gsi.de, Telefon: +49-3641-947606, Raum 204)

Sunday 16$^{\text{th}}$ December, 2018

Contents

1. An overview about JAC. Structure of this Manual

1.1. Goals of the JAC toolbox

Purpose of the JAC module:

- The Jena Atomic Calculator (JAC) provides tools for performing atomic (structure) calculations at various degrees of complexity and sophistication. This toolbox has been designed to calculate not only atomic level structures and properties [g-factors, hyperfine and isotope-shift parameters, etc.] or transition amplitudes between bound-state levels [dipole operator, Schiff moment, parity non-conservation, etc.] but, in particular, also (atomic) transition probabilities, Auger rates, photoionization cross sections, radiative and dielectronic recombination rates as well as cross sections and parameters for many other (elementary) processes.
- JAC also facilitates interactive computations, the simulation of atomic cascades and atomic responses, the time-evolution of statistical tensors as well as various semi-empirical estimates of atomic properties. It provides a diverse and wide-ranging, yet consistent set of methods which can be applied in different fields.
- In addition, the JAC module has been designed to readily support the display of level energies, electron and photon spectra, radial orbitals and several others entities.
- Since the theoretical background and various data, implemented in JAC, have been drawn from many sources, we also hope to develop JAC as a repository of previous experience that is here to be further refined, expanded and developed.
- The code, documentation as well as a number of tutorials and examples are available from our Web site https://www.github.com/sfritzsche/JAC.jl.
- In order to support all these goals, several types of computation need to be distinguished in the JAC toolbox.

Types of computations:

- Atomic computations, based on explicitly specified electron configurations: A typical computation, that is based on explicitly specified electron configurations, refers to level energies, atomic states and to either one (or several) atomic properties for levels from a given multiplet or to the rates and cross sections of just one selected process. For further details, see the supported amplitudes, properties and processes below.
- Restricted active-space computations (RAS): A RAS computation refers to systematically-enlarged calculations of atomic states and level energies due to a specified (and usually restricted) active space of orbitals as well as due to the number and/or kind of virtual excitations to be included. Such RAS computations are internally performed *stepwise* by utilizing the self-consistent field from some prior step but have not yet been properly implemented so far.
- Interactive computations: In an interactive computation, the functions/methods of the JAC program are applied interactively, either directly within the REPL or by just a short JULIA script, in order to compute energies, expansion coefficients, transition matrices, rates, cross sections, etc. An interactive computation typically first prepares and generates (instances of) of JAC's data structures, such as orbitals, (configuration-state) bases, multiplets, and later applies them to obtain the desired information. More generally, all methods from JAC and its submodules can be utilized interactively, although some specialized methods are often already available and may facilitate the computations. Like for other JULIA methods, the methods provided by JAC can be seen as (high-level) language elements for performing computations at various degrees of sophistication.
- Atomic cascade computations: A cascade computation typically refers to three or more charge states of an atom, and which are connected to each other by various atomic processes, such as photoionization, dielectronic recombination, Auger decay, radiative transitions, etc. Different (cascade) approaches have been predefined in order to deal with atomic cascades. The particular atomic processes that are to be taken into account for the inidividual steps of the cascade need to be specified explicitly; these cascade computations have been only partly implemented so far.
- Atomic responses: Atomic response computations will support simulations of how atoms *respond* to an incident (beam of) light pulses and particles, such as field-induced ionization processes, high-harmonic generation and others. For these responses, the detailed atomic structure is often not considered in much detail, though it will become relevant s more elaborate and accurate measurements are carried out. These response computations have not yet been implemented so far.
- Time evolution of statistical tensors in (intense) light pusles: A time evolution of statistical tensors always proceeds within a pre-specified set of sublevels; all further (decay) processes that lead the system *out of these sublevels* must be treated by loss rates. Although such a

time evolution can deal with pulses of different shape, strength and duration, it is assumed that they are *weak enough* to not disturb the level structure and level sequence of the atoms in their neutral or ionic stage substantially, i.e. that every sublevel can still be characterized by its (given total) energy and symmetry. This time-evolution has not yet been implemented so far. No attempt will be made to solve the time-dependent (many-electron) Schrödinger equation explicitly.

➢ Semi-empirical estimates of atomic properties, cross sections, asymptotic behaviour, etc.: A semi-empirical 'estimate' refers to some simple model computation or to the evaluation of fit functions in order to provide such atomic data, that cannot be generated so easily by *ab-initio* computations. These semi-empirical estimations are typically built on — more or less — sophisticated models and external parameter optimizations, although only a very few of such estimates have been implemented so far.

1.2. Notations

Atomic multipoles:

➢ The multipole components (fields) of the radiation field occur at many different places in atomic theory due to the electron-photon interaction, though often within slightly different contexts. We here use the standard notations for the E1 (electric-dipole), M1 (magnetic-dipole), E2 (electric-quadrupole), etc. components and refer to them briefly as *multipoles* $\mathbb{M}$ of the radiation field.

➢ These multipoles or multipole components of the radiation field frequently occurs also in terms of *multipole operators* $\mathbb{O}^{(\mathbb{M})}$ as well as in summations $\sum_{\mathbb{M}} \ldots$ over such operators and/or the associated transition amplitudes (matrix elements).

Atomic level notations.

➢ Bound (many-electron) levels and states: $|\alpha\mathbb{J}\rangle \equiv |\alpha J^P\rangle$; $|\alpha\mathbb{J}M\rangle \equiv |\alpha J^P M\rangle$.

Here, the multi-index α refers to all additional quantum numbers that are needed for a unique specification of some many-electron level or state. — For instance, we shall often use below $|\alpha_i\mathbb{J}_i\rangle$ and $|\alpha_f\mathbb{J}_f\rangle$ in order to denote the initial and final-ionic bound states of some atomic amplitude and process.

➢ (Many-electron) resonances with a single free electron: $|(\alpha\mathbb{J},\, \varepsilon\kappa)\, \mathbb{J}_t\rangle \equiv |(\alpha J^P,\, \varepsilon\kappa)\, J_t^{P_t}\rangle$

describes a many-electron scattering wave with a single free electron in the partial wave $|\epsilon\kappa\rangle$; $\mathbb{J}_t$ denotes the overall symmetry of the many-electron scattering state (level).

1.3. A quick overview about the considered amplitudes, level properties and processes

In Jac (partly) implemented amplitudes:

➢ Selected many-electron (reduced) amplitudes that are accessible within the JAC program. Further details about the call of these amplitudes can be found in the manual [**?**] or interactively by `?<module>.amplitude`.

Amplitude	Call within JAC	Brief explanation
$\langle \alpha\mathbb{J} \,\|\| \mathbb{T}^{(1)} \|\| \beta\mathbb{J}' \rangle$, $\langle \alpha\mathbb{J} \,\|\| \mathbb{T}^{(2)} \|\| \beta\mathbb{J}' \rangle$	Hfs.amplitude	Amplitude for the hyperfine interaction with the magnetic-dipole and electric-quadrupole field of the nucleus.
$\langle \alpha\mathbb{J} \,\|\| \mathbb{N}^{(1)} \|\| \beta\mathbb{J}' \rangle$	LandeZeeman.amplitude	Amplitude for the ineraction with an external magnetic field.
$\langle \alpha_f\mathbb{J}_f \,\|\| \mathbb{O}^{(\mathbb{M},\,\text{emission})} \|\| \alpha_i\mathbb{J}_i \rangle$	Radiative.amplitude	Transition amplitude for the emission of a multipole ($\mathbb{M}$) photon.
$\langle \alpha_f\mathbb{J}_f \,\|\| \mathbb{O}^{(\mathbb{M},\,\text{absorption})} \|\| \alpha_i\mathbb{J}_i \rangle$	Radiative.amplitude	Transition amplitude for the absorption of a multipole ($\mathbb{M}$) photon.
$\langle (\alpha_f\mathbb{J}_f, \varepsilon\,\kappa)\,\mathbb{J}_t \,\|\| \mathbb{O}^{(\mathbb{M},\,\text{photoionization})} \|\| \alpha_i\mathbb{J}_i \rangle$	PhotoIonization.amplitude	Photoionization amplitude for the absorption of a multipole ($\mathbb{M}$) photon and the release of an electron in the partial wave $\|\varepsilon\,\kappa\rangle$.
$\langle \alpha_f\mathbb{J}_f \,\|\| \mathbb{O}^{(\mathbb{M},\,\text{recombination})} \|\| (\alpha_i\mathbb{J}_i, \varepsilon\kappa)\mathbb{J}_t \rangle$	PhotoRecombination.amplitude	Photorecombination amplitude for the emission of a multipole ($\mathbb{M}$) photon and the capture of an electron in the partial wave $\|\varepsilon\,\kappa\rangle$.
$\langle (\alpha_f\mathbb{J}_f,\, \varepsilon\,\kappa)\,\mathbb{J}_t \,\|\| \mathbb{V}^{(\text{Auger})} \|\| \alpha_i\,\mathbb{J}_i \rangle$	Auger.amplitude	Auger transition amplitude due to the electron-electron interaction and the release of an electron in the partial wave $\|\varepsilon\,\kappa\rangle$.
$\langle \alpha_f\mathbb{J}_f \,\|\| \sum \exp i\,\mathbf{q}\cdot\mathbf{r}_i \,\|\| \alpha_i\mathbb{J}_i \rangle$	FormFactor.amplitude	Amplitude for a momentrum transfer $\mathbf{q}$.
$\langle \alpha_f\mathbb{J}_f \,\|\| \mathbb{O}^{(\text{PNC})} \|\| \alpha_i\mathbb{J}_i \rangle$	PNC.amplitude	Parity-nonconservation amplitude.

In Jac (partly) implemented atomic level properties:

➢ In JAC implemented or partly-implememted atomic properties. For these properties, different parameters (observables) can be obtained by performing an `Atomic.Computation(..., properties=[id1, id2, ...])`, if one or more of the given identifiers are specified. For each of these properties, moreover, the corresponding (default) `Settings` can be overwritten by the user to control the computations.

Property	id	Brief explanation.
$\|\alpha\mathbb{J}\rangle \longrightarrow \|\alpha(J)\,\mathbb{F}\rangle$	HFS	Hyperfine splitting of an atomic level into hyperfine (sub-) levels with $F = \|I-J\|,\ ..., I+J-1,\ I+J$; hyperfine A and B coefficients; hyperfine energies and interaction constants; representation of atomic hyperfine levels in a IJF -coupled basis.
$\|\alpha\mathbb{J}\rangle \longrightarrow \|\alpha\,\mathbb{J}M\rangle$	LandeJ	Zeeman splitting of an atomic level into Zeeman (sub-) levels; Lande $g_J \equiv g(\alpha\mathbb{J})$ and $g_F \equiv g(\alpha\mathbb{F})$ factors for the atomic and hyperfine levels.
$K^{(\mathrm{MS})},\ F$	Isotope	Isotope shift of an atomic level for two isotopes with masses $A,\ A'$: $\Delta E^{AA'} = E(\alpha\mathbb{J};\ A) - E(\alpha\mathbb{J};\ A')$; mass-shift parameter $K^{(\mathrm{MS})}$ and field-shift parameter F.
α-variations	AlphaX	Differential sensitivity parameter $\Delta q(\delta\alpha)$ of an atomic level; $\Delta E(\delta\alpha;\ \beta\mathbb{J})$, $\Delta q(\delta\alpha;\ \beta\mathbb{J})$, $K(\beta\mathbb{J})$.
$F(q;\ \alpha\,\mathbb{J})$	FormF	Standard and modified atomic form factor of an atomic level $\|\alpha\mathbb{J}\rangle$ with a spherical-symmetric charge distribution.
$\omega(\alpha\mathbb{J}) + a(\alpha\mathbb{J}) = 1$	Yields	Fluorescence & Auger decay yields of an atomic level.
$\alpha^{(\mathbb{M})}(L,\omega)$		Static and dynamic (ac, multipolar) polarizibilities.
$E(\alpha\mathbb{J};$ plasma model)	Plasma	Plasma shift of an atomic level as obtained for different but still simple plasma models.
$\|\alpha_i\mathbb{J}_i\rangle \longrightarrow \|\alpha_f\mathbb{J}_f\rangle + \hbar\omega$	EinsteinX [a]	Photon emission from an atom or ion; Einstein A and B coefficients and oscillator strength between levels $\|\alpha_i\mathbb{J}_i\rangle \rightarrow \|\alpha_f\mathbb{J}_f\rangle$ that belong to a single multiplet (representation).

[a] Although the Einstein coefficients are not the property of a single level, we here still support a quick computation of these coefficients by means of the `Einstein` module for two levels that are represented by a single CSF basis.

In Jac (partly) implemented atomic processes:

➢ In JAC implemented or partly-implememted atomic processes. For *one* process at a time, different parameters (observables) can be obtained by performing an `Atomic.Computation(..., process=id)`, if the corresponding identifier is specified. For this particular property, moreover, the corresponding (default) `Settings` can be overwritten by the user to control the computations.

Process	id	Brief explanation
$A^* \longrightarrow A^{(*)} + \hbar\omega$	RadiativeX	Photon emission from an atom or ion; transition probabilities; oscillator strengths; angular distributions.
$A + \hbar\omega \longrightarrow A^*$	PhotoExc	Photoexcitation of an atom or ion; alignment parameters; statistical tensors.
$A + \hbar\omega \longrightarrow A^{+*} + e_p^-$	PhotoIon	Photoionization of an atom or ion; cross sections; angular parameters; statistical tensors.
$A^{q+} + e^- \longrightarrow A^{(q-1)+} + \hbar\omega$	Rec	Photorecombination of an atom or ion; recombination cross sections; angular parameters.
$A^{q+*} \longrightarrow A^{(q+1)+(*)} + e_a^-$	AugerX	Auger emission (autoionization) of an atom or ion; rates; angular and polarization parameters.
$A^{q+} + e^- \rightarrow A^{(q-1)+*} \rightarrow A^{(q-1)+(*)} + \hbar\omega$	Dierec	Dielectronic recombination (DR) of an atom or ion; resonance strengths.
$A + \hbar\omega_i \longrightarrow A^* \longrightarrow A^{(*)} + \hbar\omega_f$	PhotoExcFluor	Photoexcitation of an atom or ion with subsequent fluorescence emission.
$A + \hbar\omega \longrightarrow A^* \longrightarrow A^{(*)} + e_a^-$	PhotoExcAuto	Photoexcitation & autoionization of an atom or ion.
$A + \hbar\omega_i \longrightarrow A^{(*)} + \hbar\omega_f$	Compton	Rayleigh or Compton scattering of photons at an atom or ion; angle-differential and total cross sections.
$A + n\,\hbar\omega \longrightarrow A^*$ or $A^* \longrightarrow A^* + n\,\hbar\omega$	MultiPhoton	Multi-photon (de-) excitation of an atom or ion, including two-photon decay, etc.
$A + Z_p \longrightarrow A^* + Z_p$	CoulExc	Coulomb excitation of an atom or ion by fast, heavy ions; energie-differential, partial and total Coulomb excitation cross sections.
$A + \hbar\omega \rightarrow A^* + e_p^- \rightarrow A^{(*)} + e_p^- + \hbar\omega'$	PhotoIonFluor	Photoionization of an atom or ion with subsequent fluoescence emission.
$A + \hbar\omega \rightarrow A^* + e_p^- \rightarrow A^{(*)} + e_p^- + e_a^-$	PhotoIonAuto	Photoionization of an atom or ion with subsequent autoionization.
$A^{q+} + e^- \rightarrow A^{(q-1)+*} \rightarrow A^{(q-1)+(*)} + \hbar\omega \rightarrow A^{(q-1)+} + \hbar\omega + \hbar\omega'$	DierecFluor	Dielectronic recombination of an atom or ion with subsequent fluorescence.

Process	id	Brief explanation
$e_s^- + A \longrightarrow A^* + e_s^{-'}$	Eimex	Electron-impact excitation of an atom or ion; collision strength.
$A + e_s^- \rightarrow A^* + e_s^{-'} \rightarrow A^{+(*)} + e_s^{-'} + e_a^-$	EimexAuto	Electron-impact excitation and subsequent autoionization of an atom or ion.
$A^{q+*} \longrightarrow A^{(q+1)+(*)} + (e_a^- + \hbar\omega)$	RadAuger	Radiative-Auger (autoionization) of an atom or ion.
$A + n\,\hbar\omega \longrightarrow A^{(*)} + e_p^-$	MultiIon	Multi-photon ionization of an atom or ion.
$A + n\,\hbar\omega \longrightarrow A^{(*)} + e_{p_1}^- + e_{p_1}^-$	MultiDoubleIon	Multi-photon double ionization of an atom or ion.
$A^{q+}[\text{nucleus}^*] \longrightarrow A^{(q+1)+*} + e_c^-$	Conversion	Internal conversion, i.e. electron emission due to nuclear de-excitation.

1.4. Short comparison of JAC with other existing codes

We here compile some (incomplete) information about other existing codes for atomic structure computations, remind to some of their special features and briefly summarize how they differ from the implementation of the JAC toolbox.

GRASP (Grant *et al.*, 1980; Parpia *et al.*, 1992; Jönsson *et al.*, 2013):

➢ Level energies & ASF: GRASP has originally been devoloped since the late 60s in order to provide level energies and eigenvector for quite general open-shell atoms. Much emphasize during the last two decades was placed upon the systematic improvement of these energies. While we also provide such level energies and atomic state functions by the JAC toolbox, we *do not* intent to facilitate such extensive wave function expansions. Instead, approximate level energies and ASF are always considered as the *technically necessary preposition* for describing other properties and processes. With the restricted-active space (RAS) computations, however, we shall provide in JAC useful features for a systematic improvement of such *ab-initio* computations.

➢ Transition probabilities & oscillator strength: Apart from the level energies, GRASP has been extensively applied in order to compute and tabulate transition probabilities for many atoms and ions throughout the periodic table of elements. With JAC, we provide analogue or even simpler tools for such computations. Moreover, the (many-electron amplitudes that arise from the) coupling of the radiation field provides the natural *building blocks* for a large number of other atomic processes, cf. section 7 on atomic processes below.

RATIP (Fritzsche, 2001, 2012):

- Relativistic CI (RELCI): While RATIP has always used the SCF computations and orbitals from the GRASP code, it supports relativistic CI computations. For many years, it helped define a new standard for performing the angular intergration (angular coefficients; Gaigalas *et al.*, 2002)). These angular coefficients are also utilized in JAC by an interface to the Fortran modules of RATIP.
- Atomic properties and processes: RATIP was (one of) the first codes that made use of GRASP's systematically improved wave functions in order to compute a good number of atomic properties and processes, such as relaxed-orbital transition probabilities (REOS; Fritzsche and Froese Fischer 1999), Auger rates, photoionization cross sections and angular parameters, radiative and dielectronic recombination rates, electron-impact excitation cross sections, and several others. The experience with RATIP has been found central for the development of JAC and has find its continuation here.

CATS (Cowan: 'Theory of Atomic Spectra', 1980):

- CATS relies on a semirelativistic self-consistent potential and by using either a nonlocal Hartree-Fock (HF) or local Hartree-Fock-Slater (HFS) approach in order to deal with the exchange interaction.
- Level energies & ASF: Since the late 60s, Cowan's HFX code has set some standard for many experimentalist and has, together with his well-known textbook, helped many physicist to understand and make use of atomic structure theory. While these earlier developments are highly appreciated (and are still utilized for various applications), CATS has several severe limitations which are hard to *overcome*. The same applies also for the computation of various atomic properties, such at transition probabilities, photo-excitation and ionization cross sections, Auger rates.
- Display of data & spectra: Several tools and facility-programs have been developed for CATS in order to display the computed data and to compared them with each other and with experiment. The success of some of these tools have motivated us for developing some graphical interfaces for the display of (radial) orbitals, line spectra, etc. also for thte JAC toolbox.
- Comparison with JAC: JAC provides methods to display, for instance, radial functions and line spectra; cf. `JAC.display()`.

FAC (Gu 2008):

- FAC is a well-known relativistic code based on the fit of free parameters in defining the atomic potential and on some a local approximation for dealing with exchange interactions, based on the standard Dirac-Fock-Slater method.
- Level energies & wave functions: The simplified and more object-oriented treatment of wave functions in the FAC code, when compared with GRASP, has stimulated the development of the JAC program. While JAC will enable the user to perform also systematic improvements on the underlying computational models, the support of simple approximations has been found crucial, for example, for dealing with cascades and time-evolutions.

LASER (Fontes *et al.*, 2015):

- LASER, i.e. the Los Alamos suite of relativistic atomic physics code, comprises various codes for fundamental atomic structure calculations as well as for various processes, such as photoexcitation, electron-impact excitation and ionization, photoionization and autoionization, within a consistent framework. It may help develop atomic physics models in either configuration- average and fine-structure modes, and by including a proper self-consistency. This suite has been developed for more than 20 years.
- Applications of this code: The LASER has been applied to the collisional-radiative modeling of of plasmas, for ine identifications in plasma spectroscopy and for testing relativistic atomic and quantum electro-dynamics (QED) theories. The code has been applied also for feasibility studies of the collisional-radiative modeling of non-LTE (optically thin) gold plasmas for and to questions from inertial confinement fusion.
- Approximations: LASER mainly employs the semi-relativistic, similar and as obtained from Cowans atomic structure code (CATS). The bound-electron wavefunctions are obtained from the semi-relativistic approach in CATS, while the continuum-electron wavefuctions are obtained as solutions of the Schrödinger equation from some specialized routines. Typically, therefore, the bound and continuum radial wave functions are single-component type wavefunctions associated with the Schrdinger equation, rather than the four-component spinors associated with the Dirac equation.
- Features: Cross sections and other properties can be calculated for five fundamental processes: photo-excitation, photo-ionization, electron-impact excitation and ionization and autoionization. The code supports the IPCRESS (Independent of Platform and Can be Read by Existing Software Subroutines) random-access binary file format that is used to store large amounts of data and which can be ported to any platform.
- Limitations: The use of the (local-exchange) Slater potential in generating the bound-electron wave functions limits the range of accuracy to highly charged ions, typically half-ionized or even more. Moreover, while distances are used internally in units of the Bohr radius, all

energies are handle in Rydbergs. Oscillator strength are typically calculated only in dipole approximation and Auger rates with just the Coulomb operator.

QEDMOD (Shabaev *et al.*, 2015):

- Self energy, $\mathbb{h}^{(\mathrm{QED})}$: Computes a model QED operator $\mathbb{h}^{(\mathrm{QED})}$ that accounts for the Lamb shift in accurate atomic-structure calculations. However, there are various difficulties with QEDMOD which make a direct application of the code and its combination with GRASP or JAC rather cumbersome. In JAC, we therefore presently treat the QED corrections still at a slightly less advanced level, following an earlier suggestion by Yong-ki Kim (2000).
- Advantages: The QEDMOD code provides one-electron matrix elements that, in principle could be directly added to any CI matrix and, hence, to the computation of level energies and multiplets. For the vacuum polarization, it includes automatically both, the Uehling and Wichmann-Kroll terms.

GEANT4 (Amako *et al.*, 2005):

- GEANT4 is an object-oriented toolkit for analyzing and simulating the passage of particeles through matter that provides a variety of semi-empirical models to describe the underlying electromagnetic and hadronic interactions. GEANT4 combines theorical models with experimental data or parameterizations of such data.
- GEANT4 is especially based on a number of separate packages to deal with the electromagnetic interactions of (either) electrons, muons, positrons, photons, hadrons and ions as well as for specific energy range of the processes considered.

1.5. To-do's, next steps & desired features of the JAC program

Encouragement for external users and developers:

➢ While we (will further) develop JAC for several frequently-requested applications, here I shall compile a number of desired features which could or will make JAC more powerful and/or easy to use. For these *additional features*, we wish to encourage collaboration with external developers. We welcome in particular all help from outside if the overall style of the program is maintained and if some prior consensus exist how to add and implement certain features.

1.5.a. To-do lists

Urgent to-do's:

➢ xx

Short-term to-do's:

➢ Implement ... `Jac.modify("level energies:  interactive", multiplet::Multiplet)`

➢ Implement ... `Jac.display("level energies:  HFS", multiplets::ArrayHFSMultiplet,1)`

➢ Implement ... `Jac.display("level energies", multiplets::ArrayMultiplet,1)`

➢ Implement ... `Jac.display("configuration list:  from basis", basis::Basis)`

Medium-term to-do's:

➢ Tutorials: To advertise the JAC program, we should have a good set of 'tutorials' for getting started with the code and to show the features explicitly. A few tutorials can be presently accesses already by the method `Jac.tutorials()`.

➢ Breit interaction in CI: Implement at least a zero-frequency treatment of the Breit interaction, i.e. an effective strength `Jac.InteractionStrength.XL_Breit(L::Int64, a::Jac.Radial.Orbital, b::Jac.Radial.Orbital, c::Jac.Radial.Orbital, d::Jac.Radial.Orbital)`

1.5.b. Questions about the (further) implementation

To be discussed:

- Further documentation of the code: How can the internal .doc-strings be combined with the websites ??
- Parallelization and performance of the code: How can on make the code parallel without that the user need to know and provide much information about the cluster that is used for computations.
- Modern input forms in scientific computing: ... with constructors ?? ... constructor of constructors ?? ... what is the maximum depth ?? ... which simple graphical (applet) features exist ? ... configuration format tomel.jl ??

1.5.c. Further desired features of the Jac program

Plotting and vizualization:

- Implement ... `Jac.plot("radial orbitals", orbitals::ArrayOrbital,1)`
- Implement ... `Jac.plot("spectrum: oscillator strength over energy, emission", lines::ArrayRadiativeLine,1; widths=value::Float64)` and
  `Jac.plot("spectrum: oscillator strength over energy, absorption", lines::ArrayRadiativeLine,1; widths=value::Float64)`
- Implement ... `Jac.plot("spectrum: transition rates over energy, Gaussian", lines::ArrayRadiativeLine,1; widths=value::Float64)` and
  `Jac.plot("spectrum: transition rates over energy, Lorentzian", lines::ArrayRadiativeLine,1; widths=value::Float64)`
- Implement ... `Jac.plot("spectrum: transition rates over energy", lines::ArrayRadiativeLine,1; widths=value::Float64)`
- Visualize the convergence of results as function of the size of computation and/or model space.
- Visualize the level structure of a given multiplet, for instance, by displaying the level energies in different colors for different (leading) configurations or groups of such configurations.
- Visualize the level structure of a given multiplet together with further level or transition properties, such as lifetimes, HFS parameters, isotope parameters, etc.

More physics in Jac ?

- ➢ Atomic spectra: Evaluate the photoabsorption spectra from calculated photoexcitation and photoionization cross sections.
- ➢ Single-electron properties:
  - Subshelldependent differential and total photoionization cross sections (Eichler and Meyerhof, 1995, Eqs. 9.34 and 9.47)
  - Nonrelativistic total Kshell/subshell radiative recombination cross section; general and Stobbe cross section (Eichler & Meyerhof, 1995, Eqs. 9.49, 9.50)
  - Dirac energy (subshell); Dirac r^k expectation values; Dirac-matrices; `Dirac.Omega(subshell,theta,phi)`.
  - CoulombGreens functions ... for some given hydrogenic orbital.
- ➢ Collisional-radiative models: have been frequently applied to describe the evolution of plasma and to derive information for plasma diagnostics. JAC provides many, if not all, the rates and cross sections to built-up such models for selected (plasma) environments.
- ➢ Quantum dot in magnetic fields: Fock-Darwin states of hyhdrogenic systems are often used to understand the electronic structure of artificial atoms in magnetic fields.

1.6. Implementation of JAC

Why Julia ?

- ➢ Here, we just recall a few remarks from the literature as well as about our own experience why Julia have been found helpful for developing the Jac program. Some of these arguments are taken from the work of Bezanson *et al.* (2017).
- ➢ Julia is often said to stand for the combination of productivity and performance through a careful language design and carefully chosen technologies; it never forces the user to resort to C or Fortran for fast computations. — Julia's design allows for gradual learning of modern concepts in scientific computing; from a manner familiar to many users and towards well-structured and high-performance code.
- ➢ High-level languages: Most traditional high-level languages are hampered by the overhead from the interpretor, and which typically results into more run-time processing of what is strictly necessary. One of these hindrances is (missing) type information, and which then results in the request for supporting vectorization. Julia is a 'verb'-based language in contrast to most object-oriented 'noun'-based language, in which the generic functions play a more important role than the datatypes.

- Multiple dispatch: refers to the dynamically selected implementation and to the concept of running the right code at the right time. This is achieved by overloading by multiple-argument function, a very powerful abstraction. Multiple dispatch makes it easier to structure the programs close to the underlying science.
- Julia's type system: Julia's expressive type system allows optional type annotations; this type system supports an agressive code specializiation against run-time types. Over a large extent, however, Julia code can be used without any mentioning of types (in contrast to C and Fortran); this is achieved by data-flow interference. — User's own types are also first class in Julia, that is there is no meaningful distinction between built-in and user-defined types. There are mutable and (default: immutable) composite types.
- Performance: There are helpful macros, such as @timing function_call(parameters) or @benchmark function_call(parameters) to analyze the performance of the program and to find (and resolve) bottlenecks.

2. Dirac's hydrogenic atom

2.1. Energies and wave functions

Dirac's (one-electron) energies:

➢ The (relativistic) bound-state energy spectrum for electrons with principal quantum number n and angular-momentum quantum number κ is given by

$$\varepsilon_{n\kappa} \;=\; mc^2\, W_{n\kappa} \;=\; \frac{mc^2}{\left[1 \,+\, \left(\frac{\alpha Z}{n' + s}\right)\right]}$$

where α is the fine-structure constant, $n' = n - |\kappa| = 0,\, 1,\, 2,\, ...$ the number of nodes and $s = \sqrt{\kappa^2 \,-\, (\alpha Z)^2}$.

➢ Since $W_{n\kappa} < 1$, it can be expanded in terms of (αZ) and written as

$$W_{n\kappa} \;=\; 1 \,-\, \frac{1}{2}\,\frac{(\alpha Z)^2}{n^2} \,-\, \frac{1}{2}\,\frac{(\alpha Z)^4}{n^3}\,\left(\frac{1}{j + 1/2} \,-\, \frac{3}{4\,n}\right) \,-\, ...$$

where the second term, multiplied with mc^2 , represents the nonrelativistic binding energy of a hydrogenic atom.

➢ For a given (principal) shell n, the eigenvalues are the same for equal values of j but are different for equal values of ℓ . For a given value of ℓ, the spin-orbit splitting between states with $j = \ell + 1/2$ and $j = \ell - 1/2$ gives rise to the fine-structure in the spectrum of hydrogen-like atoms. The equation above shows that the relativistic corrections to the one-electron energies decreases rapidly with n. The relativistic correction to the non-relativistic energy is therefore important, especially for highly-charged ions with rather large Z.

Relativistic radial orbitals:

➢ Analogue to the nonrelativistic case, the solution $\psi(\mathbf{r})$ of the Dirac equation can be separated for a spherical potential into a radial and angular part

$$\psi_{\kappa m}(r,\vartheta,\varphi) \;=\; \frac{1}{r}\begin{pmatrix} P(r)\,\Omega_{\kappa m}(\vartheta,\varphi) \\ i\,Q(r)\,\Omega_{-\kappa m}(\vartheta,\varphi) \end{pmatrix},$$

where $\Omega_{\kappa m}(\vartheta,\varphi)$ denotes a standard Dirac spin-orbital function, and where $\kappa = \pm\,(j+1/2)$ for $\ell = j \pm 1/2$ is called the *relativistic* angular-momentum quantum number.

➢ Owing to the definition of $\kappa = \pm 1, \pm 2, \ldots$, this relativistic quantum number carries information about both, the total angular momentum j and the parity $(-1)^\ell$ of the wavefunction.

➢ Dirac spin-orbital: As usual, the Dirac spin-orbitals can be written in terms of the spin-1/2 Pauli spinors $\chi_\pm$ and the spherical harmonics by

$$\Omega_{\kappa m}(\vartheta,\varphi) \;=\; \sum_{m_\ell} \langle \ell\, m_l,\; 1/2, m-m_\ell \,|\, jm\rangle \; Y_{\ell m_\ell}(\vartheta,\varphi)\; \chi_{m-m_\ell}\,.$$

➢ Kinetic-balance condition: In JAC, we provide approximate radial (relativistic bound-state) orbitals by applying the kinetic-balance condition to the non-relativistic radial orbital from above and by re-normalizing them appropriately;
cf. `JAC.HydrogenicIon.radialOrbital()`:

$$Q(r) \;=\; \frac{1}{2m\,c}\left(\frac{d}{dr} + \frac{\kappa}{r}\right) P(r)$$

2.2. Coulomb-Greens function

Relativistic radial Coulomb-Greens function:

➢ Radial Green function of the Dirac equation: Following Yerokhin and Shabaev (1999, appendix D), the radial Green function of the Dirac equation for electrons with the angular-momentum symmetry κ can be written in the form:

$$G_\kappa(\omega, r_1, r_2) \;=\; -\,\frac{1}{W_\kappa(\omega)}\,\Big[\boldsymbol{\phi}_\kappa^{\infty}(\omega, r_1)\;\boldsymbol{\phi}_\kappa^{0^T}(\omega, r_2)\,\Theta(r_1 - r_2) \;+\; \boldsymbol{\phi}_\kappa^{0}(\omega, r_1)\;\boldsymbol{\phi}_\kappa^{\infty^T}(\omega, r_2)\,\Theta(r_2 - r_1)\Big]$$

where $\boldsymbol{\phi}_\kappa^{0}(\omega, r)$ and $\boldsymbol{\phi}_\kappa^{\infty}(\omega, r)$ are solutions of the radial Dirac equation, bounded at the origin and at the infinity, and where $W_\kappa(\omega)$ is the Wronskian.

➢ The functions $\boldsymbol{\phi}_\kappa^{0}(\omega, r)$ and $\boldsymbol{\phi}_\kappa^{\infty}(\omega, r)$ can be calculated in terms of the Whittaker functions of the first and second kind, although special care has to be taken.

2.3. Matrix elements with Dirac orbitals

2.3.a. Matrix elements with radial orbitals

Matrix elements with non-relativistic radial orbitals:

➢ Special non-relativistic r^k expectation values: These expectation values are displayed by Marxer (1991)

$$\big\langle r^{-1}\big\rangle \;=\; \frac{Z}{a_o\, n^2}$$

$$\big\langle r^{-6}\big\rangle \;=\; \left[\frac{Z}{a_o}\right]^6 \frac{35n^4 \;-\; n^2\,[30\ell\,(\ell+1) \;-\; 25] \;+\; 3(\ell-1)\,\ell\,(\ell+1)\,(\ell+2)}{8n^7\,(\ell-3/2)\,(\ell-1)\,(\ell-1/2)\,\ell\,(\ell+1/2)\,(\ell+1)\,(\ell+3/2)\,(\ell+2)\,(\ell+5/2)}$$

$$\big\langle r^{-k\,-\,2}\big\rangle \;=\; \left[\frac{Z}{a_o}\right]^{k+2} \frac{1}{n^{k+3}\;\ell^{k+1}}\;\mathcal{P}_{k,\ell}\left(\frac{n}{\ell}\right), \qquad\qquad \mathcal{P}_{k,\ell}(x) \;=\; \frac{(2\ell)^{k+1}\,(2\ell-k)!)}{(2\ell+1)!}\;{}_3F_2(-k, k+1, \ell+1-\ell\,x;\; 1, 2\ell+2;\; 1)$$

Matrix elements with relativistic Dirac wavefunctions:

➢ An analytical expression of the matrix elements with operators $r^k\, e^{-sr}$ can be found (also) for Dirac's relativistic wavefunctions. In order to derive such expressions, it is typically more convenient first to re-write the standard representation of the hydrogenic functions in terms of a series expansion in r as it was suggested originally by Rose (1961).

2.3.b. Matrix elements including the angular part of Dirac orbitals

Matrix elements of spherical tensors:

➢ Matrix elements of the $\mathbb{C}^K$ tensors: Gaidamauskas *et al.* (2011) use the following definition:

$$\left\langle \kappa_a \left\| \, \mathbb{C}^{(K)} \, \right\| \kappa_b \right\rangle \;=\; (-1)^{j_a\,+\,1/2}\,[j_a,\,j_b]^{1/2} \begin{pmatrix} j_a & K & j_b \\ 1/2 & 0 & -1/2 \end{pmatrix} \delta_{\ell_{\rm a}+\ell_{\rm b}+1,\,\rm even}$$

2.4. Partial-wave expansions of free electrons

Partial-wave expansion:

➢ The computation of partial (and total) ionization cross sections often requires an integration over all possible angles $\Omega_p = (\vartheta_p, \varphi_p)$ of the photoelectrons, emitted in 4π. In practice, this integration over Ω_p can be carried out rather easily by making use of the *decomposition* of the free-electron wavefunction $|\mathbf{p}\, m_s\rangle$ into *partial-wave* components.

➢ In practice, however, this expansion generally depends on the choice of the quantization axis.

➢ If the quantization axis is taken along $\mathbf{e}_z$, this expansion is given by

$$|\mathbf{p}\, m_s\rangle \;=\; \sum_{\kappa\, m} i^{\ell}\, e^{-i\,\Delta_\kappa}\; \langle l m_\ell,\, 1/2\, m_s \,|\, jm\rangle\; Y^*_{\ell m_\ell}(\hat{p})\; |\epsilon\kappa m\rangle \;,$$

and where the summation runs over all partial waves, $\kappa = \pm 1, \pm 2, ...$, while $m = -j, ..., j$. Here, Δ_κ is the Coulomb phase shift, and the (nonrelativistic orbital angular momentum) quantum number ℓ just distinguishes the parity of the partial waves.

2.5. B-splines

Properties of B-splines:

➢ Knot sequence: A sequence of (radial) grid points $\{t_1, t_2, ..., t_m\}$ with $t_1 \le t_2 \le ... \le t_m$

➢ Set of B-splines: Set of piecewise polynomial functions of order k, the so-called B-splines:

$$\left\{B_1^{(k)}(x),\, B_2^{(k)}(x),\, ...,\, B_n^{(k)}(x)\right\}, \qquad B_i^{(1)}(x) \;=\; \begin{cases} 1 & \text{for } t_i \le x \le t_{i+1} \\ 0 & \text{otherwise} \end{cases} \qquad i \;=\; 1, 2, ..., m-1$$

➢ Recursion relation:

$$B_i^{(k)}(x) \;=\; \frac{x \,-\, t_i}{t_{i+k-1} \,-\, t_i}\, B_i^{(k-1)}(x) \;+\; \frac{t_{i+k} \,-\, x}{t_{i+k} \,-\, t_{i+1}}\, B_{i+1}^{(k-1)}(x) \qquad\qquad i \;=\; 1, 2, ..., m-k$$

The number of B-splines $n = m - k\; (k < m)$ is determined by the order k and the number of knots m. For B-splines of a given order, it is therefore sufficient to use the notation $B_i(x)$

2.6. Generation of continuum orbitals

Simple approximations:

➢ For a first estimate of continuum processes, we have implemented a number of (rather) simple approximations for the continuum orbitals that occur frequently at various places in the program. In JAC, the particular method can be selected by (re-) defining the global variable `JAC_CONTINUUM` by a proper call to `Jac.define("method: continuum; ...)`.

➢ In particular, the following four methods have been implemented: (a) spherical Bessel functions; (b) non-relativistic Coulomb waves, together with the kinetic-balance condition to obtain a relativistic continuum orbital; (c) superposition of neighboured continuum oribtals; (d) Galerkin method for a continuum orbital in a given atomic potential.

2.6.a. Spherical Bessel functions

Implementation and numerical details:

➢ Generating equation and solutions: The spherical Bessel functions obey the equation for the one-electron energy $k^2 = 2\,\varepsilon$

$$R_{\varepsilon\ell}(r) \;=\; j_\ell(|\mathbf{k}|\,r) \;=\; j_\ell(\sqrt{2\,\varepsilon}\,r) \qquad \Longleftrightarrow \qquad j_\ell''(r) \,+\, 2\,\frac{j_\ell'(r)}{r} \,+\, \left(1 \,-\, \frac{\ell(\ell+1)}{r^2}\right) j_\ell(r) \;=\; 0$$

2.6.b. Quasi-relativistic free Coulomb waves

Implementation and numerical details:

➢ Non-relativistic free Coulomb waves: The free solutions to the radial Schrödinger equation, which satisfy the boundary condition, are:

$$P_{\varepsilon\ell}(0) \;=\; 0; \qquad P_{\varepsilon\ell}(r\to\infty) \;\simeq\; \sqrt{\frac{2}{\pi\,k}}\,\sin\left(kr \,+\, \frac{\bar{Z}}{k}\,\ln(2k\,r) \,-\, \frac{\ell\,\pi}{2} \,+\, \sigma_\ell^{(\mathrm{Coulomb})} \,+\, \delta_\ell\right)$$

where $k^2 = 2\,\varepsilon$, $\bar{Z} = Z - N$ is the effective charge seen by the free electron at large distance and $\sigma_\ell^{(\mathrm{Coulomb})} = \arg\,\Gamma(\ell + 1 - i\,\bar{Z}/k)$ is the (well-known) Coulomb phase. Note that this solution is normalized on the energy scale.

➢ The phase-shift δ_ℓ is the non-Coulombic phase shift and is set to $\delta_\ell = 0$ in this approximation.

➢ In JAC, this solution is used together with the kinetic-balance condition to obtain a *small* component if `Jac.define("method: continuum; (non-relativistic) Coulomb)` is called prior to the computations.

2.6.c. Continuum waves in an atomic potential: Galerkin method

Implementation and numerical details:

➢ While the Schrödinger and Dirac equations have formally a solution for every positive energy ε, a diagonalization in a B-spline representation only provides a discrete set of solutions due to the boundary condition $P(r_{\max}) = Q(r_{\max}) = 0$, and where $r_{\max}$ denotes the size of the 'numerical box'.

➢ Despite the discrete representation, these solutions describe *free* electrons within the given potential.

➢ One of the great advantages of using B-splines is that, in principle, solutions can be found for any energy $\varepsilon > 0$ by properly adopting $r_{\max}$.

2.7. Nuclear potentials

Nuclear charge distributions:

➢ Fermi model: for a nucleus with *root-mean-square* (rms) radius $R = \sqrt{\langle r^2 \rangle}$

$$\rho(r,R) = \frac{N}{1 + \exp[(r-c)/a]}, \qquad \int dr\, \rho(r,R) = 1$$

where the thickness parameter a is often chosen as $a = 2.3/4 \ln 3$.

➢ With high accuracy, the parameters N and c can be obtained from analytical formulas

$$N = \frac{3}{4\pi c^3} \left(1 + \frac{\pi^2 a^2}{c^2}\right)^{-1}, \qquad c = \sqrt{\frac{5}{3}\langle r^2 \rangle - \frac{7}{3}\pi^2 a^2}$$

Nuclear potential:

➢ Potential of extended nucleus:

$$\mathbb{V}^{(\mathrm{nuc})}(r;R) = -4\pi\alpha Z \int_0^\infty dr'\, r^2 \frac{\rho(r',R)}{r_>}, \qquad r_> = \max(r,r')$$

3. Many-electron atomic interactions, state functions, density operators and statistical tensors

3.1. Electron-electron interaction

Motivation:

➢ In the (non-relativistic) limit of a rather slow motion of the electrons, each electron pair just interact by the instantaneous Coulomb repulsion

$$\frac{1}{r_{12}} \equiv \frac{1}{|\mathbf{r}_1 - \mathbf{r}_2|}$$

Already this quite simple (interaction) operator results mathematically in various complications and is in all many-particle computations the major source of electron-electron correlations.

➢ For moving charges, Maxwell's theory predicts both, current-current and retarded interactions, to which we briefly refer as Breit interactions in atomic physics. — These relativistic contributions to the electron-electron interactions must be added to the electro-static Coulomb repulsion.

Effective interaction strength $X^{(L)}(abcd)$ of scalar electron-electron interactions:

➢ All operators of the (scalar) electron-electron interaction can be generally represented as spherical tensors in the form and further factorized

$$g_{12} \equiv g(\mathbf{r}_1, \mathbf{r}_2) = \sum_L g_L(r_1, r_2) \left(\mathbb{T}^{(L)}(\vartheta_1, \varphi_1) \cdot \mathbb{T}^{(L)}(\vartheta_2, \varphi_2) \right)$$

$$\langle n_a \kappa_a m_a\,(1)\; n_b \kappa_b m_b\,(2) \,|\, \mathfrak{g}_{12} \,|\, n_c \kappa_c m_c\,(1)\; n_d \kappa_d m_d\,(2) \rangle = \sum_{L\,M} (-1)^{L-M+j_a-m_a+j_b-m_b} \begin{pmatrix} j_a & L & j_c \\ -m_a & M & m_c \end{pmatrix} \begin{pmatrix} j_b & L & j_d \\ -m_b & -M & m_d \end{pmatrix} X^{(L)}(abcd),$$

and where the magnetic quantum numbers (i.e. the angular dependence) of the matrix elements only occurs in the phase and the Wigner $3-j$ symbols.

➢ Effective interaction strength $X^{(L)}(abcd)$ of order L: describe the physical interaction and are specific for every operator. They are often used as the building blocks in order to handle the electron-electron interactions efficiently in eletronic structure computations.

Effective interaction strength $X^{(L,\,\mathrm{Coulomb})}(abcd)$ of the Coulomb repulsion:

➢ Coulomb repulsion: The decomposition of the Coulomb operator is given by:

$$\frac{1}{r_{12}} = \sum_{L=0}^{\infty} U_L(r,s)\, P_L(\cos(\vartheta)) = \sum_{L=0}^{\infty} U_L(r,s) \left(\mathbb{C}^{(L)}(\vartheta_1, \varphi_1) \cdot \mathbb{C}^{(L)}(\vartheta_2, \varphi_2) \right), \qquad U_L(r,s) = \begin{cases} \frac{r^L}{s^{L+1}} & r < s \\ \frac{s^L}{r^{L+1}} & r > s\,. \end{cases}$$

In this expansion, $P_L(x)$ denotes a Legendre-polynomial and $\vartheta = \mathbf{r}\cdot\mathbf{s}/rs$ the angle between the two electron coordinates.

➢ Effective interaction strength of the Coulomb repulsion:

$$X^{(L,\,\mathrm{Coulomb})}(abcd) = \delta(j_a, j_c, L)\, \delta(j_b, j_d, L)\, \Pi^e(\kappa_a, \kappa_c, L)\, \Pi^e(\kappa_b, \kappa_d, L)\, (-1)^L \left\langle \kappa_a \left\| \mathbb{C}^{(L)} \right\| \kappa_c \right\rangle \left\langle \kappa_b \left\| \mathbb{C}^{(L)} \right\| \kappa_d \right\rangle \; R^L(abcd)\,,$$

$$\delta(j_a, j_b, j_c) = \begin{cases} 1 & |j_a - j_b| \le j_c \le |j_a + j_b| \quad \text{and cyclic interchanged} \\ 0 & \text{otherwise}\,, \end{cases}$$

and where $\Pi^e(\kappa, \kappa', L)$ represent the angular momentum and parity selection rules.

3.2. Multi-configuration Dirac-Fock (MCDF) method

Motivation:

- The multi-configuration Dirac-Fock (MCDF) method has been found a versatile tool for calculating the level structure and approximate wave functions for atoms and ions of all elements across the periodic table. Not much need to be said about this method which has been presented at several places elsewhere (Grant 1989; Parpia *et al.* 1996; Fritzsche 2002).
- Similar to the well-known Hartree-Fock (HF) method from non-relativistic quantum theory, in which the state of a quantum system is approximated by a single (symmetry-adapted) Slater determinant, an atomic state function (ASF) is written in the MCDF model as linear combination of configuration state functions (CSF) with well adapted symmetry

$$|\alpha\ \mathbb{J}M\rangle \ \equiv\ \psi_\alpha(\mathbb{J}M)\ =\ \sum_{r=1}^{n_c} c_r(\alpha)\ |\gamma_r\, PJM\rangle\ .$$

In this ansatz, n_c is the number of CSF, $\mathbb{J} \equiv J^P$ the total angular momentum and parity of the state, and α refers to all (further) quantum numbers that are needed to specify the state uniquely. Moreover, $\{c_r(\alpha)\}$ denotes the representation of the atomic state in the given basis.

Complete active spaces:

- To include the *correlated* motion of the bound electrons in a more systematic fashion, the (complete) active space (CAS) method has been found useful for simple shell structures and has been applied along various isoelectronic sequences. The idea of this method is to account for an excitation of the *active* electrons from the outer shells (into a number of predefined *unoccupied* orbitals), while some 'electronic core' remains usually fixed in the set-up of the CAS.
- For a complete active space, it is supposed that all possible excitations (distributions) of these valence electrons can be taken into account among the set of active orbitals. In practice, the concept of a *complete* active space is often not only unfeasible but also unnecessary for predicting many atomic properties, since only those CSF with a "total excitation energy" in the same region as the reference configurations need often to be included into the MCDF expansion.

3.3. Atomic interaction amplitudes

Concept of interaction amplitudes:

➢ The (scalar) Hamiltonian matrix elements below describe the interaction energy between the two CSF $|\gamma_r\, P_r J_r M_r\rangle$ and $|\gamma_s\, P_s J_s M_s\rangle$, and these Hamiltonian matrix elements are perhaps the most simplest interaction amplitudes in atomic structure computations: $\langle\psi_\alpha \,|\, \mathbb{H} \,|\, \psi_\beta\rangle = \langle \alpha\, JM \,\|\, \mathbb{H} \,\|\, \beta J' M'\rangle \;=\; \sum_{rs}\; c_r^*(\alpha)\; H_{rs}\; c_s(\beta)\; \delta_{JJ'}\; \delta_{MM'}$.

➢ In relativistic atomic structure theory, in particular, $E_\alpha \;=\; \big\langle \alpha\, \mathbb{J} \,\big|\, \mathbb{H}^{(\mathrm{DCB})} \,\big|\, \alpha \mathbb{J}\big\rangle \;\approx\; \big\langle \alpha\, \mathbb{J} \,\big|\, \mathbb{H}^{(\mathrm{DC})} \,\big|\, \alpha \mathbb{J}\big\rangle$ is the total energy of a given level $|\alpha \mathbb{J}\rangle$.

Reduced matrix elements of spherical tensor operators for two CSF:

➢ For two CSF of well-defined symmetry, the reduced matrix elements of spherical tensor operators take always the form

$$\big\langle \gamma_r P_r J_r \,\big\|\, \mathbb{T}^{(K)} \,\big\|\, \gamma_s P_s J_s \big\rangle \;=\; \sum_t\; u(a_t b_t; K)\, X(a_t b_t; K), \qquad \mathbb{T}^{(K)} \;=\; \sum_j\; \mathbb{t}^{(K)}(;) \qquad \text{... one part. operators}$$

$$\big\langle \gamma_r P_r J_r \,\big\|\, \mathbb{T}^{(K)} \,\big\|\, \gamma_s P_s J_s \big\rangle \;=\; \sum_t\; v_{L_t}(a_t b_t c_t d_t; K)\, X_{L_t}(a_t b_t c_t d_t; K), \qquad \mathbb{T}^{(K)} \;=\; \sum_{i<j}\; \mathbb{T}^{(K)}(i,j) \quad \text{... symmetric two part. operators,}$$

and where $X(a_t b_t; K)$ and $X^{L_t}(a_t b_t c_t d_t; K)$ are called one- and two-particle (effective) interaction strengths, cf. section 3.1. These interaction strengths are specific to the particular transition or interaction operator under consideration, and special care has to be taken that the same phase convention applies if different interaction amplitudes are to be combined with each other.

➢ In practice, there are two steps in the computation of the transition amplitudes above for pairs of CSF that need to be performed separately: The (pure) angular coefficients are usually calculated by means of some proper program, for instance ANCO, for either a pair or a whole set of CSF, and all the non-vanishing coefficients are then returned together. For these coefficients, the associated one- or two-particle interaction strengths are evaluated and summed up to form the requested matrix element T_{rs} of the transition matrix.

Electron-electron interaction:

➢ The interaction among the electrons is described by the scalar operator that occurs in the Dirac-Coulomb-Breit Hamiltonian; cf. section 3.1

$$\mathbb{V}^{(\mathrm{e-e})} \;=\; \mathbb{V}^{(\mathrm{Coulomb})} + \mathbb{V}^{(\mathrm{Breit})} \;=\; \sum_{i<j} \left(\frac{1}{r_{ij}} + b_{ij} \right) .$$

➢ The Dirac-Coulomb-Breit Hamiltonian gives rise to the (reduced) interaction amplitudes

$$\langle \gamma_r P_r J_r \,\|\, \mathbb{V} \,\|\, \gamma_s P_s J_s \rangle \;=\; \langle \gamma_r P_r J_r \,\|\, \mathbb{V}^{(\mathrm{Coulomb})} \,\|\, \gamma_s P_s J_s \rangle \;+\; \langle \gamma_r P_r J_r \,\|\, \mathbb{V}^{(\mathrm{Breit})} \,\|\, \gamma_s P_s J_s \rangle \,.$$

For scalar operators, the full and reduced matrix elements coincide with each other and need not to be distinguished, since the Clebsch-Gordan coefficient in the Wigner-Eckert theorem simply evaluates to $\langle J_r M_r, 00 \,|\, J_s M_s \rangle \;=\; \delta_{J_r J_s}\, \delta_{M_r M_s}$ for $K = Q = 0$.

3.4. Atomic potentials

3.4.a. In JAC implemented potentials

Atomic potentials:

➢ Core-Hartree potential:

$$V^{(\mathrm{core-Hartree})}(r) \;=\; \int_0^\infty dr' \, \frac{\rho_c(r')}{r_>}, \qquad r_> \;=\; \max(r, r'), \qquad \rho_c(r) \;=\; \sum_a \left(P_a^2(r) \;+\; Q_a^2(r) \right)$$

and where the summation runs over all *core* orbitals of electron configurations with typically just a single valence electron (alkali atoms). In JAC, this potential can be obtained for a given level from `Jac.computePotentialCoreHartree(grid::Radial.Grid, level::Level)`.

➢ Dirac-Fock-Slater potential:

$$V^{(\mathrm{DFS})}(r) \;=\; \int_0^\infty dr' \,\frac{\rho_t(r')}{r_>} \;-\; \left(\frac{3}{4\pi^2\, r^2}\,\rho_t(r)\right)^{1/3}, \qquad r_> \;=\; \max(r,r'), \qquad \rho_t(r) \;=\; \sum_a \left(P_a^2(r) \;+\; Q_a^2(r)\right)$$

and where the summation runs over *all* orbitals (electrons). In Jac, this potential can be obtained for a given level from `Jac.computePotentialDFS(grid::Radial.Grid, level::Level)`.

➢ Hartree potential:

$$V^{(\mathrm{Hartree})}(r) \;=\; -\sum_a \,\bar{q}_a \; r\, Y^0_{aa}(r)$$

where $\bar{q}_a$ is the generalized occupation number and where the summation runs over all orbitals. In Jac, this potential can be obtained for a given level from `Jac.computePotentialHartree(grid::Radial.Grid, level::Level)`.

➢ Hartree-Slater potential:

$$V^{(\mathrm{HS})}(r) \;=\; -\sum_a \,\bar{q}_a\, Y^0_{aa}(r) \;+\; \frac{3}{2}\,\left(\frac{3}{4\pi^2\, r^2}\,\rho(r)\right)^{1/3}\,\frac{r}{2} \qquad \rho(r) \;=\; \sum_a \bar{q}_a\, \left(P_a^2(r) \;+\; Q_a^2(r)\right)$$

and where the summation runs over *all* orbitals. In Jac, this potential can be obtained for a given level from `Jac.computePotentialDFS(grid::Radial.Grid, level::Level)`.

➢ Kohn-Sham potential:

$$V^{(\mathrm{Kohn-Sham})}(r) \;=\; \int_0^\infty dr' \,\frac{\rho_t(r')}{r_>} \;-\; \frac{2}{3\,r}\,\left(\frac{81}{32\,\pi^2}\, r\,\rho_t(r)\right)^{1/3}, \qquad r_> \;=\; \max(r,r'), \qquad \rho_t(r) \;=\; \sum_a \left(P_a^2(r) \;+\; Q_a^2(r)\right)$$

and where the summation runs over *all* orbitals (electrons). In Jac, this potential can be obtained for a given level from `Jac.computePotentialKohnSham(grid::Radial.Grid, level::Level)`.

3.5. Atomic self-consistent-field and configuration-interaction calculations

Hamiltonian matrix elements:

➢ For a given CSF basis, the representation of an atomic state in the MCDF ansatz above (i.e. the mixing coefficients $\mathbf{c}(\alpha) \equiv (c_1(\alpha), c_2(\alpha), \ldots, c_{n_c}(\alpha))$ is obtained by solving the secular equation

$$\det\left(\mathbf{H} - E_\alpha^{(n_c)}\,\mathbf{I}\right) = 0\,,$$

where $E_\alpha^{(n_c)}(PJ)$ denotes the eigenvalue and

$$\mathbf{H} = (H_{rs}) = \left(\left\langle \gamma_r\, PJM \,|\, \mathbb{H} \,|\, \gamma_s\, \bar{P}\bar{J}\bar{M}\right\rangle\, \delta_{P\bar{P}}\, \delta_{J\bar{J}}\, \delta_{M\bar{M}}\right)$$

the Hamiltonian matrix which is blockdiagonal in the total parity and angular momentum of the atom, independent of the particular choice of the electron-electron interaction in the Hamiltonian.

➢ Since the Hamiltonian matrix is real and symmetric, all atomic states are orthogonal for $E_\alpha \neq E_\beta$ or can be chosen in this way for $E_\alpha = E_\beta$. In practice, an efficient decomposition of the many-electron matrix elements H_{rs} in the Hamiltonian matrix above is central to every implementation of the MCDF method.

3.6. Atomic density operators

Motivation

➢ The electron-photon, electron-electron interaction and electron-nucleus interaction amplitudes from above are the building blocks to form the (scattering or) transition matrix for all atomic processes of interest and, hence, the density matrices of the system at the various steps of some particular excitation or decay process. For scattering states with a single electron in the continuum, these interaction amplitudes can be readily calculated by means of the JAC tools.

Density operator of an atom in level $|\alpha \mathbb{J}\rangle$:

➢ For an atom in a well-defined and isolated level $|\alpha \mathbb{J}\rangle$, a general mixed state with regard to its magnetic projections M can always be written as

$$\hat{\rho} \;=\; \sum_{MM'} c_{MM'} \; |\alpha\, \mathbb{J} M\rangle \, \langle \alpha\, \mathbb{J} M'| \, .$$

➢ Often, however, it is more convenient to represent the intermediate state of the ions in terms of its so-called statistical tensors

$$\rho_{k_f q_f}(\alpha_f \mathbb{J}_f) \;=\; \sum_{M_f M'_f} (-1)^{J_f - M'_f} \, \left\langle J_f M_f,\, J_f\, (-M'_f) \,|\, k_f q_f \right\rangle \, \left\langle \alpha_f \, J_f M_f \,|\, \rho_f \,|\, \alpha_f \, \mathbb{J}_f M'_f \right\rangle \, .$$

and which are non-zero only for $0 \;\le\; k_f \;\le\; 2\, J_f$ and $-k_f \;\le\; q_f \;\le\; k_f$.

3.7. Frequent radial integrals

Grant's radial integrals for the coupling of the radiation field:

➢ Grant (1988) defines the following radial integrals that frequently occur in the coupling of the radiation field

$$I^o_L(q;\, ab) \;=\; \int_0^\infty dr \; j_L(qr) \;\; [P_a \, Q_b]$$

$$I^\pm_L(q;\, ab) \;=\; \int_0^\infty dr \; j_L(qr) \;\; [P_a \, Q_b \;\pm\; Q_a \, P_b]$$

$$J_L(q;\, ab) \;=\; \int_0^\infty dr \; j_L(qr) \;\; [P_a \, P_b \;+\; Q_a \, Q_b]$$

➢ These integrals are useful also if the spherical Bessel function occurs in the integrant as $j_L(qr)/qr$, and where the following recursion relations can be used:

$$\frac{j_L(x)}{x} \;=\; \frac{1}{2L+1}\,[j_{L-1}(x) \;+\; j_{L+1}(x)]$$

Further radial integrals from one-electron spherical tensor operators:

➢ In the treatment of the electron nucleus (hyperfine) interaction and the interaction with an external magnetic field, some radial integrals occur frequently:

$$I_L^{[r]}(ab) \;\equiv\; [r^L]_{ab} \;=\; \int_0^\infty dr\, r^L\; [P_a\, Q_b \;+\; Q_a\, P_b]$$

$$J_L^{<r>}(ab) \;=\; \langle r^L\rangle_{ab} \;=\; \int_0^\infty dr\, r^L\; [P_a\, P_b \;+\; Q_a\, Q_b]$$

➢ Vinti-Integral: In the treatment of the (relativistic) mass shift, the (so-called) Vinti-Integrals occur

$$R^{(\mathrm{Vinti})}(a,b) \;=\; \int_0^\infty dr\, P_a \left[\frac{d}{dr} \;-\; \frac{\kappa_a(\kappa_a+1) \;-\; \kappa_b(\kappa_b+1)}{2r}\right] P_b \quad+\quad \int_0^\infty dr\, Q_a \left[\frac{d}{dr} \;-\; \frac{-\kappa_a(-\kappa_a+1) \;+\; \kappa_b(-\kappa_b+1)}{2r}\right] Q_b$$

4. Atomic interactions with the radiation field

4.1. Electron-photon interaction. Notations

Amplitudes for photon absorption:

- ➢ Photon absorption: by an atom or ion $|\alpha_i \mathbb{J}_i\rangle + \hbar\omega \longrightarrow |\alpha_f \mathbb{J}_f\rangle$
- ➢ Total (absorption) amplitude: for the absorption of a photon with wave vector $\mathbf{k} \,||\, \mathbf{e}_z$, energy ω and helicity $\lambda = \pm 1$ by an atom or ion due to a bound atomic transition $|\alpha_i \mathbb{J}_i\rangle \to |\alpha_f \mathbb{J}_f\rangle$

$$\left\langle \alpha_f\, \mathbb{J}_f M_f \,\middle|\, \mathbb{T}^{\,(\text{absorption})}(\mathbf{k},\lambda) \,\middle|\, \alpha_i\, \mathbb{J}_i M_i \right\rangle \;\equiv\; \left\langle \alpha_f\, \mathbb{J}_f M_f \,\middle|\, \mathbb{T}^{\,(\text{absorption})}(\omega,\lambda) \,\middle|\, \alpha_i\, \mathbb{J}_i M_i \right\rangle \;=\; \left\langle \alpha_f\, \mathbb{J}_f M_f \,\middle|\, \sum_{j=1}^{N} \boldsymbol{\alpha}_j\, \mathbf{u}_\lambda\, e^{i\,\mathbf{k}\cdot\mathbf{r}_j} \,\middle|\, \alpha_i\, \mathbb{J}_i M_i \right\rangle$$

$$= \sqrt{2\pi} \sum_{\mathbb{M}}^{\infty} i^L \sqrt{\frac{2L+1}{2J_f+1}}\, (i\lambda)^p \left\langle J_i M_i,\, L\lambda \,|\, J_f M_f \right\rangle \left\langle \alpha_f \mathbb{J}_f \,\middle\|\, \mathbb{O}^{\,(\mathbb{M},\,\text{absorption})}(\omega) \,\middle\|\, \alpha_i \mathbb{J}_i \right\rangle \,,$$

and where $p = 0$ refers to the magnetic and $p = 1$ refers to the electric multipoles. For plane waves, energy and wave vector are of course related by the standard dispersion relation: $\omega = c\,k$.

4.2. Representation and parametrization of photons

Representation and Stokes parametrization of a photon:

➢ Most naturally, the spin state of an incident photon is expressed within its helicity representation

$$\rho_\gamma \;=\; \sum_{\lambda\,\lambda'} c_{\lambda\lambda'}\,|\mathbf{k}\,\lambda\rangle\,\langle\mathbf{k}\,\lambda'|\,,$$

where the helicity λ is the spin projection of the photon upon the direction of its propagation (momemtum r wave vector $\mathbf{k}$.

Pure polarization states of photons:

➢ In the following, we will restrict ourselves to pure polarization states of the incoming photons, i.e. $P_1^2 + P_2^2 + P_3^2 = 1$. This is equivalent to $\rho^2 = \rho$, and where the density matrix of photon ρ is defined above. In this particular case, an arbitrary polarization state can be described as the linear combination

$$|\mathbf{e}\rangle \;=\; g_{+1}\mathbf{u}_{+1} + g_{-1}\mathbf{u}_{-1}\,,$$

where $\mathbf{u}_\lambda$ $(\lambda = \pm 1)$ are unit polarization vectors in the circular basis and $|g_{+1}|^2 + |g_{-1}|^2 = 1$. For example, the state of photon linearly polarized along some direction φ_0 in the xy-plane can be written in the form

$$|\mathbf{e}_{\varphi_0}\rangle \;=\; -\frac{1}{\sqrt{2}}\left(e^{-i\,\varphi_0}\mathbf{u}_{+1} - -e^{i\,\varphi_0}\mathbf{u}_{-1}\right)\,.$$

Polarization parameters for different types of polarization:

➢ In the (primed) coordinates Σ' as associated with some given pulse, the polarization cofficients are

$$g_{+1} = 1, \qquad g_{-1} = 0 \qquad \text{(for 'helicity : } +1')$$

$$g_{+1} = 0, \qquad g_{-1} = 1 \qquad \text{(for 'helicity : } -1')$$

$$g_{+1} = -\frac{1}{\sqrt{2}}\, e^{-i\phi_0}, \qquad g_{-1} = \frac{1}{\sqrt{2}}\, e^{i\phi_0} \qquad \text{(for 'linear' and given } \phi_0)$$

➢ Hierarchy of angles in defining the em pulses: All angles are defined with respect to a fixed laboratory frame $\Sigma = (x, y, z)$. All coordinate systems are assumed to be properly 'right-handed'.

Polarizaton of plane-wave photons:

➢ Monochromatic plane-wave light: Such plane-wave light is determined uniquely already by either the **E**- or **B**-field. We here consider a plane-wave along $\mathbf{k} \,||\, \mathbf{e}_z$.

➢ Complex electric field $\mathbf{E} = (E_{0x},\, E_{0y}, 0)$: The transverse, real **E** -Feld is given by

$$\left.\begin{aligned} E_{0x} &= |E_{0x}|\, e^{i\,\gamma} \\ E_{0y} &= |E_{0y}|\, e^{i\,(\gamma+\delta)} \end{aligned}\right\} \qquad \mathbf{E} = \Re\left[(E_{0x}\,\mathbf{e}_x + E_{0y}\,\mathbf{e}_y)\, e^{i\,(k\,z\,-\,\omega t)}\right] = E_x\,\mathbf{e}_x + E_y\,\mathbf{e}_y$$

$$E_x = |E_{0x}|\,\cos(k\,z - \omega t + \gamma), \qquad E_y = |E_{0y}|\,\cos(k\,z - \omega t + \gamma + \underbrace{\delta}_{!!}) \quad \text{... real}$$

➢ Relative phase δ to distinguish different polarization: This relative phase refers to the complex field amplitudes E_{0x} and E_{0y}

4.3. Multipole decomposition of the radiation field

4.3.a. Elements from the theory of multipole transitions

Motivation:

- The decomposition of the transition amplitudes into multipole components can be extended ans systematized as, for instance, outlined by Johnson (2008).
- For a one-electron atom, the transition amplitude from state $a = |n_a \kappa_a m_a\rangle \rightarrow b$ due to the interaction with a plane-wave radiation field, described by the transverse-gauge vector potential $\mathbf{A}^{(\mathrm{transverse})}(\mathbf{r}, \omega)$, is

$$T_{ba} = \int d^3\mathbf{r}\, \psi_b^*\, \boldsymbol{\alpha} \cdot \mathbf{A}^{(\mathrm{transverse})}(\mathbf{r}, \omega)\, \psi_a$$

4.3.b. Multipole emission and absorption amplitudes

Jac's standard multipole amplitudes for photon emission:

- Photon emission: from an atom or ion $|\alpha_i \mathbb{J}_i\rangle \longrightarrow |\alpha_f \mathbb{J}_f\rangle + \hbar\omega$
- Care has to be taken about the many-electron multipole amplitudes which appear in many expressions. Although we need formally to distinguish between the absorption a_L^λ and emission operators $a_L^{\lambda+}$ operators, all (one- and many-electron) matrix elements are always evaluated *in absorption*. For any photon emission process, however, this requires to 'exchange' the sequence *final-state — operator — initial-state*. This would be a (very) high price in such a large software project, since it affects the intuitive description of many processes in terms of initial-intermediate-final levels as well as possibly subsequent (final) states/levels.

Electron-photon interaction:

➢ Transition operator $\hat{\mathcal{R}}(\hat{\boldsymbol{k}})$: If the quantization axis is chosen along the electron momentum $\mathbf{p}$, the electron-photon interaction operator can be decomposed the in terms of spherical tensors, i.e. in terms of the electric and magnetic multipole fields. For a photon with wave vector $\boldsymbol{k}$, this multipole decomposition is defined by

$$\boldsymbol{u}_\lambda\, e^{i\boldsymbol{k}\cdot\boldsymbol{r}} \;=\; \sqrt{2\pi}\sum_{L=1}^{\infty}\sum_{M=-L}^{+L} i^L\sqrt{2L+1}\,\mathcal{A}^{(\lambda)}_{LM}\,D^L_{M\lambda}(\hat{\boldsymbol{n}}), \qquad \mathcal{A}^{(\lambda)}_{LM} \;=\; \mathcal{A}^{(m)}_{LM}+i\lambda\mathcal{A}^{(e)}_{LM} \;=\; \sum_{p=0,1}(i\lambda)^p\,\mathcal{A}^{(p)}_{LM}$$

for the magnetic ($p = 0$) and electric ($p = 1$) multipole fields. Here, the Wigner D-function or Wigner rotation matrices of rank L, $D^L_{M\lambda}(\hat{\boldsymbol{n}}) = D^L_{M\lambda}(\boldsymbol{k}\to\boldsymbol{e}_z)$, takes into account the fact that we have chosen the direction of the electron momentum $\boldsymbol{p}$ as the quantization instead of the photon momentum $\boldsymbol{k}$.

4.4. Electromagnetic light pulses

4.4.a. High-intensity pulses

Motivation:

➢ The exposure of atoms and matter to high-intensity laser fields is known to give rise to high-harmonic generation, above-threshold ionization and well as laser-induced dissociation and plasma formation that are all fundamentally different from processes in the weak-field regime.

4.4.b. Pulse shapes and optical cycles

Motivation:

➢ Pulse shaping generally refers to the the process of changing the waveform of a (transmitted)pulses, for instance, in order to make a transmitted signal better suited for a particular communication channel. In telecommunication, for example, pulse shaping is essential in order to ensure that the signal fit to a given frequency band.

➢ In femtosecond physics and chemistry, pulse shaping describes a technology for generating nearly arbitrary pulses with user defined, ultrafast optical waveforms, and by controlling its phase, amplitude, and polarization. Here, the most widely applied technique is Fourier transform pulse shaping.

Frequently applied pulse shapes for time-dependent atomic computations:

➢ All (symmetric) light pulses are usually defined in terms of a central frequency ω and a (delay) time T_d for the arrival of the pulse center with regard to reference time $t_0 = 0$. Moreover, the shape function is always normalized to $\max[f_s(t)] = \max[f(t)/f_o] = 1$ and, hence, the intensity of the em field must be captured properly into the constant f_o.

➢ In JAC, the following (symmetric) shapes of the em pulses have been pre-defined: `'sin^2'`, `'sin^2: plateau'`, `'sin^2: cycles'` and `'gaussian'`. Further pulses shapes might be added if the need arises from the side of experiment.

➢ `'sin^2'` pulse: The `'sin^2'` pulses is internally defined by a FWHM time $T_{\rm fwhm}$; with this input, the shape function is

$$f_s(t) = \begin{cases} 0 & t < T_d - \pi/2a \\ sin^2\left(a(t - T_d + \pi/2a)\right) & T_d - \pi/2a \le t \le T_d + \pi/2a \\ 0 & t > T_d + \pi/2a \end{cases} \qquad a = \frac{\pi}{2\,T_{\rm fwhm}}, \qquad a \ll \omega\,.$$

The number of optical cycles is then $k_c = \mathrm{NINT}(\omega/2a) = \mathrm{NINT}(\omega T_{\rm fwhm}/\pi)$.

➢ `'sin^2: plateau'` pulse: `'sin^2: plateau'` pulses are defined in terms of a FWHM time $T_{\rm fwhm}$ (that characterizes the beginning and the end of the pulse) and a plateau time T_p. With these parameters, the pulse-shape function is defined as

$$f_s(t) = \begin{cases} 0 & t < T_d - \pi/2a - T_p/2 \\ sin^2\left(a(t - T_d + \pi/2a + T_p/2)\right) & T_d - \pi/2a - T_p/2 \le t \le T_d - T_p/2 \\ 1 & T_d - T_p/2 \le t \le T_d + T_p/2 \\ sin^2\left(a(t - T_d + \pi/2a - T_p/2)\right) & T_d + T_p/2 \le t \le T_d + T_p/2 + \pi/2a \\ 0 & t > T_d + T_p/2 + \pi/2a \end{cases} \qquad a = \frac{\pi}{2\,T_{\rm fwhm}}, \qquad a \ll \omega\,.$$

4.4.c. Vector potential and maximum pulse intensity

Motivation:

➢ Amplitude of the vector potential: This amplitude need to be derived from the (maximum) intensity of a laser pulses that is typically given in W/cm^2. In general, this relation between the intensity and amplitude is not trivial since the relationship between the intensity and the electric field slightly depends also on the polarization. A simple relation only occurs if a linearlypolarized beam is assumed.

Vector potential:

➢ Vector potential for the time evolution of statistical tensors: In the general evolution of the statistical tensor, the vector potential appears in the form

$$\mathrm{A}(\mathrm{r},t) = \mathrm{A}(\mathrm{r}) f(t) e^{-i\omega t} + \mathrm{A}^*(\mathrm{r}) f^*(t) e^{i\omega t}$$

where A(r) denotes the spatial part, normalized to one photon per unit volume, and $f(t) = f_o\, f_s(t)$ is the (real) pulse envelope. In this factorization, $f_s(t)$ describes the pulse shape as defined in the last subsection and f_o the field amplitude, related to the (maximum) intensity. In the program, we use the conversion

$$f_o\,[\mathrm{a.u.}] \;=\; -c \times 5.34 \cdot 10^{-9} \sqrt{I[W/cm^2]}\,.$$

Pulse geometry and intensity:

➢ The atomic unit of electric field is $m_e^2\, e^5/\hbar^4 = 5.1422 \cdot 10^9$ V/cm. From this we have

$$E_0\,[a.u.] = 5.34 \cdot 10^{-9}\, \sqrt{I\,[W/cm^2]}$$

4.4.d. Bichromatic laser fields

Motivation:

➢ bichromatic laser fields. Of particular interest will be the case where the field is composed of two components of commensurate frequencies, usually consisting of a fundamental component and one of its low harmonics 2 or 3. These two components are in general out of phase by an angle .

Bichromatic laser fields:

➢ Linearly polarized bichromatic fields: The electric field can be written as

$$E(t) \;=\; F(t)\,\Big[\cos(\omega\,t \,+\, \phi_1^{(\mathrm{cep})}) \,+\, \eta\,\cos(2\,\omega\,t \,+\, \phi_2^{(\mathrm{cep})})\Big]$$

with frequencies ω of the fundamental radiation and $2\,\omega$ from the second harmonic. Here, the same envelope function $F(t)$ is applied for both, the fundamental and the second harmonic, while the ratio of the corresponding amplitudes is specified by the real parameter $\eta\,(\eta\,>\,0)$. The carrier-envelope phases (CEP) are denoted by $\phi_1^{(\mathrm{cep})})$ and $\phi_2^{(\mathrm{cep})})$, respectively.

4.5. Parity- and time-violating atomic interactions

4.5.a. Interactions beyond the standard model

Standard electro-weak model:

➢ The success of the standard electro-weak model of elementary particles is indeed extraordinary. It has been tested with many physical processes that cover more ten orders of magnitude in momentum transfer. The standard model correctly predicted the existence of new particles, such as the neutral Z boson.

➢ CP symmetry: This symmetry refers to the combined symmetry of charge conjugation C and parity P.

- Violation of CP symmetry: The violation of CP symmetry was first discovered in 1964 in the decays of the neutral K mesons and is taken into account by the standard electro-weak model by a single complex phase in the quark mixing matrix (the so-called Kobayashi-Maskawa mechanism). — Alternatively, the standard model of particle physics is sometimes said to violate time-reversal (T) invariance, but again only through just a single phase in the Cabibbo-Kobayashi-Maskawa matrix that mixes quark flavors.
- For a rather long time, K mesons remained the only system in which CP-violation had been observed. In 2001 only, the BaBar and Belle collaborations detected CP violation also for neutral B mesons, although this is consistent again with the predictions of the standard model.
- If CPT is *conserved* as suggested by gauge theories, then CP-violation must be accompanied by T (time-reversal) violation. Until the present, however, there has been no (undisputed) direct observation of T violation and its detection is of fundamental interest by itself. A direct detection of T-violation may shed light also on the origin of CP-violation. The measurement of a permanent electric dipole moment (EDM) of neutrons, atoms, or molecule would be direct evidence of T-violation.

High-precision measurements on fundamental symmetries of atoms:

- High-precision measurements on the (violation of fundamental) symmetries in atoms are suitable to test the standard model of elementary particles and to search for new physics beyond it. Such precision experiments in atomic physics complement measurements at high energies.
- Indeed, atomic experiments played an important role in the verification of the standard model already more than 30 years ago. While the first evidence for neutral-weak currents, i.e. the existence of the neutral Z boson, was discovered in neutrino scattering, a parity violation was first established in atomic experiments, and before it was observed also in high-energy electron scattering.
- Today, atomic physics plays a major role in the search for *new* physics beyond the standard model.
- For example, the cesium measurement on parity non-conservation in atomic physics have been found in excellent agreement with the standard model.

4.5.b. Parity-violating (P-odd, T-even) interactions

Motivation:

➢ Parity nonconservation (PNC) effects arises in atoms largely due to the exchange of Z^0-bosons between atomic electrons and the nucleus.

➢ There is also another contribution to atomic parity violation due to the exchange of Z^0 bosons between electrons; however, this effect is negligibly small for heavy atoms and suppressed by a factor $10^{-3} \ldots 10^{-4}$. This contribution is usually neglected in most PNC studies.

Nuclear-spin independent electron-nucleus interactions:

➢ Nuclear-spin independent Hamiltonian: For non-relativistic nucleons, the nuclear-spin independent Hamiltonian for the electron-nucleus interaction is given by the effective single-electron operator

$$\mathbb{H}^{(\mathrm{weak-charge})} \;=\; -\frac{G}{\sqrt{2}}\,\gamma_5\;\left[Z\,C_{1p}\,\rho_p(r)\;+\;N\,C_{1n}\,\rho_n(r)\right]\,,$$

where Z and N are the number of protons and neutrons, and where the proton and neutron densities are normalized to unity.

➢ If the proton and neutron densities coincide, $\rho_p = \rho_n = \rho$, the nuclear-spin independent Hamiltonian simplifies and can be described in terms of a nuclear-weak charge Q_W,

$$\mathbb{H}^{(\mathrm{weak-charge})} \;=\; -\frac{G}{2\sqrt{2}}\,\gamma_5\,Q_W\rho\,.$$

➢ Nuclear weak charge Q_W: This charge is very close to the neutron number and is in lowest order in the electroweak interaction given by

$$Q_W \;=\; -N + Z\,(1 - 4\sin^2\theta_W) \;\approx\; -N\,.$$

This value for Q_W is modified by radiative corrections.

Nuclear-spin dependent electron-nucleus interactions:

➢ Interaction that depend on the nuclear spin I: There are different interactions that depend on the nuclear spin I due to:
i) the neutral weak current; ii) hyperfine-induced neutral currents; or iii) the nuclear anapole moment.

➢ Interaction with the nuclear anapole: The anapole moment gives typically the dominant nuclear-spin dependent electron-nucleus interaction. The nuclear anapole moment arises P-odd interactions inside the nucleus. This interaction manifests itself in atoms through a slightly modified electromagnetic interaction of the nucleus with atomic electrons.

Anapole moment:

➢ The notion of the anapole moment was introduced by Zel'dovich just after the discovery of parity violation.

➢ However, an nuclear anapole moment was unambiguously detected only 30 years later. In 1997, a group at Boulder measured a nuclear anapole moment in ^{133}Cs to an accuracy of 14 % in an atomic experiment. This is considered as the first observation of an electromagnetic moment that violates fundamental discrete symmetries.

➢ A P-odd, T-even anapole moment of the nucleus arises due to the presence of a parity violating weak interaction between nucleons.

Further information:

➢ Several PNC experiments in rare-earth atoms have been suggested for close-lying levels of opposite parity in order to enhance the PNC effects. Moreover, rare-earth often have various stable isotopes and, hence, the dependence on atomic theory can be removed by taking ratios of the measured PNC contributions for different isotopes.

➢ The possibility of performing PNC measurements on a singly trapped Ba^+ and Ra^+ ion is currently being considered at Seattle. Preliminary atomic PNC calculations indicate that the accuracy of such Ba^+ calculations could readily compete with those for neutral cesium.

4.5.c. Time-reversal violating (P-odd, T-odd) interactions

Motivation:

➢ Many physical systems and processes are asymmetric under time reversal. In classical mechanics, for example, a velocity $v\,to\,-v$ reverses its direction under time reversal, while an acceleration does not. This asymmetry is often associated with some dissipation and, hence, with the second law of thermodynamics. Without dissipation, the laws of mechanics are usually considered to be invariant with regard to time reversal.

➢ In nuclei, P-odd and T-odd nuclear moments can arise due to an intrinsic EDM of an external nucleon or due to P-odd and T-odd nuclear forces. The P-odd and T-odd nuclear forces induce larger nuclear moments than a single nucleon EDM. The study of the different sources for an EDM atomic experiments so competitive compared to neutron experiments in probing CP-violation in the hadron sector (Ginges and Flambaum, 2004).

P-odd & T-odd Hamiltonians due to electron-nucleus interactions:

➢ Different contributions to the P-odd and T-odd electron-nucleus interaction: (i) the scalar-pseudoscalar, (ii) the pseudoscalar-scalar, and (iii) the tensor P-odd and T-odd electron-nucleon interactions.

➢ Electron-nucleus interaction for nucleons with infinite mass: If the nucleons have an infinite mass, the electron-nucleus interaction simplifies to

$$\mathbb{H}^{(\text{scalar}-\text{pseudoscalar})} = i\,\frac{G}{\sqrt{2}}\,\left(Z\,C_p^{\text{SP}} + N\,C_n^{\text{SP}}\right)\,\gamma_0\,\gamma_5$$

$$\mathbb{H}^{(\text{tensor})} = i\,\frac{2\,G}{\sqrt{2}}\,\rho(r)\,\left(C_p^{\text{T}}\sum_p \sigma_p \,+\, C_n^{\text{T}}\sum_n \sigma_n\right)\cdot\boldsymbol{\gamma}$$

while the pseudoscalar-scalar term vanishes in this approximation. In these Hamiltonians, the dimensionless constants C_N^{SP}, C_N^{PS} and C_N^{T} can be determined from measurements of the atomic EDM.

➢ Note the similarity between the expressions for $\mathbb{H}^{(\text{scalar}-\text{pseudoscalar})}$ and $\mathbb{H}^{(\text{weak charge})}$ as well as $\mathbb{H}^{(\text{I}-\text{independent})}$, respectively. However, here the matrix elements are real. Therefore the electron-nucleus interactions from above mixes atomic states of opposite parity and induces static electric dipole moments in atoms.

P-odd & T-odd nuclear moments:

- The operators $\mathbb{H}^{(\text{scalar}-\text{pseudoscalar})}$ and $\mathbb{H}^{(\text{tensor})}$ have both electronic and nuclear components. While these Hamiltonians are overall scalar, the electronic and nuclear operators can be of any (equal) rank. To obtain any non-zero matrix element, therefore, the triangle rule for coupling of angular momenta imposes restrictions on the angular momenta of the electron and nuclear states.
- For example, the interaction of the electrons with the nuclear magnetic quadrupole moment cannot mix s and $p_{1/2}$ (electron) states, since we must have $|j_1 - j_2| \leq j \leq j_1 + j_2$. Similarly, a static magnetic quadrupole moment of the nucleus cannot arise in nuclei with total angular momentum $I \leq 1$.
- The nuclear EDM exceeds the EDM of single nucleons by one to two orders of magnitude. Similarly, P-odd and T-odd nuclear forces generate all P-odd and T-odd nuclear moments, such as the Schiff and MQM moments. These nuclear moments can be 10-to-100 times larger than those generated by the presence of a nucleon EDM.
- Nuclear moments that violate parity and time-reversal invariance: electric dipole, magnetic quadrupole, electric octupole. For an nuclear electric-dipole moment, the Hamiltonian must be of the form $\mathbb{H}^{(\text{Schiff moment})}$ to mix electron states of opposite parity.

4.5.d. Time-reversal violating atomic electric-dipole moments

Motivation:

- A non-zero electric-dipole moment (EDM) of atoms require P-odd and T-odd interactions, either among the nucleons or the electrons and the nucleus.
- Therefore, the null measurements of EDM in atoms place severe restrictions upon new sources of CP-violation that often arise in models beyond the standard model, such as supersymmetry.

Physics of the atomic EDM:

- An atomic EDM that is associated with an atomic level $|\alpha \mathbb{J}\rangle$ due to the admixture of levels (states) $|\nu \mathbb{J}\_nu\rangle$ with opposite-parity wave functions has the form

$$\mathbb{d}^{(\text{atomic EDM})} = 2 \sum_{\nu} \frac{\langle \alpha \mathbb{J} | \mathbb{D} | \nu \mathbb{J}\_nu \rangle \langle \nu \mathbb{J}\_nu | \mathbb{H}^{(\text{PT})} | \alpha \mathbb{J} \rangle}{E_\alpha - E_\nu} = d^{(\text{atomic EDM})} \frac{\mathbf{F}}{F},$$

where $\mathbb{D}$ is the electric dipole operator, $\mathbb{H}^{(\mathrm{PT})}$ the P-odd and T-odd operator that mixes $|\alpha \mathbb{J}\rangle$ with the set of wave functions $|\alpha_\nu \mathbb{J}_\nu\rangle$, and F is the total angular momentum of the atom corresponding to the state $|\alpha \mathbb{J}\rangle$.

➢ A typical EDM experiment is performed in parallel electric and magnetic fields and can be described by the Hamiltonian

$$\mathbb{H}^{(\text{em field})} = -\mu \cdot \mathbf{B} - \mathbf{d} \cdot \mathbf{E}.$$

➢ A linear Stark shift is measured by observing the change in frequency when the electric field is reversed since it is sensitive to the P-odd and T-odd term $\mathbf{E} \cdot \mathbf{B}$).

➢ Measurements of EDMs in paramagnetic systems (that is, with nonzero total electron angular momentum) are most sensitive to leptonic sources of P- and T-violation, in particular the electron EDM, while measurements of EDMs in diamagnetic systems (zero total electron angular momentum) are most sensitive to P-odd and T-odd mechanisms in the hadronic sector.

Enhancement of atomic EDM:

➢ The effects of P- and T-violation increase in atoms with: (i) a high nuclear charge Z. P- and T-odd effects in atoms increase rapidly with ZZ [GF:223,GF:224]. Therefore, it is best to search for atomic EDMs in heavy atoms. (ii) close levels of opposite parity. From above, we can see that if H_{PT} mixes opposite parity levels with energies $E_1 \approx E_2$, then the atomic EDM induced will be enhanced, $d_{\mathrm{atom}} \propto 1/(E_1 - E_2)$.

➢ An enhancement occurs, for example, in rare-earth atoms, where there are anomalously close levels of opposite parity.

➢ The best limits on the electron electric dipole moment are derived from measurements of atomic EDMs. Salpeter first noted the possibility of an enhancement of the electron EDM in atoms through consideration of the metastable $2s$ state in hydrogen.

5. Atomic amplitudes

5.1. In JAC implemented amplitudes

5.1.a. Dipole amplitudes (MultipoleMoment)

Amplitude & notations:

- Formal quantum notation: $\langle \alpha_f \mathbb{J}_f \| \mathbb{D} \| \alpha_i \mathbb{J}_i \rangle$ = selection rules
- Using JAC: Call `MultipoleMoment.dipoleAmplitude(level`$_f$`::Level, level`$_i$`::Level)` or `MultipoleMoment.dipoleAmplitude(level`$_f$`::Level, level`$_i$`::Level; display=true)`, if you wish print also the value of the amplitude to screen.

5.1.b. Electro-magnetic multipole amplitudes (MultipoleMoment, Radiative)

Amplitude & notations:

- Formal quantum notation: $\langle \alpha_f \mathbb{J}_f \| \mathbb{M} \| \alpha_i \mathbb{J}_i \rangle$ = selection rules
- Using JAC: Call `MultipoleMoment.multipoleAmplitude(level`$_f$`::Level, mp::EmMultipole, level`$_i$`::Level)` or `MultipoleMoment.multipoleAmplitude(level`$_f$`::Level, mp::EmMultipole, level`$_i$`::Level; display=true)`, if you wish print also the value of the amplitude to screen.

Multipole operators:

- Start here from Walter Johnson's book.

5.1.c. Momentum transfer amplitudes (FormFactor)

Amplitude & notations:

- Formal quantum notation: $\langle \alpha_f \mathcal{J}_f \| \sum \exp i\,\mathbf{q}\cdot\mathbf{r}_i \| \alpha_i \mathcal{J}_i \rangle$ = selection rules
- Using JAC: Call `FormFactor.amplitude(level`$_f$`::Level, level`$_i$`::Level, ...)` or `FormFactor.amplitude(level`$_f$`::Level, level`$_i$`::Level, ...; display=true)`, if you wish print also the value of the amplitude to screen.

Momentum transfer amplitude:

- ...

5.1.d. Parity non-conservation amplitudes (ParityNonConservation)

Amplitude & notations:

- Formal quantum notation: $\langle \alpha_f \mathcal{J}_f \| \ldots \| \alpha_i \mathcal{J}_i \rangle$ = selection rules
- Using JAC: Call `ParityNonConservation.weakChargeAmplitude(level`$_f$`::Level, level`$_i$`::Level, ...)` or `ParityNonConservation.weakChargeAmplitude(level`$_f$`::Level, level`$_i$`::Level, ...; display=true)`, if you wish print also the value of the amplitude to screen.

P-odd, T-even weak-charge amplitude:

➢ ...

5.2. In JAC partly-implemented amplitudes

5.2.a. Schiff-moment amplitudes (ParityNonConservation)

Amplitude & notations:

➢ Formal quantum notation: $\langle \alpha_f \mathbb{J}_f \| ... \| \alpha_i \mathbb{J}_i \rangle$ = selection rules

➢ Using JAC: Call `ParityNonConservation.schiffMomentAmplitude(level`$_f$`::Level, level`$_i$`::Level, ...)` or `ParityNonConservation.schiffMomentAmplitude(level`$_f$`::Level, level`$_i$`::Level, ...; display=true)`, if you wish print also the value of the amplitude to screen.

P-odd, T-odd Schiff moment amplitude:

➢ ...

5.2.b. Anapole-moment amplitudes (ParityNonConservation)

Amplitude & notations:

- Formal quantum notation: $\langle \alpha_f \mathbb{J}_f \| \ldots \| \alpha_i \mathbb{J}_i \rangle$ = selection rules
- Using JAC: Call `ParityNonConservation.anapoleMomentAmplitude(level`$_f$`::Level, level`$_i$`::Level, ...)` or `ParityNonConservation.anapoleMomentAmplitude(level`$_f$`::Level, level`$_i$`::Level, ...; display=true)`, if you wish print also the value of the amplitude to screen.

P-odd, T-odd anapole moment amplitude:

- ...

5.3. Further amplitudes, not yet considered in JAC

5.3.a. Scalar-pseudo-scalar amplitudes

P-odd, T-odd scalar-pseudo-scalar amplitude:

- ...

5.4. Composed many-electron amplitudes, not yet considered in JAC

5.4.a. Parity-violating (non-diagonal, second-order) amplitude

Motivation:

- Parity violation: This (effective) violating interaction is caused by the exchange of a Z_o boson between atomic electrons and the nucleus and typically results in nonvanishing off-diagonal electric-dipole matrix element between two atomic states of the same parity.
- The exchange of Z_o bosons is described by the Weinberg-Salam theory. It leads to phenomena such as circular dichroism and optical rotation which have been investigated to detect P-violation in cesium, thallium, bismut and plumbum.

5.4.b. Charge-parity-violating (diagonal, second-order) amplitude

Motivation:

- Charge-parity violation: An intrinsic electron electric dipole moment d_e leads to CP-violation in atoms and also induces an atomic electric dipole moment.

5.4.c. Electric-dipole moment enhancement factor

Motivation:

- An intrinsic electric-dipole moment of the electron can enhanced the EDM of the atom.
- :

6. Atomic properties

6.1. In JAC implemented level properties

6.1.a. Transition probabilities for a single multiplet (Einstein)

Process & notations:

- Photon emission: from an atom or ion $A^* \longrightarrow A^{(*)} + \hbar\omega$
- Formal quantum notation: $|\alpha_i \mathbb{J}_i\rangle \longrightarrow |\alpha_f \mathbb{J}_f\rangle + \hbar\omega$
- Using JAC: Perform an `Atomic.Computation(.., properties=[EinsteinX, ..], configs=[..], einsteinSettings= Einstein.Settings(..), ..)` or call directly functions from the module `Einstein`.

Motivation:

- Calculations of Einstein A and B coefficients and oscillator strength for levels $|\alpha\mathbb{J}\rangle$ from a single multiplet; although these coefficients do not refer to (some property of) a single level, we still support with the `Einstein` module the computation of these coefficients for levels that are represented within a single CSF basis.
- This module helps for obtaining either a quick overview about the Einstein coefficients of just a few configurations or with cascade computations, although it does not allow to include relaxation effects.

6.1.b. Hyperfine parameters (Hfs)

Property & notations:

➢ Hyperfine splitting of an atomic level into hyperfine (sub-) levels: $|\alpha\mathbb{J}\rangle \longrightarrow |\alpha(J)\,\mathbb{F}\rangle\,, \qquad F = |I-J|, ..., I+J-1, I+J$.

➢ Formal quantum notation: $|\alpha\mathbb{J}\rangle \longrightarrow |\alpha\,\mathbb{F}\rangle \equiv |\alpha(J)\,\mathbb{F}\rangle \equiv |\alpha(IJ)\,\mathbb{F}\rangle \equiv |\alpha(IJP)\,F\rangle$ or
$|\alpha\mathbb{J}M_J\rangle \longrightarrow |\alpha\,\mathbb{F}M\rangle \equiv |\alpha(J)\,\mathbb{F}M\rangle \equiv |\alpha(IJ)\,\mathbb{F}M\rangle \equiv |\alpha(IJP)\,FM\rangle$.

➢ Using Jac: Perform an `Atomic.Computation(.., properties=[HFS, ..], configs=[..], hfsSettings=Hfs.Settings(..), ..)` or call directly functions from the module `Hfs`.

Motivation:

➢ If the nucleus has a *non-zero* spin $I > 0$, a hyperfine splitting of (all) atomic levels occurs, since each atomic electron then also interacts with the electric and magnetic (multipole) fields of the nucleus.

➢ In atomic physics, this interaction is better known as "hyperfine interaction" whose two dominant contributions arise from the nuclear magnetic-dipole field $\mathbf{A} = \frac{\boldsymbol{\mu}\times\mathbf{r}}{r^3}$ and the electric-quadrupole field $\Phi(r) = \sum_{ij} \frac{r_i\, r_j}{2\, r^5}\, Q_{ij}$, respectively. In these expressions, $\boldsymbol{\mu}$ is the nuclear magnetic moment operator and Q_{ij}, $i,j = 1..3$ are the Cartesian components of the nuclear quadrupole operator.

Hyperfine interaction Hamiltonian:

➢ Relativistic hyperfine interaction Hamiltonian: For many-electron systems, this Hamiltonian can be written as

$$H^{(\mathrm{hfs})} = \sum_K \mathbb{W}^{(K)} \cdot \mathbb{T}^{(K)}$$

where $\mathbb{W}^{(K)}$ and $\mathbb{T}^{(K)}$ represent the spherical tensor operators of rank K that occur in the nucleonic and electronic sectors, respectively.

➢ The reduced nuclear matrix elements are determined geometrically by

$$\left\langle I \left\| \mathbb{W}_1^{(K)} \right\| I \right\rangle = \mu_I \sqrt{\frac{I+1}{I}}, \qquad \left\langle I \left\| \mathbb{W}_2^{(K)} \right\| I \right\rangle = \frac{Q}{2} \sqrt{\frac{(I+1)\,(2I+3)}{I\,(2I-1)}},$$

while the corresponding electronic amplitudes require, in contrast, detailed atomic structure calculations. Values of nuclear magnetic dipole and electric quadrupole moments can be found in the compilation by Stone (2005).

Atomic (hyperfine) IJF -coupled basis:

➢ This basis is obtained by the standard coupling of the nuclear states $|IM_I\rangle$ and the ASF $|\alpha\, \mathbb{J}M_J\rangle$

$$|\alpha(I,J)\,\mathbb{F}M\rangle \equiv |(I,\,\alpha'\,\mathbb{J})\,\mathbb{F}M\rangle = \sum_{M_I\,M_J} |IM_I\rangle\,|\alpha'\,\mathbb{J}M_J\rangle\,\langle IM_I,\,JM_J\,|\,FM\rangle\,.$$

Atomic hyperfine amplitudes and levels:

➢ Atomic hyperfine levels: For the combined system "nucleus+electrons", the atomic hyperfine states (sub-levels) can be formed as linear combination

$$|\alpha\,\mathbb{F}M\rangle = \sum_{r=1} \tilde{c}_r(\alpha)\,|(I,\,\beta_r\,\mathbb{J}_r)\,\mathbb{F}M\rangle$$

of hyperfine (basis) states $|(I,\,\beta_r\mathbb{J}_r)\,FM\rangle$ of the same total angular momentum F and (the same electronic) parity P, and where $\{\tilde{c}_r(\alpha)\}$ denotes the representation of these states in the atomic hyperfine-coupled basis (Johnson, 2010).

➢ Analogue as for the ASF $|\alpha\mathbb{J}\rangle$ in the standard MCDF ansatz, the representation $\{\tilde{c}_r(\alpha)\}$ of an atomic hyperfine state is obtained by diagonalizing the Hamiltonian $\mathbb{H} = \mathbb{H}^{(\mathrm{DFB})} + \mathbb{H}^{(\mathrm{hfs})}$ of the combined system "nucleus+electrons", where we can make use of $\mathbb{H}^{(\mathrm{DFB})}\,|(I,\,\beta_r\,\mathbb{J}_r)\,\mathbb{F}M\rangle = E(\beta_r\,\mathbb{J}_r)\,|(I,\,\beta_r\,\mathbb{J}_r)\,\mathbb{F}M\rangle\,.$

Hyperfine energies and interaction constants:

➢ Hyperfine interaction constants: Usually the hyperfine splitting is considered independently for each atomic level $|\alpha\mathbb{J}\rangle$ and without specifying the hyperfine levels $|\alpha\mathbb{F}\rangle$ explicitly. Then, the energy splitting of an atomic level $|\alpha\mathbb{J}\rangle$ into hyperfine levels $|\alpha\mathbb{F}\rangle$ can be

expressed most conviniently in terms of the (hyperfine interaction) constants

$$A(\alpha\,\mathbb{J}) \;=\; \frac{\mu_I}{I}\;\frac{1}{\sqrt{J(J+1)}}\;\langle \alpha\,\mathbb{J}\,\|\mathbb{T}^{(1)}\|\,\alpha\,\mathbb{J}\rangle\,, \qquad\qquad B(\alpha\,\mathbb{J}) \;=\; 2Q\,\sqrt{\frac{J(2J-1)}{(J+1)(2J+3)}}\;\langle \alpha\,\mathbb{J}\,\|\mathbb{T}^{(2)}\|\,\alpha\,\mathbb{J}\rangle$$

➢ Hyperfine energy splitting: With these constants, the hyperfine energy shifts with regard to the electronic level energy $E(\alpha\mathbb{J})$ is given by

$$\Delta\,E_F \;=\; \frac{A(\alpha\,\mathbb{J})\,C}{2} \;+\; B(\alpha\,\mathbb{J})\,\frac{3/4\,C(C+1)\;-\;I(I+1)\,J(J+1)}{2I\,(2I-1)\,J\,(2J-1)}, \qquad\qquad C \;=\; F(F+1)\;-\;J(J+1)\;-\;I(I+1)$$

6.1.c. Representation of hyperfine levels within a IJF-coupled hyperfine basis (`Hfs`)

Property & notations:

➢ Formal quantum notation: $|\alpha\mathbb{J}\rangle \;\longrightarrow\; |\alpha\,\mathbb{F}\rangle \equiv |\alpha(J)\,\mathbb{F}\rangle \equiv |\alpha(IJ)\,\mathbb{F}\rangle \equiv |\alpha(IJP)\,F\rangle$ or
$|\alpha\mathbb{J}M_J\rangle \;\longrightarrow\; |\alpha\,\mathbb{F}M\rangle \equiv |\alpha(J)\,\mathbb{F}M\rangle \equiv |\alpha(IJ)\,\mathbb{F}M\rangle \equiv |\alpha(IJP)\,FM\rangle$.

➢ Using Jac: Perform an `Atomic.Computation(.., properties=[IJF_Expansion, ..], configs=[..], hfsSettings= Hfs.Settings(..), ..)` or call directly functions from the module `Hfs`.

Motivation and implementation:

➢ Apart from the hyperfine parameters $A(\alpha\,\mathbb{J})$ and $B(\alpha\,\mathbb{J})$, we also provide in Jac a representation of the atomic hyperfine levels that can be utilized, for instance, to compute hyperfine quenched transitions probabilities.

➢ In the Jac program, such a representation of a hyperfine multiplet is obtained by diagonalizing the Hamiltonian $\mathbb{H} = \mathbb{H}^{(DCB)} + \mathbb{H}^{(hfs)}$ within the hyperfine IJF-coupled basis, if a `IJF_Expansion` was selected to be calculated as one of the supported properties in

`Atomic.Computation`. For this hyperfine multiplet, we only tabulate (hyperfine) level energies $E_{\alpha\,\mathbb{F}}$ and the energies relative to the lowest (hyperfine) level.

6.1.d. Lande g_J factors and Zeeman splitting of fine-structure levels (`LandeZeeman`)

Property & notations:

- ➢ Zeeman splitting of an atomic level into Zeeman (sub-) levels: $|\alpha\mathbb{J}\rangle \longrightarrow |\alpha\,\mathbb{J}M\rangle\,, \qquad M = -J, ..., J-1, +J$.
- ➢ Formal quantum notation: $|\alpha\mathbb{J}M\rangle$.
- ➢ Using JAC: Perform an `Atomic.Computation(.., properties=[LandeJ, ..], configs=[..], zeemanSettings= LandeZeeman.Settings(..), ..)` with `calcLandeJ=true` or call directly functions from the module `LandeZeeman`.

Motivation:

- ➢ The Zeeman effect describes the (level) splitting of an atomic level $|\alpha\mathbb{J}\rangle$ into its sub-levels $|\alpha\mathbb{J}M\rangle$ for the presence of a static magnetic field.
- ➢ More general, any external magnetic field may cause a splitting of the spectral lines into several components, analogous to the Stark effect for the splitting of a spectral line in the presence of an electric field.

Zeeman Hamiltonian $\mathbb{H}^{(\mathrm{mag})}$:

➢ If the z-axis is chosen along the magnetic field $\mathbf{B} \,||\, \mathbf{e}_z$ and if we neglect diamagnetic contributions, the magnetic (Zeeman) Hamiltonian can be written in terms of spherical tensors (Andersson and Jönsson, 2008)

$$\mathbb{H}^{(\mathrm{mag})} \;=\; \left(\mathbb{N}_0^{(1)} \;+\; \Delta\, \mathbb{N}_0^{(1,\,\mathrm{QED})} \right)\, B$$

$$\mathbb{N}^{(1)} \;=\; \sum_j^N \mathbb{n}^{(1)}(j) \;=\; \sum_j^N -i\,\frac{\sqrt{2}}{2\,\alpha}\, r_j \;\; \left(\boldsymbol{\alpha}_j \, \mathbb{C}^{\,(1)}(j) \right)^{(1)}$$

$$\Delta\, \mathbb{N}^{(1)} \;=\; \sum_j^N \Delta\, \mathbb{n}^{(1)}(j) \;=\; \sum_j^N \frac{g_s \;-\; 2}{2}\, \beta_j \;\boldsymbol{\Sigma}_j, \qquad\qquad \boldsymbol{\Sigma} \;=\; \begin{pmatrix} \boldsymbol{\sigma} & 0 \\ 0 & \boldsymbol{\sigma} \end{pmatrix},$$

and where the second term in the magnetic Hamiltonian above is (so-called) Schwinger's QED correction. Here, $g_s \;=\; 2.00232$ is the g-factor of the electron, including some leading QED corrections.

➢ (Reduced single-electron) Zeeman interaction strengths: Following Andersson and Jönsson (2008), the single-electron Zeeman interaction strengths of the magnetic operators are given by

$$\left\langle n_a\kappa_a \left\| \, \mathbb{n}^{(1)} \right\| n_b\kappa_b \right\rangle \;=\; -\frac{1}{2\,\alpha}\, \left\langle -\kappa_a \left\| \, \mathbb{C}^{\,(1)} \right\| \kappa_b \right\rangle \; I_1^{[\mathrm{r}]}(ab)$$

$$\left\langle n_a\kappa_a \left\| \, \Delta\, \mathbb{n}^{(1)} \right\| n_b\kappa_b \right\rangle \;=\; \frac{g_s \;-\; 2}{2}\, (\kappa_a \;+\; \kappa_b \;-\; 1)\, \left\langle -\kappa_a \left\| \, \mathbb{C}^{\,(1)} \right\| \kappa_b \right\rangle \; J_0^{<\mathrm{r}>}(ab)$$

and where the radial integrals $I_L^{[\mathrm{r}]}(ab)$ and $J_L^{\langle \mathrm{r} \rangle}(ab)$ are defined in section 3.7.

➢ In the Jac program, the Zeeman amplitudes $\left\langle \beta_r \mathbb{J}_r \left\| \, \mathbb{N}^{(1)} \right\| \beta_s \mathbb{J}_s \right\rangle$ and $\left\langle \beta_r \mathbb{J}_r \left\| \, \Delta\, \mathbb{N}^{(1)} \right\| \beta_s \mathbb{J}_s \right\rangle$ can be obtained from the function `Jac.LandeZeeman.amplitude()`.

Lande factor $g_J \equiv g(\alpha\mathbb{J})$ and Zeeman splitting of an electronic level $|\alpha\,\mathbb{J}\rangle$:

➢ Zeeman splitting of an atomic level $|\alpha\mathbb{J}\rangle$: If the splitting due to the magnetic field is small, when compared with the fine-structure splitting, it can be expressed in first-order perturbation theory by

$$\Delta E^{(\mathrm{mag})} = \left\langle \alpha\,\mathbb{J}M \left| \mathbb{N}_0^{(1)} + \Delta\,\mathbb{N}_0^{(1,\,\mathrm{QED})} \right| \alpha\,\mathbb{J}M \right\rangle = (-1)^{J-M} \begin{pmatrix} J & 1 & J \\ -M & 0 & M \end{pmatrix} \sqrt{2J+1}\, \left\langle \alpha\,\mathbb{J} \left\| \mathbb{N}^{(1)} + \Delta\,\mathbb{N}^{(1,\,\mathrm{QED})} \right\| \alpha\,\mathbb{J} \right\rangle B$$

$$= \frac{M}{\sqrt{J\,(J+1)}} \left\langle \alpha\,\mathbb{J} \left\| \mathbb{N}^{(1)} + \Delta\,\mathbb{N}^{(1,\,\mathrm{QED})} \right\| \alpha\,\mathbb{J} \right\rangle B$$

and with regard to the unperturbed energy $E(\alpha\mathbb{J}) = E(\alpha\mathbb{J},\, M=0)$.

➢ Lande g_J factor of an atomic level $|\alpha\mathbb{J}\rangle$: Usually, the dependence on M quantum number is factored out and the energy splitting is expressed for a single level $|\alpha\mathbb{J}\rangle$ in terms of its Lande factor $g_J \equiv g(\alpha\mathbb{J})$

$$\Delta E^{(\mathrm{mag})} = g(\alpha\mathbb{J})\, M\, \frac{B}{2}, \qquad g(\alpha\mathbb{J}) \equiv g_{\mathbb{J}} = 2\, \frac{\left\langle \alpha\,\mathbb{J} \left\| \mathbb{N}^{(1)} + \Delta\,\mathbb{N}^{(1,\,\mathrm{QED})} \right\| \alpha\,\mathbb{J} \right\rangle}{\sqrt{J\,(J+1)}}$$

6.1.e. Lande g_F factors and Zeeman splitting of hyperfine levels (LandeZeeman)

Property & notations:

➢ Zeeman splitting of an atomic hyperfine level into Zeeman (sub-) levels: $|\alpha(J)\mathbb{F}\rangle \longrightarrow |\alpha\,(J)\mathbb{F}M\rangle$, $M = -F, ..., F-1, +F$.

➢ Formal quantum notation: $|\alpha(J)\mathbb{F}M\rangle$.

➢ Using JAC: Perform an `Atomic.Computation(.., properties=[LandeJ, ..], configs=[..], zeemanSettings= LandeZeeman.Settings(..), ..)` with `calcLandeF=true` or call directly functions from the module `LandeZeeman`.

Motivation:

➢ The Lande g-factor (also kown as g value or dimensionless magnetic moment) is a dimensionless entity that characterizes the gyromagnetic ratio of an atomic or hyperfine level. The Lande g-factor is basically a proportionality constant how efficient a particle, spin or quantum state with given total angular momentum s contributes to the splitting in an external magnetic fiel B.

➢ In JAC, we also support the computation of $g_F \equiv g(\alpha\mathbb{F})$ factors for hyperfine levels.; cf. Section 6.1.d.

Lande factor $g_F \equiv g(\alpha\mathbb{F})$ of an hyperfine level $|\alpha\,\mathbb{F}\rangle$:

➢ Zeeman splitting of an hyperfine level $|\alpha\mathbb{F}\rangle$: If the splitting due to the magnetic field is small, when compared with the hyperfine-splitting, it can be expressed in first-order perturbation theory in terms of the reduced electronic Zeeman amplitudes by

$$\begin{aligned}
\Delta E^{(\mathrm{mag})} &= \Big\langle (I,\,\alpha\,\mathbb{J})\,FM \Big|\, \mathbb{N}_0^{(1)} \,+\, \Delta\,\mathbb{N}_0^{(1,\,\mathrm{QED})} \,\Big|\, (I,\,\alpha\,\mathbb{J})\,FM \Big\rangle \\
&= M\,\frac{F(F+1)\,+\,J(J+1)\,-\,I(I+1)}{2\,F(F+1)}\;\frac{\Big\langle \alpha\,\mathbb{J} \Big\|\, \mathbb{N}_0^{(1)} \,+\, \Delta\,\mathbb{N}_0^{(1,\,\mathrm{QED})} \,\Big\|\, \alpha\,\mathbb{J} \Big\rangle}{\sqrt{J(J+1)}} \\
&= M\,\frac{F(F+1)\,+\,J(J+1)\,-\,I(I+1)}{2\,F(F+1)}\;g(\alpha\mathbb{J})\,\frac{B}{2}\,,
\end{aligned}$$

and expressed with regard to the unperturbed hyperfine energy $E(\alpha(IJ)\mathbb{F}) \,=\, E(\alpha\mathbb{F},\,M=0)$.

➢ Lande factor $g_F \equiv g(\alpha\mathbb{F})$ and Zeeman energy splitting of an hyperfine level $|\alpha\mathbb{F}\rangle$:

$$g(\alpha\mathbb{F}) \;=\; \frac{F(F+1)\,+\,J(J+1)\,-\,I(I+1)}{2\,F(F+1)}\;g(\alpha\mathbb{J}) \qquad\Longrightarrow\qquad \Delta E^{(\mathrm{mag})} \;=\; g(\alpha\mathbb{F})\,M\,\frac{B}{2}$$

6.1.f. Isotope-shift parameters (IsotopeShift)

Property & notations:

➢ Isotope shift of an atomic level for two isotopes A, A' with nuclear masses M, M': $E(\alpha\mathbb{J};A) \longrightarrow E(\alpha\mathbb{J};A')$.

➢ Formal quantum notation: $\Delta E(\alpha\mathbb{J};A,A')/h = \frac{M'-M}{M\,M'}\,K^{(\mathrm{MS})} + F\,\delta\,\langle r^2\rangle \ldots$.

➢ Using JAC: Perform an `Atomic.Computation(.., properties=[Isotope, ..], configs=[..], isotopeSettings= IsotopeShift.Settings(..), ..)` with `calcLandeF=true` or call directly functions from the module `LandeZeeman`.

Motivation:

➢ Owing to the conservation of the total momentum, the (total non-relativistic) mass shift is a sum of two parts, the (so-called) normal mass shift (NMS) and the specific mass shift (SMS):

$$\mathbb{H}^{(\mathrm{MS,\,nr})} = \mathbb{H}^{(\mathrm{NMS,\,nr})} + \mathbb{H}^{(\mathrm{SMS,\,nr})} = \frac{1}{2\,M}\sum_j \mathbf{p}_j^2 + \frac{1}{2\,M}\sum_{i\neq j}\mathbf{p}_i\cdot\mathbf{p}_j$$

While the normal mass shift operator is obviously a one-particle operator, the specific mass shift is a two-particle operator. The sum of these two parts is known also as the total recoil operator within the nonrelativistic theory.

Relativistic recoil (Hamilton) operator:

➢ Recoil Hamiltonian: Within the lowest-order relativistic approximation ($\sim v^2/c^2$) and in first order of m/M, the recoil corrections are given by means of the (recoil) Hamiltonian:

$$\mathbb{H}^{(\mathrm{recoil})}(M) = \frac{1}{2\,M}\sum_{ij}\left[\mathbf{p}_i\cdot\mathbf{p}_j - \frac{\alpha\,Z}{r_i}\left(\boldsymbol{\alpha}_i + \frac{(\boldsymbol{\alpha}_i\cdot\mathbf{r}_i)\,\mathbf{r}_i}{r_i^2}\right)\cdot\mathbf{p}_j\right]$$

➢ The expectation value of $\mathbb{H}^{(\mathrm{recoil})}(M)$ with relativistic wave function from $\mathbb{H}^{(\mathrm{DCB})}$ gives the recoil correction to the energy of the atomic energy $|\alpha \mathbb{J}\rangle$ in first order of m/M .

➢ Decomposition of the relativistic recoil Hamiltonian: As in the non-relativistic theory, the (relativistic) recoil operator above can be written as (Tupitsyn *et al.*, 2003; Gaidamauskas *et al.*, 2011)

$$\begin{aligned}
\mathbb{H}^{(\mathrm{recoil})}(M) &= \mathbb{H}^{(\mathrm{NMS,\,relativistic})} + \mathbb{H}^{(\mathrm{SMS,\,relativistic})} \\
&= \frac{1}{2\,M}\sum_i \left[\mathbf{p}_i^2 - \frac{\alpha\,Z}{r_i}\left(\boldsymbol{\alpha}_i + \frac{(\boldsymbol{\alpha}_i\cdot\mathbf{r}_i)\,\mathbf{r}_i}{r_i^2}\right)\cdot\mathbf{p}_i\right] + \frac{1}{2\,M}\sum_{i\neq j}\left[\mathbf{p}_i\cdot\mathbf{p}_j - \frac{\alpha\,Z}{r_i}\left(\boldsymbol{\alpha}_i + \frac{(\boldsymbol{\alpha}_i\cdot\mathbf{r}_i)\,\mathbf{r}_i}{r_i^2}\right)\cdot\mathbf{p}_j\right] \\
&= \frac{1}{2\,M}\sum_i \left[\mathbf{p}_i^2 - \frac{\alpha\,Z}{r_i}\boldsymbol{\alpha}_i\cdot\mathbf{p}_i - \frac{\alpha\,Z}{r_i}(\boldsymbol{\alpha}_i\cdot\mathbb{C}_i^{(1)})\,\mathbb{C}_i^{(1)}\cdot\mathbf{p}_i\right] + \frac{1}{2\,M}\sum_i \left[\mathbf{p}_i\cdot\mathbf{p}_i - \frac{\alpha\,Z}{r_i}\boldsymbol{\alpha}_i\cdot\mathbf{p}_j - \frac{\alpha\,Z}{r_i}(\boldsymbol{\alpha}_i\cdot\mathbb{C}_i^{(1)})\,\mathbb{C}_i^{(1)}\cdot\mathbf{p}_j\right] \\
&= \mathbb{H}^{(\mathrm{NMS})} + \mathbb{H}^{(\mathrm{SMS,\,A})} + \mathbb{H}^{(\mathrm{SMS,\,B})} + \mathbb{H}^{(\mathrm{SMS,\,C})}
\end{aligned}$$

Reduced one-electron matrix elements of the recoil (Hamilton) operator:

➢ Recoil Hamiltonian: While the normal mass-shift Hamiltonian is a one-particle operator, the specific mass-sift is a (symmetric) two-particle operator

$$\mathbb{H}^{(\mathrm{NMS})} = \sum_j \mathbb{h}^{(\mathrm{NMS})}(\mathbf{r}_j), \qquad \mathbb{H}^{(\mathrm{SMS,\,k})} = \sum_{i\neq j}\mathbb{h}^{(\mathrm{SMS,\,k})}(\mathbf{r}_i,\mathbf{r}_j) = \sum_{i\neq j} g(r_i,k)\,g(r_j,k)\left(\mathbb{T}_i^{(1)}\cdot\mathbb{T}_j^{(1)}\right), \qquad k = A,B,C$$

The particular tensorial structure of the two-particle specific mass-shift Hamiltonian ensures that the reduced (one-electron) matrix elements can be expressed in terms of the first-rank effective interaction strength $X^{(1;\,\mathrm{SMS,\,k})}$ that are specified below for $k = A,B,C$.

Parametrization of the isotope shift:

➢ Mass shift of two isotopes: Within lowest order of m/M, the (isotope) mass shift for an atomic level $|\alpha\, \mathbb{J}\rangle$ is determined by the difference of the expectation values of $\mathbb{H}^{(\mathrm{recoil})}(M)$ for two different isotopes:

$$\Delta E^{(\mathrm{MS})}(M, M') = \left\langle \alpha\, \mathbb{J} \left| \mathbb{H}^{(\mathrm{recoil})}(M) - \mathbb{H}^{(\mathrm{recoil})}(M') \right| \alpha\, \mathbb{J} \right\rangle = \frac{M' - M}{M\, M'}\, K$$

$$\frac{K}{M} = \left\langle \alpha\, \mathbb{J} \left| \mathbb{H}^{(\mathrm{recoil})}(M) \right| \alpha\, \mathbb{J} \right\rangle = \left\langle \alpha\, \mathbb{J} \left\| \mathbb{H}^{(\mathrm{recoil})}(M) \right\| \alpha\, \mathbb{J} \right\rangle,$$

and where the Wigner-Eckardt is used here in a special form that is consistent with GRASP and that is required by the implementation of corresponding angular coefficients.

➢ In JAC, the mass-shift parameters $K^{(\mathrm{MS})} = K^{(\mathrm{NMS})} + K^{(\mathrm{SMS})}$ is calculated and tabulated for the reference nucleus with a Fermi distribution and given mass M.

➢ Field shift of two isotopes: is caused by their different nuclear charge distributions and can be parametrized by:

$$\Delta E^{(\mathrm{FS})}(M, M') = -\left\langle \alpha\, \mathbb{J} \left| \sum_{j=1}^{N} \left(\mathbb{V}^{(\mathrm{nuc})}(r_j; R') - \mathbb{V}^{(\mathrm{nuc})}(r_j; R) \right) \right| \alpha\, \mathbb{J} \right\rangle = \left\langle \alpha \mathbb{J} \left\| \sum_{j=1}^{N} \delta\, \mathbb{V}^{(\mathrm{nuc})}(r_j;\, R, R') \right\| \right\rangle = -F\, \delta \left\langle r^2 \right\rangle$$

$$F = \frac{\left\langle \alpha\, \mathbb{J} \left| \sum_j \left(\mathbb{V}^{(\mathrm{nuc})}(r_j; R') - \mathbb{V}^{(\mathrm{nuc})}(r_j; R) \right) \right| \alpha\, \mathbb{J} \right\rangle}{R' - R}$$

where $\delta \langle r^2 \rangle = R' - R$ is the difference of the *root-mean-square* (rms) charge radii of the two isotopes with masses M', M.

➢ The conversion factor between the mass-shift parameters $K^{(\mathrm{MS})}$ in the frequently applied units is: $K^{(\mathrm{MS})}/[\mathrm{GHz\,u}] = 3609.4824\, K^{(\mathrm{MS})}/[\mathrm{a.u.}]$.

6.2. In JAC partly-implemented level properties

6.2.a. Sensitivity of level energies with regard to variations of α (AlphaVariation)

Property & notations:

➢ Differential sensitivity parameter $\Delta q\,(\delta\alpha;\ \beta\mathbb{J})$ of an atomic level: For an atomic level $|\beta\mathbb{J}\rangle$, the level energy depends of course on the fine-structure constant α. Therefore, an energy shift arises for any variation $\delta\alpha = \alpha - \alpha_o$ of the fine-structure constant and for a non-zero differential sensitivity parameter $\Delta q\,(\delta\alpha;\ \beta\mathbb{J})$:

$$\Delta E(\delta\alpha;\ \beta\mathbb{J}) \;=\; \Delta q\,(\delta\alpha;\ \beta\mathbb{J}) \left[\left(\frac{\alpha}{\alpha_o} \right)^2 - 1 \right],$$

and where α_o is the (current) reference value.

➢ Formal quantum notation: $\Delta E(\delta\alpha;\ \beta\mathbb{J})$, $\Delta q\,(\delta\alpha;\ \beta\mathbb{J})$, $K(\beta\mathbb{J})$.

➢ Using JAC: Perform an `Atomic.Computation(.., properties=[AlphaVar, ..], configs=[..], alphaSettings= AlphaVariation.Settings(..), ..)` or call directly functions from the module `AlphaVariation`.

Motivation:

➢ Fine-structure constant α: The dimensionless constant α becomes dynamical, i.e. explicitly time-dependent, in a number of (quantum-field) theories that go beyond the standard model and general relativity.

➢ Search for variations of fundamental constants: This search is related also to several, so-far still unexplained phenomena of the Universe, such as the nature of dark matter.

Enhancement and sensitivity of atomic levels with regard to variations of $\delta\alpha$:

➢ Enhancement of energy shifts due to $\delta\alpha$ variations: The sensitivy of an atomic level energy $E(\beta\mathbb{J};\,\alpha)$ on $\delta\alpha$ can be re-written also in terms of the dimensionless enhancement factor $K = 2\,\Delta q/\,\Delta E$ as: in the form:

$$\frac{E(\beta\mathbb{J};\,\alpha) - E(\beta\mathbb{J};\,\alpha_o)}{E(\beta\mathbb{J};\,\alpha_o)} = K\,\frac{\alpha - \alpha_o}{\alpha_o} = K\,\frac{\delta\alpha}{\alpha_o}$$

6.2.b. Atomic form & scattering factors and scattering functions (FormFactor)

Property & notations:

➢ Form factor $F(q;\,\alpha\,\mathbb{J})$ of an atomic level with spherical-symmetric charge distribution:.

➢ Formal quantum notation: $F^{\,(\text{standard})}(q;\,\alpha\,\mathbb{J})$, $F^{\,(\text{modified})}(q;\,\alpha\,\mathbb{J})$.

➢ Using JAC: Perform an `Atomic.Computation(.., properties=[FormF, ..], configs=[..], formSettings= FormFactor.Settings(..), ..)` or call directly functions from the module `FormFactor`.

Motivation:

➢ Atomic form factor (known also as atomic scattering factor): Typically, such form factors are a measure of the (scattering) amplitude for the scattering of some incident quantum wave by an isolated and spherical symmetric atom.

➢ Therefore, the atomic form factor depends on the type of scattering, elastic or inelastic as well as incident radiation, such as photons, electrons or neutrons. As usual, We here consider the atomic form factor for photon (x-ray) scattering.

Definition of atomic form factors:

➢ Standard atomic form factor: For an atom in the level $|\alpha\, \mathbb{J}\rangle$ with a spherically-symmetric charge distribution $\rho(r)$, the standard atomic form factor is givenby

$$F^{\,(\text{standard})}(q;\, \alpha\, \mathbb{J}) \;=\; 4\pi \int dr\; r^2\; \rho(r)\; \frac{\sin(qr)}{q\, r} \;=\; \big\langle \alpha\, \mathbb{J} M \,\big|\, \mathbb{T}^{(1)}(\mathbf{q}) \,\big|\, \alpha\, \mathbb{J} M \big\rangle$$

is just equal to the Fourier transform of the charge density $\rho(r)$, if this density is normalized by $4\pi \int dr\, r^2 \rho(r) = N$ to the number of bound electrons.

Anomalous scattering factors g', g''

➢ Anomalous scattering factor: The real $g'(\omega)$ and imaginary $g''(\omega)$ anomalous scattering factors are frequently employed to express the coherent (Rayleigh) scattering factor $G(\omega)$, for incident photons with energy $\hbar\omega$.

➢ Rayleigh scattering factor For the photon energy $\hbar\omega$, the coherent (Rayleigh) scattering factor in forward direction can be written fas (Zhou *et al.*, 1990)

$$G(\omega) \;=\; F(0) \;+\; g'(\omega) \;+\; i\, g''(\omega)$$

where F is the atomic form factor. Therefore, the (Rayleigh) scattering factors can be readily defined with regard to the standard (atomic) form factor (FF) or with regard to the modified form factor (MFF).

Incoherent scattering function $S(\mathbf{q})$

➢ Incoherent scattering function: This scattering function can be expressed by means of the generalized atomic form factor

$$S(\mathbf{q}; \alpha_o \mathbb{J}_o M_o) \;=\; \sum_{e \neq o} |F^{\,(\text{generalized})}(q;\, \alpha_e \mathbb{J}_e M_e; \alpha_o \mathbb{J}_o M_o)|^2 \;=\; \big\langle \alpha_o \mathbb{J}_o \,\big|\, \mathbb{T}^{(2)}(\mathbf{q}) \,\big|\, \alpha_o \mathbb{J}_o \big\rangle \;-\; |F^{\,(\text{standard})}(q; \alpha_o \mathbb{J}_o)|^2 \,.$$

Here, the sum over e includes a summation over all discrete levels and the integration over the continuum. In the second expression, the two-electron momentum-transfer operator $\mathbb{T}^{(2)}(\mathbf{q}) = \sum_{m,n=1}^{N} \exp[i\, \mathbf{q} \cdot (\mathbf{r}_m - \mathbf{r}_n)]$ need to be applied, while then only matrix elements are necessary with regard to the ground state $|\alpha_o \mathbb{J}_o M_o\rangle$.

6.2.c. Level-dependent fluorescence an Auger yields (DecayYield)

Property & notations:

➢ Fluorescence *versus* Auger decay of an (excited) atomic level: $A^{q+*} \longrightarrow \begin{bmatrix} A^{q+(*)} + \hbar\omega \\ A^{(q+1)+(*)} + e_a^- \\ \ldots \end{bmatrix}$.

The corresponding fluorescence and Auger yields just describe the fraction (of atoms in a particular level or configuration) that decay by fluorescence or Auger electron emission.

➢ Formal quantum notation: $|\alpha \mathbb{J}\rangle \longrightarrow \begin{bmatrix} \{\, |\alpha_r \mathbb{J}_r\rangle + \hbar\omega\,(\{\mathbb{M}\})\,\} \\ \{\, |\alpha_a \mathbb{J}_a\rangle + |\varepsilon\,\kappa\rangle\,\} \\ \ldots \end{bmatrix}$.

➢ Using JAC: Perform an `Atomic.Computation(.., properties=[Yields, ..], configs=[..], yieldSettings= DecayYield.Settings(..), ..)` or call directly functions from the module `DecayYield`.

Motivation:

➢ Fluorescence yields $\omega(\alpha\mathbb{J})$: This yield typically represents the probability of an inner-shell (core) hole to be filled by some radiative decay process, in contrast and in competition with other nonradiative processes.

➢ Auger yields $a(\alpha\mathbb{J})$: This yield desribes the (complementary) probability for an inner-shell hole level to decay by an non-radiative process, hence: $\omega(\alpha\mathbb{J}) + a(\alpha\mathbb{J}) = 1$. The Auger yield is sometimes further partioned into an Auger and Coster-Kronig yield: $a(\alpha\mathbb{J}) = a^{(\text{Auger})}(\alpha\mathbb{J}) + a^{(\text{Coster-Kronig})}(\alpha\mathbb{J})$.

Fluorescence and Auger yields:

➢ More often than not, the fluorescence and Auger yields are determined for either K - and L -shell states (holes), and for which usually no distinction need to be made for different fine-structure levels $(\alpha\mathbb{J})$.

➢ Typically, it is completely sufficient to include only electric-dipole decay channels, although other multipoles can be defined explicitly in the computations.

6.2.d. Approximate many-electron Green function for atomic levels `(GreenFunction)`

Property & notations:

➢ Green function of an atomic level: .

➢ Formal quantum notation: .

➢ Using JAC: Perform an `Atomic.Computation(.., properties=[Greens, ..], configs=[..], greensSettings= GreensFunction.Settings(..), ..)` or call directly functions from the module `GreensFunction`.

Motivation:

➢ Greens functions of an atomic level $(\alpha \mathbb{J})$:

Approximate many-electron Green's function:

➢ ... can be obtained by

6.2.e. Multipole polarizibilities (MultipolePolarizibility)

Properties & notations:

- General multipole polarizibility of an atomic level: .
- Dynamic polarizibility of an atomic level: .
- Formal quantum notation: .
- Using JAC: Perform an `Atomic.Computation(.., properties=[Polarity, ..], configs=[..], polaritySettings= MultipolePolarizibility.Settings(..), ..)` or call directly functions from the module `MultipolePolarizibility`.

Motivation:

- Frequency-dependent (multipole) polarizibilities are important in various fields of physics.
- The ac Stark shift of a clock transition, for example, is determined by the frequency-dependent electric-dipole polarizibilities of the clock states. The (so-called) magic wavelengths of a clock transition can be determined by finding the frequencies where the ac electric-dipole polarizabilities of the two clocks states are the same.
- In JAC, we calculate and tabulate by default the scalar electric-dipole polarizibility for all selected levels.

Multipole polarizibilities:

- Multipole (ac 2^L-pole) polarizibility: of a level $|0\rangle$ is (Porsev *et al.*, 2018)

$$\alpha^{(\mathbb{M})}(\omega,\, \beta_o \mathbb{J}_o) \;=\; \frac{L+1}{L}\,\frac{2L+1}{[(2L+1)!!]^2}\,(\alpha\,\omega)^{2L-2}\,\sum_{\nu}\,\frac{(E_\nu - E_o)\,\left|\langle \alpha_\nu \mathbb{J}_\nu \,\|\, \mathbb{T}^{(\mathbb{M})} \,\|\, \beta_o \mathbb{J}_o\rangle\right|^2}{(E_\nu - E_o)^2 \;-\; \omega^2}$$

where $\mathbb{T}^{(\mathbb{M})}$ is the corresponding multipole operator for E1, M1, ... transitions.

Dynamic electric-dipole polarizibility:

➢ The (dynamic) electric-dipole polarizibility is defined as (Derivianko *et al.*, 1999)

$$\alpha^{(\mathrm{E1})}(i\,\omega,\ \beta_o \mathbb{J}_o) \ = \ \frac{2}{3} \sum_{\nu} \frac{E_\nu \ - \ E_o}{(E_\nu \ - \ E_o)^2 \ + \ \omega^2} \ |\langle \alpha\_nu \mathbb{J}_\nu \,|\, \mathbf{R} \,|\, \beta_o \mathbb{J}_o \rangle|^2$$

and which includes for $\alpha^{(\mathrm{E1})}(\omega \equiv 0)$ the static electric-dipole polarizibility.

Scalar and tensor polarizibility:

➢ The scalar polarizability of a level $\alpha\mathbb{J}$ in a light field at frequency ω can be expressed as the sum over intermediate states that are allowed by the electric-dipole selection rules (Safronova *et al.*, 2018)

$$\alpha_0(\omega) \ = \ \frac{2}{3\,(2J+1)} \sum_{k} \frac{(E_\nu \ - \ E_o)\ \langle \alpha_\nu \mathbb{J}_\nu \,\|\mathbb{D}\|\, \beta_o \mathbb{J}_o \rangle}{(E_\nu \ - \ E_o)^2 \ - \ \omega^2} \,,$$

and where the frequency ω of the incident light is assumed to be off resonance by at least several linewidths with regard to any of the intermediate levels $\{|\alpha_\nu \mathbb{J}_\nu\rangle\}$.

➢ The expression for the tensor polarizability has a similar structure.

6.2.f. Energy shifts in plasma environments (PlasmaShift)

Property & notations:

➢ Plasma shift of an atomic level: $E(\alpha\mathbb{J}) \ \longrightarrow \ E(\alpha\mathbb{J};\ \text{plasma model and parameters})$.

➢ Formal quantum notation: $\Delta\, E^{\,(\text{plasma})}(\alpha\mathbb{J}) \ = \ E(\alpha\mathbb{J};\ \text{plasma model and parameters}) \ - \ E(\alpha\mathbb{J};\ \text{unperturbed})$.

➢ Using JAC: Perform an `Atomic.Computation(.., properties=[Plasma, ..], configs=[..], plasmaSettings= PlasmaShift.Settings(..), ..)` or call directly functions from the module `PlasmaShift`.

Motivation:

➢ Plasma shift: high plasma densities can be expected to affect all atomic parameters, either by changing the atomic structures and associated rates, or by lowering the ionization potentials, increasing the importance of collisional processes.

➢ In JAC, the plasma shifts are calculated and tabulated for the Debye-Hückel plasma model for the plasma parameter $\lambda = 1$. Here, the Debye-Hückel interaction is treated only in first-order perturbation theory with the CI matrix.

Frequently applied plasma models in atomic structure calculations:

➢ Debye-Hückel model: This model has been commonly used in order to incorporate plasma effects into atomic structure calculations. However, the validity of this model is rather questionable because it is valid only when the *correlation* time of the ion is much longer than the lifetime of excited atomic states. Therefore, this perturbative approach is at best valid for weakly-coupled plasmas and should not be applied for modeling of high-density plasmas.

➢ In the Debye-Hückel model, the (pairwise) Coulomb interaction among the charged particles is modified for an ion with nuclear charge Z to

$$V^{(\mathrm{DH})}(r,\,\lambda) \;=\; -\sum_{i}^{N}\frac{Ze^{-\lambda r_i}}{r_i} + \sum_{i>j}^{N}\frac{e^{-\lambda r_{ij}}}{r_{ij}} \;=\; \sum_{i}^{N} V^{(\mathrm{e-n,\,DH})}(r_i,\,\lambda) \;+\; \sum_{i>j}^{N} V^{(\mathrm{e-e,\,DH})}(r_{ij},\,\lambda).$$

Here, N is the number of bound electrons in the ion, r_i is the distance of the i-th electron from the nucleus, and r_{ij} the distance between the electrons i and j.

➢ plasma screening parameter λ: This parameter is the inverse of the Debye shielding length for a certain plasma environment and can be expressed in terms of the electron density n_e and the temperature T_e of the plasma:

$$\lambda \;=\; \left[\frac{4\pi\, n_e}{k\, T_e}\right]^{\frac{1}{2}} .$$

➢ Ion-sphere model: In this model, the ion is typically enclosed in a spherically symmetric cell that contains the exact number of electrons in order to ensure neutrality. In the ion-sphere model, one needs to define an electron-density distribution that either obeys self-consistency equations or some simple hypothesis, such as an uniform density within the cell.

➢ In practice, the ion-sphere model has been extensively used only in its simplest form, in which the free-electron density exactly cancels the ion densities beyond the Wigner-Seitz sphere, i.e. beyond the ion-sphere radius. This refers to a completely neutral cell in which the free-electron density exactly cancels the ion density.

Free-electron distributions in plasma:

➢ The free-electron (radial) density $n_e(r)$ can follow different distributions:

➢ Maxwell-Boltzmann distribution: The Maxwell-Boltzmann statistics has been often applied to describe the free-electron distribution but is not well justified for high plasma densities or low plasma temperatures.

➢ Fermi-Dirac distribution: This distribution is preferable if the free electrons are degenerate

$$n_e(r) \;=\; \frac{4}{\sqrt{\pi}} \int_{x_o}^{\infty} dx \, \frac{\sqrt{x}}{e^{x \,-\, x_o \,-\, \mu/k\,T_e} \,+\, 1} \;=\; 2\,\lambda_{\rm th}^{-3}\,\mathcal{F}_{1/2}\left(-\frac{V(r)}{k\,T_e} \,+\, \frac{\mu}{k\,T_e}; \,-\frac{V(r)}{k\,T_e}\right) .$$

Here μ is the chemical potential of the plasma, $\mathcal{F}_{1/2}(x,y)$ the incomplete Fermi-Dirac integral and $\lambda_{\rm th} = \sqrt{2\pi \,/\, k\,T_e}$ the thermal de-Broglie thermal wavelength.

➢ Uniform electron-gas distribution: This distribution considers a sphere of radius $\mathbf{R}_0$ around the ion with N_b bound electrons , in which the the ionic charge is completely neutralized by the remaining $N_f = Z - N_b$ additional free electrons. Although all electrons inside of the sphere interact strongly with the embedded ion, the additional electrons are assumed to be distributed uniformly. For this assumption, the electrostatic potential for the i-th electron with radial coordinate r_i is given by

$$V^{\,(\rm IS)}(\mathbf{r}_i;\mathbf{R}_0) \;=\; \begin{cases} -\frac{Z}{\mathbf{r}_i} \,+\, \frac{Z-N_b}{2R_0}\left[3 - \left(\frac{\mathbf{r}_i}{\mathbf{R}_0}\right)^2\right] & \text{for} \quad \mathbf{r}_i \le \mathbf{R}_0 \\ 0 & \text{for} \quad \mathbf{r}_i > \mathbf{R}_0 \,. \end{cases}$$

In this potential above, the first term describes the interaction of the bound electron with the nucleus, while the second (repulsive) term arises from the plasma background and always causes a shift of all the level energies towards the continuum.

Gordon-Kim theory:

➢ In the Gordon-Kim theory (1972), the total energy of the system consists out of the direct Coulomb potential energy, the exchange Coulomb potential energy, the kinetic energy as well as the correlation energy. The direct Coulomb potential energy is calculated by integrating the Coulomb potential for the (apporximated) electron density, while the other contributions to the total energy are calculated by using a temperature-dependent local density functional (LDA) approach.

6.3. Further properties, not yet considered in JAC

6.3.a. Dispersion coefficients

Motivation:

➢ The long range interactions between the atoms and molecules play prominent roles in the low energy and low temperature collision experiments.

➢ The van der Waals coefficients C_6, C_8, C_{10} help describe the interaction of alkaline-earth metal dimers of two like atoms in their ground state.

Atom-wall coefficient, C_3:

➢ For an atom in a spherically-symmetric ground state $|\psi_o\rangle = |\beta_o \mathbb{J}_o M_o\rangle$, the dispersion coefficient C_3 of the Lennar-Jones interaction between an atom and a perfectly conducting wall is (Derivianko *et al.*, 1999)

$$C_3 = \frac{1}{4\pi}\int_0^\infty d\omega\ \alpha^{(\mathrm{E1})}(i\,\omega;\ \beta_o \mathbb{J}_o M_o) = \frac{1}{12}\,\langle \beta_o \mathbb{J}_o M_o \,|\, \mathbf{R}\cdot\mathbf{R} \,|\, \beta_o \mathbb{J}_o M_o\rangle\,, \qquad \mathbf{R} = \sum_{i=1}^{N} \mathbf{r}_i\,.$$

Van-der-Waals coefficient, C_6:

➢ For an atom in a spherically-symmetric ground state $|\psi_o\rangle \equiv |\beta_o \mathbb{J}_o M_o\rangle$, the dispersion coefficient C_6 of the Lennar-Jones interaction can be expressed as integral over the dynamic electric-dipole polarizibility (Derivianko *et al.*, 1999)

$$C_6 = \frac{3}{\pi}\int_0^\infty d\omega\,[\alpha^{(\mathrm{E1})}(i\,\omega;\,\beta_o \mathbb{J}_o M_o)]^2\,.$$

Long-range interaction of two atoms:

➢ For two atoms a and b in spherical-symmetric ground states, $|\psi_a\rangle = |\beta_a \mathbb{J}_a M_a\rangle$ and $|\psi_b\rangle = |\beta_b \mathbb{J}_b M_b\rangle$ the long-range interaction can be written as (Porsev and Derivianko, 2006)

$$V(R) = -\sum_{n=3}\frac{C_{2n}^{ab}}{R^{2n}}, \qquad C_{2n}^{ab} = \frac{(2n-2)!}{2\pi}\sum_{k=1}^{n-2}\frac{1}{(2k)!\,(2k')!}\int_0^\infty d\,\omega\,\alpha_k^{(\mathrm{E1})}(i\omega;\,\psi_a)\,\alpha_{k'}^{(\mathrm{E1})}(i\omega;\,\psi_b); \qquad k' = n-k-1$$

and where $\alpha_k^{(\mathrm{E1})}(i\omega;\,\psi_c)$ is the 2^k -pole dynamic (electric-dipole) polarizibility of the atom c in its state $|\alpha_c \mathbb{J}_c M_c\rangle$.

6.3.b. Stark shifts and ionization rates in static electric fields

Motivation:

➢ Different strong-field ionization mechanisms can be distinguished for different laser frequencies ω_L , (electric) field strength $E_o = |\mathbf{E}_o|$ as well as atomic ionization potentials I_p . They are often distinguished by the Keldish adiabacity parameter, $\gamma_K = \omega\sqrt{2\,I_p}/E_o$.

➢ Multiphoton regime, $\gamma_K \gg 1$: This regime is realized at high frequency and low or moderate field strength and gives rise to a a power law for the ionization rate, $\Gamma \propto E_o^n$.

Theoretical background:

➢ Complex-eigenvalue Schrödinger equation: The system 'neutral atom plus dc field' constitutes an electronic structure dependent many-electron problem ... Upon application of the field, the discrete spectrum changes into a resonance spectrum whose states correspond to the solutions of the complex-eigenvalue Schrödinger equation

$$(H - z_o)\psi = 0, \qquad H = H^{(\mathrm{atom})} + \sum_i \mathbf{F}\cdot\mathbf{r}_i, \qquad z_o = E_o + \Delta(F) - \frac{i}{2}\Gamma(F)$$

This equation can be solved in terms of function spaces which are square integrable, provided the transformation $\rho = r\,e^{i\,\theta}$ is applied. This coordinate rotation was used on the Hamiltonian operators for the computation of the LoSurdo-Stark ground-state resonance of hydrogen atoms and the solution was achieved by direct diagonalization of the non-Hermitian Hamiltonian on a large square-integrable basis set. However, for decaying states of many-electron systems, this brute-force diagonalization approach is unrealistic.

6.3.c. Dressed atomic (Floquet) states and quasi-energies in slowly varying laser fields

Motivation:

➢ For neither ultra-intense nor ultra-short laser pulses, these pulses can be modeled as a rapidly oscillating electric field with well-defined but with a slowly varying envelope (field amplitude). For such pulses, the behaviour of atoms can be described in terms of superpositions of dressed bound states that decay under the emission of photoelectrons.

➢ The dressed states of atoms in a field of constant intensity and frequency refer to particular quasistationary solutions of the time-dependent Schrödinger equation.

Dressed atomic states:

➢ Dressed atomic states: In a laser pulse of moderately varying intensity, the dressed states follow adiabatically the temporal evolution of the intensity during the passage of the pulse. The slow variation of the intensity then results into fairly slow changes in the (coefficients of the) superposition of the dressed states when compared with the optical period of the laser.

- Quasi-stationary wave function of dressed states: For sufficiently slow variations of the laser intensity, each dressed state can be written in the Floquet form, i.e. by means of a space-independent complex exponential *multiplied* by a time-harmonic function that oscillates with the same (optical) period as the incident field.
- Floquet equations: If the incident field is expanded in terms of a Fourier series, the time-dependent Schrödinger equation can be decomposed and re-written as a system of time-independent equations, the (so-called) Floquet equations. For multiphoton ionization, this system should be solved together with the radiation (Siegert) boundary conditions.
- The (complex) eigenvalues of the Floquet equations provide both, the quasienergies of the dressed states and the resonance poles of the scattering amplitudes for laser-assisted scattering.
- The Floquet approximation is typically adequate for infrared laser pulses as well as for atoms in either the ground or some Rydberg level. It may be inappropriate at laser frequencies in the UV region and for low-lying excited levels because of avoided crossings that occur between dressed levels and large non-ponderomotive ac Stark shifts at high frequencies.
- The computation of the widths of quasi-energies often requires to go beyond first-order perturbation theory.

6.3.d. Fano profiles of continuum-embedded resonances

Motivation:

- In physics, a Fano resonance is a type of resonant scattering phenomenon that gives rise to an asymmetric line-shape.
- The interference between a background and a resonant scattering process produces the asymmetric line-shape.

6.3.e. Light shifts

Motivation:

➢ The clock frequencies can be affected by (i) the thermal bath of blackbody radiation (BBR), (ii) the electric-quadrupole couplings of the ions with the trapping as well as with the residual electromagnetic fields, (iii) by ambient magnetic fields, or (iv) through various Stark shifts (Yudin *et al.*, 2014).

6.3.f. Black-body radiation shifts

Motivation:

➢ Update: The shift of a quantum energy level in an atom owing to the atom not residing in an environment at absolute zero temperature.

➢ Objects emit radiation whose wavelength depends on the object's temperature.

6.3.g. Hyperpolarizibility

Motivation:

➢ Wiki: The hyperpolarizability, a nonlinear-optical property of a molecule, is the second-order electric susceptibility per unit volume.

6.4. Other topics, related to atomic properties

6.4.a. Laser cooling, precision spectroscopy and quantum control

Quantum logic spectroscopy:

- Quantum logic is typically implemented by laser-induced coupling of the internal and external degrees of freedom of two ions, the spectroscopy and the logic one. By applying appropriate laser pulses, the information about the internal state of the spectroscopic ion can be transferred to the logic ion.
- Such a quantum-logical transfer scheme can be realized with two ions in a linear Paul trap.
- Many limitations of precision spectroscopy can be overcome by using simple quantum logic techniques that allow us to share properties between a spectroscopy and a logic ion. In this technique, the well-controllable logic ion provides sympathetic cooling, internal state preparation and detection of the ion with an interesting spectroscopic transition.
- From a simplified viewpoint, the logic ion can be viewed as both, a remote control and a sensitive quantum sensor for the internal and external state of the spectroscopy ion.

Precision spectroscopy:

- in 1995, a controlled-NOT (C-NOT) gate between a trapped atomic ion and its motional mode in the trap was experimentally realized. Since this first demonstration of coherent control over the internal and external degrees of freedom in an atomic system, quantum information processing with trapped ions has flourished, and several results, such as teleportation, error-correction and the implementation of the Deutsch-Jozsa and semi-classical Fourier transformation algorithms, have been achieved.

Further information:

- The development of laser cooling techniques made cold and ultra-cold atomic samples available for optical spectroscopy. This development allowed for long interrogation times and reduced Doppler shifts and gave eventually rise to an unprecedented uncertainty, exceeding one part in 10^{-15} in atomic clocks.
- Recently, an optical clock based on a forbidden transition in a single mercury ion has achieved an uncertainty of 7.2×10^{17}, thus exceeding the performance of the best cesium fountain standards.

➢ However these advances in precision spectroscopy were limited to atomic species that have not only an interesting spectroscopy transition, but also a suitable transition for cooling, detection and state preparation.

➢ For this reason, single ion optical clocks base on particularly interesting candidates, such as the isotopes of aluminum and boron have not been realized in the past.

6.4.b. Atomic clocks

Motivation:

➢ Recent developments in the set-up and control of optical atomic clocks has improved their precision by a factor of 1000 in less than two decades.

➢ Many clock applications are now in reach or are already realized by the improved precision and the high stability of thse clocks: (1) the study of many-body physics and quantum simulations; (2) relativistic geodesy; (3) very long baseline interferometry; (4) searches for the variation of the fundamental constants; (5) searches for dark matter candidates; (6) tests of the Lorentz invariance and several others. These and new ideas and applications, such as the use of atomic clocks for gravitational wave detection, will require even more precise clocks in the future.

Laser spectroscopy of trapped samples:

➢ Laser spectroscopy helped develop methods to simultaneously control both, the internal electronic and motional degrees of freedom of individual atoms, molecules and low-charge-state ions in traps with high accuracy.

➢ Most laser spectroscopy with trapped samples have explored a rather small class of atoms and atomic ions, including hydrogen, the alkali and alkaline-earth atoms and ions as well as few other species (Schmöger *et al.*, 2015). These atoms and ions have electronic transitions that are suited for laser cooling and that help localize the atoms for precision spectroscopy.

Further details:

➢ There are currently two types of optical atomic clocks under development, based on neutral atoms in optical lattices or based on a single trapped ion. For both types, a similar uncertainty have been reached, namely: 2.1×10^{18} for a Sr neutral atom clock (Nicholson *et al.*, 2015) and 3.2×10^{18} for a Yb^+ trapped ion clock (Huntemann *et al.*, 2016), operating on a particular electric-octupole (E3) transition.

➢ Proposals for a Yb clock: The $4f^{14}\,6s^2\ {}^1S_0 - 4f^{14}\,6s\,6p\ {}^3P_0$ transition can be induced in isotopes with nuclear spin $I \neq 0$ by hyperfine mixing and has served already as some frequency standard. However, neutral Yb has still another $4f^{14}\,6s\,6p\ {}^3P_0 - 4f^{13}\,6s^2\,5d\ (J = 2)$ (E2) transition at an easily accessible wavelength of 1695 nm, that might be suitable for the development of another frequency standard in this atom (Safronova *et al.*, 2018).

➢ ^{229m} Th clock: Thorium has one exceptional nuclear state that is known for the last 40 years and that has a very low energy of presumably below 10 eV. The currently assumed excitation energy of this isomeric state is 7.8 ± 0.5 eV, or correspondingly 159 ± 11 nm or ~ 1900 THz. This isomeric state conceptually allows for a direct laser excitation of the nucleus by using solid-state laser technology. This state has therefore been proposed for the development of a nuclear clock of extremely high stability owing to the expected high resilience against external influences and its radiative lifetime in the range of minutes to hours (von der Wense *et al.*, 2017)

6.4.c. Atom-atom and atom-ion interaction potentials

Motivation:

➢ sfmoKnowledge of the interatomic forces in (closed-shell) molecules is a key for understanding the behaviour of many systems, such as the geometry and stability of molecular solids, the properties of liquids and their phase transitions as well as collisions between molecules in gases or in molecular beams.

➢ While the theory of intermolecular forces has been developed over the last four decades, fast and reasonably reliable predictions are still often not available, especially if a whole range of intermolecular separations need to be considered.

Gordon-Kim (1972) theory for atom-atom interactions:

➢ Gordon and Kim (1972) developed a model to calculate the interactions between closed-shell atoms, ions and molecules. In this model, the electron density of the system is taken as the sum of the two separate densities, and the non-Coulombic part of the interaction potential is calculated from this density by using the electron-gas energy expression. .

➢ Assumptions of the Gordon-Kim theory: Three basic assumptions were made by Gordon and Kim (1972):

i) No rearrangement or distortion of the separate atomic densities occurs when the two atoms are brought together and, hence, the total electron density is just the sum of the two (spherically symmetric) atomic densities. This assumption neglects of course the rearrangement of electron density and, therefore, the theory to systems with a strong chemical bond, inlcuding covalent chemical bonds and for inter-atomic

distances smaller than about half of the equilibrium separation.

ii) The interatomic interaction can be evaluated from the combined atomic density, including the Coulomb interactions between all charges.

iii) Gordon and KimF applied originally Hartree-Fock wave-functions in order to obtain the electron densities of the separate atoms, although other, and perhaps more accurate, wave functions should work as well.

➢ Apart from the Coulomb interaction of the two (atomic) charge distributions, the kinetic, exchange and correlation energy contributions to the total interaction energy are obtained from the electron density and the free-electron gas approximation. f.

➢ The regions around the nuclei (in which the density varies rapidly) do overall not contribute much to the interaction energy, though it strongly affects the total energy. These contributions to the total energy cancel out if the atomic energies are substracted. Only the outer regions of the atoms, in which the atomic densities overlap, contribute significantly to the interaction energy. For these reasons, the uniform electron gas model should be reasonably accurate (Gordon and Kim, 1972).

Further information:

➢ Different regions of the molecular potential curves have been investigated by different theoretical methods. Perturbation theory has been applied, in particular, to describe the long-range attraction, and where the first- and second-order perturbation energies are often approximated by the first few terms in a multipole series expansion of the Coulombic interaction between the molecules.

➢ However, the perturbation method fails to desribe the potential at short and intermediate distances since it (i) does not include exchange interactions between the electrons, (ii) diverges for strong interatomic interactions, and (iii) because a multipole expansion generally fails when the electron distributions overlap.

➢ At intermediate distances, i.e. in the region of the minimum of the intermolecular potential, only SCF computations typically predict the potentials reasonably well if the molecule does not form strong chemical bonds.

6.4.d. Dispersive interactions in liquid and solids

Dispersive interactions in molecular-dynamics and Monte-Carlo simulations:

➢ Dispersive interactions: Dispersive forces and interactions in media often refer to contributions to the intermolecular interactions that arise from the polarization of one the atoms in the (fluctuating) instantaneous multipole field of other atoms. Therefore, dispersive interactions exist between each pair, triple, etc. of atoms or ions.

➢ Apart from inert-gas or crystallized solids of various organic molecules, the dispersive interactions are small, though not negligible. Reasonable estimates of the magnitude of the dispersion interaction are therefore necessary for many solid-state studies, such as the cohesion of matter, the behaviour of ionic crystals, for molecular liquids, the adsorption on surfaces or in porous media (Pellenq and Nicholson, 1998).

➢ In Monte Carlo and molecular dynamics simulations, for example, a reasonable accurate potential energy function is required and need to be based on quantum-mechanical estimates, even if the dynamics of the particles is described classically.

Two-body dispersive interactions:

➢ If we consider two interacting neutral atoms, time dependent perturbation theory gives rise to a long-range dispersive interaction due to charge fluctuations of the interacting species.

➢ Multipole expansion: For two spherically symmetric atoms or molecules A and B that are separated by a distance R, a multipole expansion is given by (Pellenq and Nicholson, 1998)

$$V^{(\text{dispersion,AB})}(R) = -\left[\frac{C_6}{R_6} + \frac{C_8}{R_8} + \frac{C_{10}}{R_{10}} + ...\right].$$

➢ In this expansion, the dispersion coefficient C_6 describes the interaction between two instantaneous dipoles, C_8 the interaction between a quadrupole and a dipole and C_{10} both, the interaction between an octopole and a dipole as well as between two quadrupoles.

Three-body dispersive interactions:

➢ In the multipole expansion, the terms with triplets of species A, B and C are obtained from perturbation theory at the third and fourth orders. For such a triplet, the total dispersion energy is however non-additive:

$$V^{(\text{dispersion})} = V^{(\text{dispersion, AB})} + V^{(\text{dispersion, BC})} + V^{(\text{dispersion, CA})} + V^{(\text{dispersion, ABC})} + ...$$

where $V^{(\text{dispersion, ABC})}$ represents a sum of several terms describing the three-body interaction.

6.4.e. Polarizibility and optical absorbance of nanoparticles

Motivation:

- ➢ Noble metal nanoparticles with a size comparable to the wavelength of the incident light show characteristic colors due to the strong absorption and scattering of light in the visible region.
- ➢ Localized surface plasmon resonance (LSPR). The LSPR are often explained as collective oscillation of free electrons in the nanoparticle that are induced by the electromagnetic waves. Therefore, the color of the absorbed light can be tuned by the size, shape, materials as well as the surrounding environment of the nanoparticles, and with applications in chemistry, physics and biomedical fields.
- ➢ Nanoparticles with a size below 10 nm have an extremely high surface-to-volume ratios and, thus, substantially different optical properties when compared to large nanoparticles or the bulk material. These optical properties also depend on the atomistic structure.

Methods for calculating the polarizibility of nanoparticles:

- ➢ The polarizability of a discretized medium is in general proportional to its volume.
- ➢ In a given nanoparticle, the polarizability of the i-th atom α_i can be approximated by multiplying the polarizability of the free atom $\alpha^{(\text{free})}$ with the relative volume (ratio), i.e. by dividing the effective volume $V^{(\text{eff})}$ by the volume of the free atom $V^{(\text{free})}$,

$$\alpha_i \;=\; \frac{V^{(\text{eff})}}{V^{(\text{free})}}\,\alpha^{(\text{free})} \;=\; \frac{V^{(\text{eff})}}{V^{(\text{free})}}\,\frac{e^2}{m}\sum_n \frac{f_n}{\omega_n^2 \,-\, \omega^2 \,-\, i\,\omega\,\delta}$$

  where ω_n is the n-th absorption frequency, f_n its oscillator strength and where the frequency shift δ depends on the coordination factor within the nanoparticle.

- ➢ The optical absorbance of the nanoparticle is obtained from the total polarizability by

$$\sigma^{(\text{absorption})} \;=\; \frac{4\pi\,\omega}{c}\,\Im\left\{\alpha^{(\text{total})}(\omega)\right\} \;=\; \frac{4\pi\,\omega}{c}\,\Im\left\{\sum_i^N \alpha_i^{(\text{SCF})}(\omega)\right\}$$

6.4.f. Equation-of-state relations for astro physics and condensed matter

Motivation:

- ➢ Equation of state: More often than not, the equation-of-state refers to the pressure-density of pressure-temperature relation for matter under (more or less) extreme conditions.
- ➢ When the atomic density is rather low, we can deal with isolated atoms that are in equilibrium with free electrons, while the statistical or Thomas-Fermi-Dirac has been found useful for a very high density.

Liberman's self-consistent model:

- ➢ Liberman (1979) describes a model for condensed matter in which the ions surrounding a particular atom are replaced by a positive charge distribution which is constant outside of a sphere containing the atom and zero inside. This models enables one to separate the quantities pertaining to the atom from those of the electron gas, in which it is imbedded, and hence to derive the desired equation-of-state data.
- ➢ Instead of a polyhedral cell, which are surrounded by other identical cells, a nearly equivalent spherical cell is assumed in Liberman's model, and surrounded by a uniform electron gas. The density of this electron gas as the mean density of ionic charges. Therefore, the electron gas outside will not alter the charge distribution inside the cell if its density is correctly chosen nor will the atom affect the electron gas.

6.4.g. Average-atom model for warm-dense matter

Motivation:

- ➢ Studies on the electronic structure of impurities within an electron gas have been performed in the literature as function of their density and temperature. For these investigations, one need to know the dependence of screening effects on the plasma parameters.
- ➢ At low temperatures and metallic densities, especially, the electron density often exhibits Friedel oscillations as known also from solid-state physics.

Warm-dense matter:

➢ Warm-dense matter (WDM): This term generally refers generally to some state of matter for plasma conditions that range between those of condensed matter and weakly coupled plasmas, and with typical temperatures from a few to a few hundred eV as well as densities from a few hundredths to about a hundred times of the solid density.

➢ A good understanding of the properties and behaviour of WDM, such as the equation of state, its radiation opacity, or transport properties, has been found important, for example, for modeling astrophysical objects or inertial confinement fusion experiments (Hou *et al.*, 2015).

Average-atom model:

➢ Average-atom (AA) model: This model divides the plasma into separate neutral Wigner-Seitz cells with a nucleus of charge Z and Z free electrons. Various versions of the AA model have been implemented in plasma physics for describing warm and hot dense plasma.

➢ For an isolated atom or ion, the electron density is calculated in the AA model in order to include the level broadening of the energy levels within a plasma environment. This density is applied also for studying the temperature and density effects upon the electron distributions within a statistical way.

Spectral emission from plasma in a non-local thermodynamic equilibirum:

➢ In a non-LTE (NLTE), in which the levels of each configuration are in LTE among each other, the population N_a of a given configuation is a solution of a system of rate equations

$$\frac{\partial N_a}{\partial t} = -N_a \sum_b R_{ab} + \sum_b R_{ba} N_b$$

where R_{ab} is a global transition rate that connects the configurations a and b. The rate equations includes the sum of all rates for the most important collisional and radiative processes. More precisely, $R_{ab} = \sum_p T_{ab}^{(p)}$, where for a specific process p, $T_{ab}^{(p)}$ is averaged over the initial levels of configuration a and summed over all final levels of configuation b

$$T_{ab}^{(p)} = \frac{1}{g_a} \sum_{i\in a,\, j\in b} T_{ij}^{(p)}$$

and where g_a is the statistical weight of configuration a. The direct extension of the UTA approach to a NLTE context is to evaluate the rates $T_{ab}^{(p)}$ without the explicit computation of all rates $T_{ij}^{[p]}$ between detailed levels.

6.4.h. Atomic partition functions

Motivation:

➢ The atomic partition function U(T)defined as

where the sum is taken over all bound levels. Unlike the transition parameters, information about partition functions for atoms and ions is spread throughout the literature.

6.4.i. Radial distribution functions for plasma and liquid models

Motivation:

➢ The radial distribution function for a plasma is often calculated. In these computations, quantum effects need to be taken into account for small inter-particle separations, either by using a modified path-integral technique or, equivalently, by a summation over states, together with the assumption that the charged particles interact via a shielded Coulomb potential.

➢ General expressions for the radial distribution functions in an electron-ion plasma outside of an thermal equilibrium have been obtained in the literature in first-order of the plasma parameter.

Quantal hypernetted-chain approximation:

➢ In statistical mechanics, the hypernetted-chain equation arises as a closure relation in order to solve the OrnsteinZernike equation, i.e. a relation between the direct and total correlation functions. The hypernetted-chain equation is commonly applied in fluid theory to obtain, e.g. expressions for the radial distribution function.

➢ The hypernetted chain approximation is an integral-equation method from statistical physics that arose from the theory of liquids.

6.4.j. Laser-produced plasma

Motivation:

- ➢ Laser-produced plasmas have been proposed as source of both, x-rays and multiply-charged ions. Whereas x-ray sources aim for a high radiation loss from the plasma due to the generation of highly stripped atoms, higher charge states of ions are mainly produced by a high plasma temperatur and a low radiation level (loss).
- ➢ To determine the properties, such as temperature and density, of a laser-produced plasma and, hence, its radiation emission, one needs a proper model for the coupling of the laser light with the heavy element (solid-state) target.

Ultrafast x-ray pulses from laser-produced plasma:

- ➢ A high-temperature plasma is created when an intense laser pulse is focused onto the surface of a solid (Murnane *et al.*, 1991). From such a plasma, an ultrafast pulse of x-ray radiation is emitted when the laser pulse length is less than about a picosecond.
- ➢ The emitted x-rays from such a laser-produced plasma are incoherent but have high brightness because of the small size, short lifetime and the high temperature of the radiating plasma. X-ray pulses with a duration of a picosecond or less have been observed, more than an order of magnitude shorter than those produced by any other x-ray source.
- ➢ In such plasma, hot electrons can subsequently ionize the much cooler atoms, forming an x-ray-emitting, high-temperature plasma spark at the surface of the solid (Murnane *et al.*, 1991).
- ➢ Laser-produced plasmas (LPP) have attracted recent interest because of their use in developing laboratory ion sources and pulsed light sources at short wavelengths.
- ➢ LPP will find applications in extreme ultraviolet (EUV) lithography, EUV metrology as well as in the modification of surfaces.

Scaling laws for laser-produced plasma:

- ➢ Scaling laws predict that brighter and more efficient x-ray sources will be obtained by the use of more intense laser pulses. These sources can be used for time-resolved x-ray scattering studies and for the development of x-ray lasers.
- ➢ Simple arguments can be used to derive scaling laws that predict the response of the plasma if the laser parameters are varied. If we neglect any hydrodynamic expansion during the excitation pulse, we can equate the incident heating flux to the cooling flux due to classical thermal conduction. Expressions for the electron temperature then given by $T\,[\mathrm{eV}] = 68.5\,\tau^{2/9}\,I^{4/9}$ and for heat-front penetration scale length

K [nm] $=$ 710 $\tau^{7/9}\, I^{5/9}\, / Z^*$ in terms of the laser pulse lengths τ [in units of 100 fs] and the absorbed power irrediance I [in units of 10^{16} W / cm^2], and where Z^* denotes the ionization stage. If the laser pulse has terminated, hydrodynamic cooling begins to dominate, and we have then T [eV] $\propto E^{2/3}\, / t^{2/3}$ and L [nm] $\propto E^{1/3}\, t^{2/3}$, with $E = I\, \tau$ being the absorbed energy [in J cm^{-2}].

Ionization model:

- Collisional-radiative ionization model: Such a model can be applied to laser-produced plasmas with temperatures above a few tens of eV. At these temperatures, the average state A^{q+} of a given ion is dominated by the electron plasma temperature due to electron and photon-impact excitation and ionization processes.
- Indeed, two main types of excitation and ionization processes occur in such plasma: collisional and radiative processes, and where the corresponding de-excitation and recombination arise from the same types of processes. The ionization-recombination equations for both processes are:

$$A^{(q-1)+} + e^- \longleftrightarrow A^{q+} + e_1^- + e_2^-, \qquad A^{(q-1)+} + \hbar\,\omega \longleftrightarrow A^{q+} + e_p^-.$$

- In these ionization-recombination equations, one often only considers collisions with electrons since they are much more efficient than those with heavier particles. Obviously, these equations also neglect autoionization and the (inverse) dielectronic recombination.

Deflagration model for laser-produced plasma:

- The radiative deflagration (model) describes the rapid interaction of the laser radiation by a very thin layer near to the target surface and at the (so-called) cut-off electron density $n^{(\mathrm{cut-off})} = 10^{21}\, / \lambda^2\, [\mu\,\mathrm{m}]$. Such a rapid interaction leads to a hot plasma that expands toward the incident laser light into the vacuum and that, *vice versa,* results in a shock wave into the solid due to momentum conservation.
- The properties of such a hot plasma can then be determined mainly by the power density in the focal zone and the wavelength of the radiation.

6.4.k. Plasma diagnostics

Motivation:

➢ The detailed interpretation of the spectra from laboratory plasmas and astrophysical sources has been found a challenging problem since it often requires to go beyond a local thermodynamical equilibrium (LTE) approach. Then, the solution of the rate equations require to take into account the photon emission and absorption throughout the emitting medium.

Diagnostics of astrophysical plasma:

➢ Hot plasmas are present in the universe in a variety of astrophysical systems, from stellar coronae to the intergalactic medium in clusters of galaxies. The good quality data obtained in the last few decades and up to date from space observatories like EINSTEIN, ROSAT, ASCA and SAX allowed to study in many details the physical condition of several astrophysical plasmas.

➢ To determine the relevant physical parameters describing both astrophysical plasmas and laboratory plasmas, i.e. electron temperature, density distribution, ion and element abundances, we need to compare observed data with a theoretical spectral model.

➢ The solar corona plasma is low-density plasma and believed to be dominated by the spontaneous decay and radiative recombination. For these two processes, the rates are much higher than collisional decay and three-body recombination and, hence, plasma is not in a local thermodynamic equilibrium and cannot be described by Saha or Boltzmann equations.

➢ In general, collisions between particles cause energy exchange and changes in the state distribution changes.

➢ Standard models of static stellar atmospheres lead to a self-consistent calculation, where the atomic (or ionic) populations, the radiative field, the temperature, and density are obtained through the rate equation system and radiative transfer equation with some constraints such as statistical equilib- rium, radiative equilibrium, and hydrostatic equilibrium.

Diagnostics of laboratory plasma:

➢ For ITER, various concepts have developed to reduce the peak heat at the plasma-facing components of the tokamak. Indeed, much of the experimental and theoretical work in fusion research focus on the question of how to transfer the heat from the plasma to the wall of the main and divertor chambers.

➢ To analyse this heat transfer and to enroll the relative importance of the primary atomic processes, simple quasi-analytic models and refined rate coefficients and cross sections have been utilized. Important processes refer to the radiation losses through bremsstrahlung, impurity

radiation losses from the plasma edge, the charge exchange and hydrogen radiation losses from outer layer as well as impurity radiation losses from the divertor plasma.

Laboratory *versus* astrophysical plasma:

- ➢ Laboratory plasmas can differ from astrophysical sources in various ways.
- ➢ Laboratory plasmas can be short lived so that they do not reach statistical equilibrium.
- ➢ Even if often much larger density occur in laboratory plasma, when compared to typical astrophysical sources, not all lines are optically thick and, in partiular, the ree-bound and free-free transitions (continuum radiation) is usually optically thin.

Atomic physics of tungsten:

- ➢ Atomic physics has been crucial for understanding the plasma energy balance and for diagnostic development. In particular, tungsten is used on present-day tokamaks in preparation for ITER.
- ➢ Tungsten has become of high importance since it will be a constituent of ITER plasmas as it is applied as a plasma-facing component able to withstand high heat loads and with a lower tritium retention than other possible materials.
- ➢ The ITER Core Imaging X-ray Spectrometer (CIXS) has been designed to measure the ion temperature and bulk plasma motion of ITERs plasma core, based especially on the x-ray emission of neon-like W^{64+} ions (Beiersdorfer *et al.*, 2015). The emission from tungsten will be measured by extreme ultraviolet (EUV) and optical spectrometers to determine its concentration in the plasma and to assess power loss and the tungsten sputtering rate.

Atomic physics of lanthanide ions:

- ➢ The radiative properties of lanthanide ions have numerous applications in solid-state laser materials, photonics and the lighting industry. Radiative transitions were observed in doped crystals and in solution with small shifts relative to those of the free ions.
- ➢ Suzuki *et al.* (2018) have systematically observed extreme ultraviolet (EUV) spectra from highly charged ions of nine lanthanide elements with atomic numbers from 60–70 in optically thin plasmas produced in the Large Helical Device (LHD). The wavelengths of the main peaks in the quasicontinuum features agree well previously measured singlet transitions of Pd-like ions as well as with the discrete spectral lines from Cu-like and Ag-like ions.

➢ The bright emission spectra from highly charged ions of lanthanide elements ($Z = 57-71$) are known to appear in the extreme ultraviolet (EUV) or soft X-ray wavelength range due to $n = 4-4$ transitions of lanthanide ions in the wavelength range of 5-12 nm. These emission spectra are strongly affected by relativistic effects and multi-electron correlations. Possibly, these emission spectra will play an important role in application to the next generation light sources for EUV lithography.

➢ In astrophysics, observationos with the Hubble Space Telescope of spectra of chemically peculiar stars have proven the presence of lanthanide ions up to doubly-charged stages. More recently, simultaneously observed emissions of electromagnetic waves and gravitational waves during two neutron stars merging increased the interest for radiative properties of higher-charged lanthanide ions.

➢ The overall uncertainty on the measured wavelengths varied between $\pm 0.003 .. 0.005$ Å. An analysis of these spectra, based on the Ritz combination principle, gives then rise to the energy levels by applying a least-squares fit in order to minimize the differences between the experimental wavenumbers and the calculated (Ritz) wavenumbers (Tchang-Brillet *et al.*, 2018).

6.4.I. Radiation damage of DNA by electron impact

Motivation:

➢ Radiation damage: This term often refers to the damage of biological material on rather short time scales, i.e. reactions and processes that occur within ns oreven less following the interaction of a high energy quantum with a living cell. These initial events may ultimately lead to the collapse of such cells, resulting in death of the individual within hours or days but may affect the matter also on much longer time scales.

➢ In contrast, an alteration of the genetic expression of DNA may cause the onset of some diseases.

➢ The absorption of high-energetic photons by biological matter often leads to low-energy electrons (LEE) that interact with the DNA. These LEE can cause specific resonant processes and may lead eventually either single or double strand breaks in DNA materials, to the damage of its molecular components and possibly to biological apoptosis (Bacarelli *et al.*, 2011).

➢ Several theoretical and computational approaches have been developed for studying the molecular processes that occur in the various steps of the energy deposition by LEE.

Electron-molecule dynamics:

➢ To understand the electron-impact of bio-molecules, a quite sizeable computational machinery need to be developed. The multiple inelastic scattering of these electrons will result in a re-distribution in the energy content and may lead to a fragmentation as well as the excitation of various vibrational modes.

6.4.m. Transport coefficients for ion mobility and diffusion in gases

Transport coefficients in gases:

➢ Ion-mobility spectrometry (IMS): This spectrometry is an analytical technique used to separate and identify ionized molecules in the gas phase based on their mobility within a a carrier buffer gas.

➢ IMS has been heavily employed for military or security purposes, such as detecting drugs and explosives, but also for the analysis of both small and large biomolecules.

➢ Ion mobility K: The ion mobility is defined as the proportionality factor between the drift velocity v_d of the ions and the applied electric field E : $v_d = K\,E$. These ion mobilities are usually reported as reduced mobilities for a standard gas density n_0 , i.e. for standard temperature $T = 273$ K and pressure $p_o = 1013$ hPa.

➢ Since this reduced ion mobility just refers to the standard density, it is still temperature dependent $K_o = K\,\frac{n}{n_o} == K\,\frac{T_o}{T}\,\frac{p}{p_o}$.

6.4.n. Exotic atoms and ions

Muonic atoms and ions:

➢ Muonic hydrogen: In muonic hydrogen, the electron is replaced by its 200 times heavier muon μ. Its larger mass results in a much about 200 times closer, when compared to the electron in regular hydrogen.

➢ Because of the finite extent of the proton, muons in their s-state have some probability to be inside the proton, and where it sees a slightly reduced electric charge of the proton. Therefore, the muon is less bound as larger proton is.

➢ Measurements of the transition energies in muonic atoms help determine nuclear parameters, such as charge radii, quadrupole moments and magnetic hyperfine constants. One of the most precise measurements of the nuclear root-mean-square radius by means of muonic atoms refer to the radius of ^{208}Pb at the 0.2 % level.

7. Atomic processes

7.1. In JAC implemented processes

7.1.a. Photo-emission. Transition probabilities (Radiative)

Process & notations:

- Photon emission: from an atom or ion $A^* \longrightarrow A^{(*)} + \hbar\omega$
- Formal quantum notation: $|\alpha_i \mathbb{J}_i\rangle \longrightarrow |\alpha_f \mathbb{J}_f\rangle + \hbar\omega$
- JAC's standard multipole amplitudes for photon emission: Although all (one- and many-electron) electron-photon interaction matrix elements are always evaluated in *absorption* within JAC, we wish to retain the intuitive description of matrix elements as typically applied in quantum mechanics: $\langle \text{final} - \text{state} \,|\, \text{operator} \,|\, \text{initial} - \text{state} \rangle$. We here therefore introduce an explicit notation for a *standard (reduced, JAC) emission as well as absorption multipole matrix element*

$$\langle \alpha_f \mathbb{J}_f \,\|\mathbb{O}^{(\mathbb{M},\,\text{emission})}\|\, \alpha_i \mathbb{J}_i \rangle \;=\; \left\langle \alpha_i \mathbb{J}_i \left\| \sum_{k=1}^{N} \boldsymbol{\alpha}_k \, a^{p}_{k,\,L} \right\| \alpha_f \mathbb{J}_f \right\rangle^{*} \;\equiv\; \langle \alpha_i \mathbb{J}_i \,\|\mathbb{O}^{(\mathbb{M},\,absorption)}\|\, \alpha_f \mathbb{J}_f \rangle^{*}$$

  which retains the right order and can be obtained from `Jac.Radiative.amplitude()`; cf. section 4.3.b. A multipole $\mathbb{M} \equiv (L, p) =$ E1, M1, E2, ... hereby contains all information about its multipolarity (angular momentum) L and type *magnetic* $(p = 0)$ or *electric* $(p = 1)$.
- Using JAC: Perform an `Atomic.Computation(.., process=Jac.RadiativeX, processSettings=Radiative.Settings(..), ..)` or call directly functions from the module `Radiative`.

Transition probabilities:

➢ With the notation of the (standard reduced, JAC) emission multipole matrix element from above, the transition probability is given by

$$W_{i\to f} \;=\; \frac{8\pi\,\alpha\,\omega}{2J_i+1}\,\sum_{\mathbb{M}}\,\left|\left\langle \alpha_f \mathbb{J}_f \left\| \mathbb{O}^{(\mathbb{M},\,\mathrm{emission})} \right\| \alpha_i \mathbb{J}_i \right\rangle\right|^2$$

and where the sum over $\mathbb{M}$ = E1, M1, E2, ... runs over all requested multipoles for a given computation.

➢ In JAC, the transition probabilities and radiative lifetimes are tabulated by default for all selected transitions $i \to f$.

Angular distribution and anisotropy (structure) parameters of the fluorescence radiation:

➢ The fluorescecne (radiation) from an excited atom is characterized not only by its frequency $\hbar\omega$ but also by the angular distribution and polarization of the emitted radiation. Both of these properties of the emitted photons depend on the sublevel occupation of the excited atom or ion and, hence, on its reduced statistical tensors $\mathcal{A}_{kq}(\alpha_i \mathbb{J}_i)$ which are associated with the prior excitation process.

➢ Angular distribution: For initially unpolarized but aligned atoms, the angular distribution of the (characteristic) fluorescence radiation is given in perturbation theory by:

$$W(\vartheta) \;=\; \frac{W_o}{4\pi}\left(1+\sum_{k=2,4,..} f_k(\alpha_i\mathbb{J}_i,\alpha_f\mathbb{J}_f)\,\mathcal{A}_{k0}(\alpha_i\mathbb{J}_i)\,P_k(cos\vartheta)\right)\,,$$

where W_o is the total decay rate and ϑ the angle of the photons with regard to the alignment axis (quantization axis).

Line strength:

➢ Conversion between gA [1/s] and S: For wavelengths λ [Å] (NIST Atomic Spectra Database)

$$S \;=\; 3.707342\,\times\,10^{-14}\,\lambda^3\,g\,A \qquad \text{(M1)}$$

$$S \;=\; 8.928970\,\times\,10^{-19}\,\lambda^5\,g\,A \qquad \text{(M1)}$$

Semi-empirical calculations of transition probabilities:

- Semi-empirical calculations of transition probabilities are often performed by using Cowan's code and, especially, the components RCN/RCN2/RCG/RCE. In a first step, Hartree-Fock calculations of radial integrals are carried out, including relativistic corrections (HFR) to generate all required atomic orbitals and average energies of configurations. The diagonalization of the Hamiltonian matrix then leads to approximate energy values and eigenvectors of levels in intermediate coupling.
- When, in addition, also experimental energies are available, RCE is run to perform an iterative least-squares fit and to minimizing the differences between the calculated and experimental energies, where the radial integrals are applied as fitted parameters. The mean error of such a fit is defined by $\Delta E = \sqrt{\sum_i \left(E_i^{(\mathrm{exp})} - E_i^{(\mathrm{calc})}\right)^2 / (N_i - N_p)}$ where N_i is the number of experimentally known energies and N_p the number of free parameters.
- In order to avoid a too large a number of free parameters, further constraints on parameters can be introduced by fixing their values or by fixing their ratios to their HFR values. After convergence, the final arameters were used in a final diagonalization, providing the best predictions for the unknown energy levels. The corresponding level compositions in the intermediate coupling scheme are used for the calculations of the Land factors and the radiative transition probabilities.

Unresolved transition arrays (UTA):

- Unresolved transition arrays: The UTA approach has become the method of choice to calculate the radiative properties of higher Z elements. Within this approach, a group of lines (i.e. a so-called array) which belongs to the same pair of electron configurations are treated globally by a Gaussian distributions whose width and position are given by analytical formulae.
- The UTA approach is computationally efficient and accurate for plasma conditions where the line broadening is such that individual line profiles merge. This approach has been further extended to a group of arrays in the so-called super-transition array method (STA) where set of arrays are treated globally.
- Resolved transition arrays (RTA): The RTA method was proposed to overcome the shortcoming of the UTA method that just a few transitions often dominate the spectral emission distribution of the array. This RTA method improves on the UTA approach by resolving the transition array into individual lines by using random lines but without performing an explicit atomic structure calculation.

➢ UTA method: For a group of lines with known transition energies E_i and corresponding the oscillator strengths g_i, the UTA is obtained by calculating the first two moments for the array of N transitions:

$$\mu^{(1)} = \frac{\sum_i^N g_i E_i}{\sum_i g_i}, \qquad \mu^{(2)} = \frac{\sum_i^N g_i E_i^2}{\sum_i g_i},$$

➢ These two moments can be utilized together with the variance $\sigma^2 = \mu^{(2)} - \left(\mu^{(1)}\right)^2$ in order to define the spectral distribution of the UTA

$$f(\rceil) = \frac{1}{\sigma\sqrt{\pi}} \exp\left[-\frac{(\rceil - \mu^1)^2}{2\sigma^2}\right].$$

➢ By avoiding the explicit calculation of the properties of each line, that belongs to a given array, the UTA method enables one to account for a large number of transitions for a rather low computational cost.

Two-electron one-photon transitions (TEOP):

➢ Two-electron one-photon transitions were postulated almost 100 years ago and are well-known from the optical region.

➢ In the early 1970s, Wölfli *et al.*. reported results for nickel and iron for which high-energetic satellites arose due to two-electron one-photon transition, where two vacancies in the K-shell were simultaneously filled by two L-shell electrons under the emission of s single photon.

➢ Since the interaction with the electromagnetic field is governed by an one-electron operator, however, the contribution of two-electron one-photon (TEOP) transitions can usually be ignored in comparison to other, allowed one-electron transitions.

7.1.b. Photo-excitation (PhotoExcitation)

Process & notations:

- Photo-excitation of an atom or ion: $A + \hbar\omega \longrightarrow A^*$
- Formal quantum notation: $|\alpha_i \mathbb{J}_i\rangle + \hbar\omega\,(\mathbf{k},\lambda) \longrightarrow |\alpha_f \mathbb{J}_f\rangle\,.$
- Using JAC: Perform an `Atomic.Computation(.., process=Jac.PhotoExc, processSettings=PhotoExcitation.Settings(..), ..)` or call directly functions from the module `PhotoExcitation`.

Photoexcitation cross sections:

- Total photoabsorption cross section: For initially unpolarized atoms and incident photons with given (photon) density matrix $\langle \mathbf{k}\lambda \,|\, \rho_\gamma \,|\, \mathbf{k}\lambda'\rangle$, the total photoabsorption cross section can be most easily defined in the limit of the *zero* linewidths as

$$\sigma(\alpha_i \mathbb{J}_i \to \alpha_f \mathbb{J}_f;\, \omega) = \frac{4\pi^2\alpha}{\omega\,(2J_i+1)} \sum_{M_i M_f,\, \lambda\lambda'} \langle \mathbf{k}\lambda \,|\, \rho_\gamma \,|\, \mathbf{k}\lambda'\rangle \,\big\langle \alpha_f\, \mathbb{J}_f M_f \,\big|\, \mathbb{T}^{\,(\text{absorption})}(\mathbf{k},\lambda) \,\big|\, \alpha_i\, \mathbb{J}_i M_i \big\rangle$$
$$\times \,\big\langle \alpha_f\, \mathbb{J}_f M_f \,\big|\, \mathbb{T}^{\,(\text{absorption})}(\mathbf{k},\lambda') \,\big|\, \alpha_i\, \mathbb{J}_i M_i \big\rangle^*\, \delta(\omega + E_i - E_f)\,,$$

  and where $\mathbb{T}^{\,(\text{absorption})}(\mathbf{k},\lambda)$ formally describes the electron-photon interaction operator for absorbing a photon $\hbar\omega\,(\mathbf{k},\lambda)\,.$

- In order to allow for a finite natural width Γ_f of the excited level, we need to replace the $\delta(\omega + E_i - E_f)$ function in the above expression by a (Lorentzian) spectral distribution

$$\sigma(\alpha_i \mathbb{J}_i \to \alpha_f \mathbb{J}_f;\, \omega) = \frac{4\pi^2\alpha}{\omega\,(2J_i+1)} \sum_{M_i M_f,\, \lambda\lambda'} \langle \mathbf{k}\lambda \,|\, \rho_\gamma \,|\, \mathbf{k}\lambda'\rangle \,\big\langle \alpha_f\, \mathbb{J}_f M_f \,\big|\, \mathbb{T}^{\,(\text{absorption})}(\mathbf{k},\lambda) \,\big|\, \alpha_i\, \mathbb{J}_i M_i \big\rangle$$
$$\times \,\big\langle \alpha_f\, \mathbb{J}_f M_f \,\big|\, \mathbb{T}^{\,(\text{absorption})}(\mathbf{k},\lambda') \,\big|\, \alpha_i\, \mathbb{J}_i M_i \big\rangle^* \;\; \frac{1}{\pi}\, \frac{\Gamma_f/2}{(\omega + E_i - E_f)^2 + \Gamma_f^2/4}$$

➢ Photoexcitation cross sections for initially unpolarized atoms: For incident plane-wave photons with (photon) density matrix $(c_{\lambda\lambda'}) = \frac{1}{2}\begin{pmatrix} 1+P_3 & P_1-iP_2 \\ P_1+iP_2 & 1-P_3 \end{pmatrix}$, which are resonant to the given transition $|\alpha_i \mathbb{J}_i\rangle \to |\alpha_f \mathbb{J}_f\rangle$, the total photoexcitation cross section is

$$\sigma(\alpha_i \mathbb{J}_i \to \alpha_f \mathbb{J}_f;\, \omega) = \frac{2\pi^3\alpha}{\omega\,(2J_i+1)} \sum_{\mathbb{M},\,\lambda} c_{\lambda\lambda} \left|\left\langle \alpha_f\, \mathbb{J}_f \left\| \mathbb{O}^{(\mathbb{M},\,\text{absorption})}(\lambda) \right\| \alpha_i\, \mathbb{J}_i \right\rangle\right|^2 \times \begin{cases} \delta(E_i + \omega - E_f) \\ \frac{1}{\pi} \frac{\Gamma_f/2}{(E_i+\omega-E_f)^2 + \Gamma_f^2/4} \end{cases}$$

➢ Photoexcitation cross sections for initially unpolarized atoms and linear-polarized, circularly-polarized or unpolarized photons: For resonant and unpolarized or completely linearly-polarized or circularly-polarized plane-wave photons, especially, the total photoexcitation cross section is

$$\sigma(\alpha_i \mathbb{J}_i \to \alpha_f \mathbb{J}_f;\, \omega) = \frac{8\pi^3\alpha}{\omega\,(2J_i+1)} \sum_{\mathbb{M}} \left|\left\langle \alpha_f\, \mathbb{J}_f \left\| \mathbb{O}^{(\mathbb{M},\,\text{absorption})}(\lambda) \right\| \alpha_i\, \mathbb{J}_i \right\rangle\right|^2 \times \begin{cases} \delta(E_i + \omega - E_f) \\ \frac{1}{\pi} \frac{\Gamma_f/2}{(E_i+\omega-E_f)^2 + \Gamma_f^2/4} \end{cases}$$

➢ In Jac, the photoexcitation cross sections are calculated by default for resonant and completely linearly-polarized plane-wave radiation.

➢ In Jac, the photoexcitation cross sections are calculated also for plane-wave radiation with given Stokes parameters (P_1, P_2, P_3) if the flag `calcStokes = true` are set in `PhotoExcitation.Settings` and if the Stokes parameters are given explicitly by `PhotoExcitation.Settings.stokes`.

Final-level statistical tensors and alignment parameters:

➢ Statistical tensors: Instead of the (final-level) density matrix above, it is often more convenient to describe the population of the magnetic sublevels in terms of the (so-called) statistical tensors of the atom or ion

$$\rho_{kq}(\alpha_f \mathbb{J}_f) = \sum_{M_f M_f'} (-1)^{J_f - M_f'} \left\langle J_f M_f,\, J_f\,(-M_f') \,|\, kq \right\rangle \left\langle \alpha_f\, \mathbb{J}_f M_f \,|\, \rho \,|\, \alpha_f\, \mathbb{J}_f M_f' \right\rangle .$$

and which are non-zero only for $0 \le k \le 2\,J_f$ and $-k \le q \le k$.

➢ Reduced statistical tensors: of the excited levels or so-called alignment parameters

$$\mathcal{A}_{kq}(\alpha_f \mathbb{J}_f) \;=\; \frac{\rho_{kq}(\alpha_f \mathbb{J}_f)}{\rho_{00}(\alpha_f \mathbb{J}_f)} \,.$$

➢ Statistical tensors for initially unpolarized atoms and incident plane-wave radiation For incident plane-wave photons with (photon) density matrix $(c_{\lambda\lambda'}) = \frac{1}{2}\begin{pmatrix} 1+P_3 & P_1 - iP_2 \\ P_1 + iP_2 & 1-P_3 \end{pmatrix}$, which are resonant to the given transition $|\alpha_i \mathbb{J}_i\rangle \to |\alpha_f \mathbb{J}_f\rangle$, the reduced statistical tensors can be written as

$$\rho_{kq}(\alpha_f \mathbb{J}_f) \;=\; ...$$

➢ Statistical tensors for initially unpolarized atoms and incident plane-wave radiation with well-defined helicity λ: For incident plane-wave photons with helicity λ, the reduced statistical tensors can be written as (Surzhykov *et al.*, 2015)

$$\rho_{kq}(\alpha_f \mathbb{J}_f) \;=\; \delta_{q0}\, C \sum_{\mathbb{M}\,\mathbb{M}'} i^{\,L+L'}\, [L,\, L]^{1/2}\, (i\,\lambda)^p\, (-i\,\lambda)^{p'}\, (-1)^{\,L'+J_f+J_i+k}\, \langle L\lambda,\, L'\, -\lambda \,|\, kq\rangle \begin{Bmatrix} L & L' & k \\ J_f & J_f & J_i \end{Bmatrix}$$

$$\times\, \left\langle \alpha_f \mathbb{J}_f \,\middle\|\, \mathbb{O}^{(\mathbb{M},\,\text{absorption})} \,\middle\|\, \alpha_i \mathbb{J}_i \right\rangle \left\langle \alpha_f \mathbb{J}_f \,\middle\|\, \mathbb{O}^{(\mathbb{M}',\,\text{absorption})} \,\middle\|\, \alpha_i \mathbb{J}_i \right\rangle^*$$

➢ In JAC, the statistical tensors $\rho_{kq}(\alpha_f \mathbb{J}_f)$ and the alignment parameters $\mathcal{A}_{kq}(\alpha_f \mathbb{J}_f)$ are calculated and tabulated for unpolarized atoms and plane-wave photons with given Stokes parameters, if the flag `calcTensors = true` is set in `PhotoExcitation.Settings` and if the Stokes parameters are given explicitly by `PhotoExcitation.Settings.stokes`.

7.1.c. Atomic photoionization (PhotoIonization)

Process & notations:

➢ Photo-ionization of an atom or ion: $A + \hbar\omega \longrightarrow A^{+*} + e^-_p$

➢ Formal quantum notation: $|\alpha_i \mathbb{J}_i\rangle + \hbar\omega\,(\mathbb{M}) \longrightarrow |\alpha_f \mathbb{J}_f\rangle + e^-_p(\mathbf{p},\, m_s)$ or $|\alpha_i \mathbb{J}_i\rangle + \hbar\omega\,(\mathbb{M}) \longrightarrow |\alpha_f \mathbb{J}_f\rangle + e^-_p(\varepsilon\,\kappa)$

➢ Using Jac: Perform an `Atomic.Computation(.., process=Jac.Photo, processSettings=PhotoIonization.Settings(..), ..)` or call directly functions from the module `PhotoIonization`.

Photoionization amplitude:

➢ Emission of an electron with asymptotic momentum $\boldsymbol{p}$ and spin projection m_s: If the atom undergoes the transition $|\alpha_i\, \mathbb{J}_i M_i\rangle \to |\alpha_f\, \mathbb{J}_f M_f\rangle$, the transition amplitude for the photoionization of an atom or ion by the absorption of a photon with wave vector $\boldsymbol{k}$ and helicity $\lambda = \pm 1$ is given by:

$$\mathcal{M}\,(M_f, m_s, \lambda, M_i) \;=\; \left(\frac{4\pi^2\alpha}{\omega}\right)^{1/2} \left\langle \alpha_f\, \mathbb{J}_f M_f,\, \boldsymbol{p}\, m_s \left| \sum_{i=1}^{N} \boldsymbol{\alpha}_i\, \mathbf{u}_\lambda\, e^{i\,\boldsymbol{k}\cdot\boldsymbol{r}_i} \right| \alpha_i\, \mathbb{J}_i M_i \right\rangle .$$

➢ The population of the magnetic sublevels $|\alpha_f\, \mathbb{J}_f M_f\rangle$ of the photoion depends (of course) on the spin projection λ of the incident photons as well as the magnetic quantum numbers M_f of the final state of the photoion, while one need to average over the initial sublevel and the spin projection of the emitted electrons.

Partial and total cross sections:

➢ Partial photoionization cross sections for the photoionization of an initially unpolarized atom: For the photoionization of an initially unpolarized atom from level $|\alpha_i \mathbb{J}_i\rangle \to |\alpha_f \mathbb{J}_f M_f\rangle$ by unpolarized plane-wave photons with wave vector $\mathbf{k} \,||\, \mathbf{e}_z$ (quantization axis), the

partial cross sections can be expressed as:

$$\begin{aligned}\sigma(\alpha_i \mathbb{J}_i \rightarrow \alpha_f \mathbb{J}_f M_f) &= \frac{1}{2(2J_i+1)} \sum_{M_i\,\lambda m_s} \int d\Omega_p \; \left|\mathcal{M}\left(M_f, m_s, \lambda, M_i\right)\right|^2 \\ &= \frac{4\pi^2\alpha}{2\,\omega\,(2J_i+1)} \sum_{M_i\,\lambda} \sum_{\kappa m} \sum_{JJ'M} \langle J_f M_f\, jm \,|\, JM\rangle \; \langle J_f M_f\, jm \,|\, J'M\rangle \left\langle (\alpha_f \mathbb{J}_f, \varepsilon\kappa)\, \mathbb{J}M \left| \sum_{i=1}^{N} \boldsymbol{\alpha}_i \, \mathbf{u}_\lambda \, e^{i\boldsymbol{k}\cdot\boldsymbol{r}_i} \right| \alpha_i \mathbb{J}_i M_i \right\rangle \\ &\quad \times \left\langle (\alpha_f J_f, \varepsilon\kappa)\, \mathbb{J}'M \left| \sum_{i=1}^{N} \boldsymbol{\alpha}_i \, \mathbf{u}_\lambda \, e^{i\boldsymbol{k}\cdot\boldsymbol{r}_i} \right| \alpha_i J_i M_i \right\rangle^* .\end{aligned}$$

Obviously, the integration over all the emission angles $\mathbf{n}_p = (\vartheta_p, \varphi_p)$ of the photoelectron here results into the *incoherent* summation over the partial waves of the electron with different κ's.

➢ Partial photoionization cross sections for initially unpolarized atoms by unpolarized plane-wave photons: The partial cross sections from above can be simplified and expressed as

$$\begin{aligned}\sigma(\alpha_i \mathbb{J}_i \rightarrow \alpha_f J_f M_f) &= \frac{8\pi^3\,\alpha}{2\omega\,(2J_i+1)} \sum_{t\lambda} \sum_{\kappa} \sum_{JJ'} \sum_{\mathbb{M}\,\mathbb{M}'} i^{L-L'}\,(i\lambda)^p\,(-i\lambda)^{p'}\,(-1)^{L+L'} \sqrt{(2L+1)(2L'+1)(2J+1)(2J'+1)} \\ &\quad \times \langle L'\lambda\, J_f M_f \,|\, t, \lambda+M_f\rangle \; \langle L\lambda\, J_f M_f \,|\, t, \lambda+M_f\rangle \begin{Bmatrix} j & J' & J_f \\ J & J_i & L \\ J_f & L' & t \end{Bmatrix} \\ &\quad \times \left\langle (\alpha_f \mathbb{J}_f, \varepsilon\kappa)\, \mathbb{J} \left\| \mathbb{O}^{(\mathbb{M},\,\text{photoionization})} \right\| \alpha_i \mathbb{J}_i \right\rangle \left\langle (\alpha_f \mathbb{J}_f, \varepsilon\kappa)\, \mathbb{J}' \left\| \mathbb{O}^{(\mathbb{M}',\,\text{photoionization})} \right\| \alpha_i \mathbb{J}_i \right\rangle^* .\end{aligned}$$

Reduced statistical tensors of the photoion:

➢ Statistical tensors of the photo-ion in level $|\alpha_f \mathbb{J}_f\rangle$ after photoionization of unpolarized atoms by unpolarized plane-wave photons: If the incident light propagates along the x-axis (quantization axis, because of its typical use in experimental discussions) and if the photoelectron remains unobserved, the statistical tensors are given by Kämpfer *et al.* (2016)

$$\rho_{kq}(\alpha_f \mathbb{J}_f) = \frac{\pi}{2J_i+1}\,\delta_{q0} \sum_{\mathbb{M}\mathbb{M}'} \sum_{\kappa J J'} \sum_{\lambda=\pm 1} i^{L+p-L'-p'}\,\lambda^{p+p'}\,[L,L',J,J']^{1/2}\,(-1)^{J+J'+J_f+J_i+j+1}\,\langle L\lambda, L'-\lambda \,|\, kq\rangle \begin{Bmatrix} J_f & j & J' \\ J & k & J_f \end{Bmatrix} \begin{Bmatrix} J' & J_i & L' \\ L & k & J \end{Bmatrix}$$

$$\times \left\langle (\alpha_f \mathbb{J}_f, \varepsilon\kappa)\mathbb{J} \left\| \mathbb{O}^{(\mathbb{M},\,\text{photoionization})} \right\| \alpha_i \mathbb{J}_i \right\rangle \left\langle (\alpha_f \mathbb{J}_f, \varepsilon\kappa)\mathbb{J}' \left\| \mathbb{O}^{(\mathbb{M}',\,\text{photoionization})} \right\| \alpha_i \mathbb{J}_i \right\rangle^{*},$$

➢ Statistical tensors of the photoion in level $|\alpha_f \mathbb{J}_f\rangle$ after photoionization of unpolarized atoms by plane-wave photons with given density matrix $(c_{\lambda\lambda'})$: If the incident plane-wave light with well-defined (photon) density matrix $(c_{\lambda\lambda'})$ propagates along the z-axis, the statistical tensors are given more generally by (Sharma *et al.*, 2010)

$$\rho_{kq}(\alpha_f \mathbb{J}_f) = \frac{\pi}{2J_i+1} \sum_{\mathbb{M}\mathbb{M}'} \sum_{\kappa J J'} \sum_{\lambda\lambda'} \left[\delta_{\lambda\lambda'}(1+\lambda P_3) + (1-\delta_{\lambda\lambda'})\,(P_1 - i\lambda P_2)\right]\, i^{\,L-L'+p-p'}\,\lambda^p\,(\lambda')^{p'}\,[L,L',\,J,J']^{1/2}$$

$$\times (-1)^{(J+J'+J_f+J_i+j+1)}\,\langle L\lambda L'-\lambda' \,|\, kq\rangle \begin{Bmatrix} J_f & j & J' \\ J & k & J_f \end{Bmatrix} : \begin{Bmatrix} J' & J_i & L' \\ L & k & J \end{Bmatrix}$$

$$\times \left\langle (\alpha_f J_f,\, \varepsilon\kappa)J \left\| \mathbb{O}^{(\mathbb{M},\,\text{photoionization})} \right\| \alpha_i J_i \right\rangle \left\langle (\alpha_f J_f,\, \varepsilon\kappa)J' \left\| \mathbb{O}^{(\mathbb{M}',\,\text{photoionization})} \right\| \alpha_i J_i \right\rangle^{*},$$

➢ In Jac, the statistical tensors of the photoion are calculated and tabulated for the photoionization of unpolarized atoms by plane-wave photons with given Stokes parameters, if the flag `calcTensors` is set in `PhotoRecombination.Settings` and of the Stokes parameters are given explicitly in `PhotoRecombination.Settings.stokes`.

Further information:

- ➢ Electron-electron correlations Often, interesting correlation effects with regard to exchange, interchannel coupling, relaxation and polarization occurs in the vincinity of the photoionization threshold.
- ➢ Giant resonances: The $4d$ subshells of xenon and barium are both characterized by a broad and delayed absorption peak with a widths of approximately 50 eV above of the $4d$ ionization threshold, a so-called giant resonance. Photoelectron spectroscopy measurements in this region have shown that a significant fraction of the absorption arise for xenon and barium due to satellite and multielectron ionization.
- ➢ Dichroism: Conventionally, the dichroism in the photoelectron emission is related to a change in the polarization of the incident light if the polarization state of the target is kept fixed.

7.1.d. Radiative recombination (PhotoRecombination)

Process & notations:

- ➢ Radiative recombination of an atom or ion: $A^{q+} + e^- \longrightarrow A^{(q-1)+} + \hbar\omega$
- ➢ Formal quantum notation: $|\alpha_i \mathbb{J}_i\rangle + |\varepsilon\kappa\rangle \longrightarrow |\alpha_f \mathbb{J}_f\rangle + \hbar\omega\,(\mathbb{M})$ or $|\alpha_i \mathbb{J}_i\rangle + |\mathbf{p}\, m_s\rangle \longrightarrow |\alpha_f \mathbb{J}_f\rangle + \hbar\omega\,(\mathbb{M})$
- ➢ Using JAC: Perform an `Atomic.Computation(.., process=Jac.Rec, processSettings=PhotoRecombination.Settings(..), ..)` or call directly functions from the module `PhotoRecombination`.

Motivation

- ➢ The photorecombination of ions is known also as radiative recombination (RR) or radiative electron capture (REC) in the literature.
- ➢ The radiative recombination (RR), which can be viewed as the time-reversed photoionization, occurs frequently in stellar and laboratory plasmas as well as in ion trap and storage ring experiments.
- ➢ If a highly-charged ion circulates in a storage ring, it may capture electrons from rest-gas atoms in the ring and will then be misbent by subsequent steering magnets. Therefore, the radiative recombination or electron capture typically results in a loss of the ion from the ring, and where the lifetime is usually proportional to the inverse of the product of the capture cross section and the target pressure.

➢ REC is dominant especially for low-Z targets in the ring. For these targets, the capture cross sections of projectile ions with low or moderate energies are proportional to Z_p^5 and, hence, the lifetimes fall by ten orders of magnitude if Z_p increases by two orders of magnitude. At (very) high projectile energies, in contrast, the lifetimes increases linearly with $\gamma = \sqrt{1 - \beta^2}$.

➢ In JAC, the total radiative recombination cross sections and angular anisotropy parameters are calculated and tabulated by default for all selected recombination lines.

Radiative recombination amplitude

➢ (Photo-) recombination amplitude: In first-order perturbation theory, most radiative recombination properties can be traced back to the evaluation of the (reduced emission) matrix element

$$\left\langle \alpha_f \mathbb{J}_f \left\| \mathbb{O}^{(\mathbb{M},\,\text{recombination})} \right\| (\alpha_i \mathbb{J}_i, \varepsilon\kappa)\mathbb{J}_t \right\rangle = \left\langle (\alpha_i \mathbb{J}_i, \varepsilon\kappa)\mathbb{J}_t \left\| \mathbb{O}^{(\mathbb{M},\,\text{photoionization})} \right\| \alpha_f \mathbb{J}_f \right\rangle^*$$

which describes the capture of a free electron with energy ε and angular momentum κ under the (simultaneous) emission of a photon with multipolarity $\mathbb{M} = (L, p)$.

➢ In JAC, these photorecombination amplitudes are the building blocks to obtain most of the properties below.

Total recombination cross sections:

➢ Total recombination cross section: If the density of states and the principle of detailed balance between the capture and the (photo-) ionization of an electron is taken into account, the total cross section reads as

$$\sigma(\alpha_i \mathbb{J}_i, \alpha_f \mathbb{J}_f) = \frac{8\alpha^3\,\pi^3\,\omega}{(2J_i+1)}\,\frac{1}{\beta^2\,\gamma^2}\left[\sum_{\mathbb{M}\,J\kappa} \left| \left\langle \alpha_f \mathbb{J}_f \left\| \mathbb{O}^{(\mathbb{M},\,\text{recombination})} \right\| (\alpha_i \mathbb{J}_i,\, \varepsilon\kappa)\mathbb{J} \right\rangle \right|^2 \right]$$

where $\beta = v/c$ and $\gamma = \sqrt{1-\beta^2}$ arise from the Lorentz transformation in going from the projectile into the laboratory frame.

➢ In JAC, the total recombination cross sections are calculated and tabulated by default for all selected photorecombination lines.

Angular distribution of emitted photons:

➢ Angular distribution of emitted photons: For initially unpolarized ions and unpolarized incident electrons, the angular distribution of the emitted (RR) photons can be readily obtained from the final-state density matrix by taking the trace $\mathrm{Tr}\,(P_{\mathbf{k}}\,\rho_f)$:

$$W(\theta) \;=\; \frac{\sigma}{4\pi}\left(1 \,+\, \sum_{\nu=1} P_\nu(\cos\theta)\,\beta_\nu^{(\mathrm{REC})}(\alpha_i \mathbb{J}_i, \alpha_f \mathbb{J}_f)\right).$$

➢ Anisotropy parameters of the emitted photons:

$$\beta_\nu^{(\mathrm{REC})} \;=\; -\frac{1}{2}\sum_{JJ'\kappa\kappa'}\sum_{\mathbb{M}\mathbb{M}'} i^{L+p-L'-p'}\,(-1)^{J_i-1/2-J_f}\,[L,L',\ell,\ell',j,j',J,J']^{1/2}\,\langle \ell 0,\,\ell' 0\,|\,\nu 0\rangle\,\langle L1,\,L'-1\,|\,\nu 0\rangle\,\left(1+(-1)^{L+p+L'+p'-\nu}\right)$$

$$\times \begin{Bmatrix} J & J' & \nu \\ L' & L & J_f \end{Bmatrix} \begin{Bmatrix} J & J' & \nu \\ j' & j & J_i \end{Bmatrix} \begin{Bmatrix} j & j' & \nu \\ \ell' & \ell & 1/2 \end{Bmatrix} \left\langle \alpha_f \mathbb{J}_f \,\middle\|\, \mathbb{O}^{(\mathbb{M},\,\mathrm{recombination})} \,\middle\|\, (\alpha_i \mathbb{J}_i,\,\varepsilon\kappa)\mathbb{J}\right\rangle^*$$

$$\times \left\langle \alpha_f \mathbb{J}_f \,\middle\|\, \mathbb{O}^{(\mathbb{M}',\,\mathrm{recombination})} \,\middle\|\, (\alpha_i \mathbb{J}_i,\,\varepsilon\kappa')\mathbb{J}'\right\rangle \quad \left[\sum_{J\kappa\,\mathbb{M}} \left|\left\langle \alpha_f \mathbb{J}_f \,\middle\|\, \mathbb{O}^{(\mathbb{M},\,\mathrm{recombination})} \,\middle\|\, (\alpha_i \mathbb{J}_i,\,\varepsilon\kappa)\mathbb{J}\right\rangle\right|^2\right]^{-1}.$$

➢ In JAC, the anisotropy parameters $\beta_\nu^{(\mathrm{REC})}$, $\nu = 1, ..., 6$ are calculated and tabulated for all selected photorecombination lines if the flag `calcAnisotropy = true` is set in `PhotoRecombination.Settings`.

7.1.e. Auger processes (Auger)

Process & notations:

- Auger emission (autoionization) of an atom or ion: $A^{q+*} \longrightarrow A^{(q+1)+(*)} + e_a^-$
- Formal quantum notation: $|\alpha_i \mathbb{J}_i\rangle \longrightarrow |\alpha_f \mathbb{J}_f\rangle + |\varepsilon\kappa\rangle$
- Using Jac: Perform an `Atomic.Computation(.., process=Jac.AugerX, processSettings=Auger.Settings(..), ..)` or call directly functions from the module `Auger`.

Motivation:

- An autoionization of an (inner-shell) excited bound state can occur (only) if the initial level is energetically embedded into the *continuum* of the next higher charge state.
- Formally, an electron emission from such an embedded resonance (level) arise due to its coupling to one or several scattering states that are degenerate with the initial state and that involve one (or more) *free* electrons.
- Reaction plane of the Auger emission: For a prior photo-absorption or particle impact, this reaction plane is usually defined by the directions of the incident photon (particle) beam and the emitted Auger electron.
- In Jac, we support the computation of nonradiative (Auger) rates, relative Auger intensities and intrinsic angular anisotropy parameters. To this end, first the (reduced) Auger amplitudes are calculated for all selected pairs of initial and final levels and, later, these amplitudes are combined into Auger rates, intrinsic anisotropic as well as (intrinsic) spin-polarization parameters.

Auger amplitudes:

➢ Following Åberg and Howat (1982), the Auger transition amplitude for the autoionization of an excited bound state $|\alpha_i\, \mathbb{J}_i M_i\rangle$ into the final scattering state $|\alpha_t\, \mathbb{J}_t M_t\rangle$, built from an ion in the final level $|\alpha_f\, \mathbb{J}_f\rangle$, can be expressed most generally as

$$\begin{aligned}\big\langle (\alpha_f \mathbb{J}_f,\, \varepsilon\, \kappa)\, \mathbb{J}_t M_t \,\big|\, \mathbb{V}^{(\mathrm{Auger})} \,\big|\, \alpha_i\, \mathbb{J}_i M_i \big\rangle &= \big\langle (\alpha_f \mathbb{J}_f,\, \varepsilon\, \kappa)\, \mathbb{J}_t \,\big\|\, \mathbb{V}^{(\mathrm{Auger})} \,\big\|\, \alpha_i\, \mathbb{J}_i \big\rangle\; \delta_{J_i,J_t}\; \delta_{M_i,M_t}\; \delta_{P_i,P_t} \\ &= \big\langle (\alpha_f \mathbb{J}_f,\, \varepsilon\, \kappa)\, \mathbb{J}_t \,\big\|\, \mathbb{H} - E \,\big\|\, \alpha_i\, \mathbb{J}_i \big\rangle\; \delta_{J_i,J_t}\; \delta_{M_i,M_t}\; \delta_{P_i,P_t}.\end{aligned}$$

This amplitude is independent of the projection M_i of the initial state owing to the rotational invariance of free atoms and the scalar character of the Hamiltonian and/or interelectronic interactions.

➢ In an autoionization process, the final scattering states $|\alpha_t\, \mathbb{J}_t M_t\rangle \equiv |(\alpha_f \mathbb{J}_f,\, \varepsilon\, \kappa)\, \mathbb{J}_t M_t\rangle$ arise from the coupling of the final state $|\alpha_f\, \mathbb{J}_f M_f\rangle$ of the ion with well-defined symmetry with the partial-wave $|\varepsilon\, \kappa\, m_j\rangle$ of the outgoing electron with energy ε and (one-electron) angular momentum $\kappa = \kappa(j,l)$ as well as magnetic projection m_j .

➢ In Jac, as in most other tools for computing autoionization processes, a common set of *orthonormal* orbitals is often supposed for the representation of the initial $|\alpha_i \mathbb{J}_i\rangle$ and final (ionic) bound levels $|\alpha_f \mathbb{J}_f\rangle$ in the evaluation of the Auger amplitudes. In this case, the Auger transition operator $\mathbb{V}^{(\mathrm{Auger})} \equiv \mathbb{H} - E \approx \mathbb{V}^{(\mathrm{e-e})}$ simplifies to the electron-electron interaction operator and the (reduced) Auger amplitude becomes

$$\big\langle (\alpha_f \mathbb{J}_f,\, \varepsilon\, \kappa)\, \mathbb{J}_t \,\big\|\, \mathbb{V}^{(\mathrm{Auger})} \,\big\|\, \alpha_i\, \mathbb{J}_i \big\rangle \;\simeq\; \big\langle (\alpha_f \mathbb{J}_f,\, \varepsilon\, \kappa)\, \mathbb{J}_t \,\big\|\, \mathbb{V}^{(\mathrm{e-e})} \,\big\|\, \alpha_i\, \mathbb{J}_i \big\rangle\; \delta_{J_i,J_t}\; \delta_{M_i,M_t}\; \delta_{P_i,P_t}\,.$$

Within the framework of the Dirac-Coulomb-Breit Hamiltonian, the interelectronic interaction is the sum of the Coulomb repulsion and Breit interaction, $\mathbb{V}^{(\mathrm{e-e})} = \mathbb{V}^{(\mathrm{Coulomb})} + \mathbb{V}^{(\mathrm{Breit})} \simeq \mathbb{V}^{(\mathrm{Coulomb})}$, although it is often approximated by just the Coulomb part.

➢ In Jac, the partikular kind of the Auger operator $\mathbb{V}^{(\mathrm{Auger})}$ can be specified by selecting `Auger.Settings.operator = ("Coulomb", "Breit", "Coulomb+Breit", ...)`.

Auger rates:

➢ Auger rates: If the (continuum) interaction between the different Auger channels is neglected, the Auger rates are given by

$$A(i \to f) \;=\; 2\pi \sum_{\kappa} \left| \left\langle (\alpha_f \mathbb{J}_f,\, \varepsilon\, \kappa)\, \mathbb{J}_i \,\middle\|\, \mathbb{V}^{(\text{Auger})} \,\middle\|\, \alpha_i\, \mathbb{J}_i \right\rangle \right|^2 ,$$

where the Auger interaction operator $\mathbb{V}^{(\text{Auger})}$ still need to be specified due to the (computational) framework and additional approximations that are made in practice.

➢ In Jac, the Auger rates and (Auger) lifetimes are tabulated by default for all selected (Auger) transitions.

Angular distribution of Auger electrons:

➢ Angular distribution of the emitted electrons: If only the Auger electrons are detected from the autoionization of an (inner-shell) excited ion in level $|\alpha_i \mathbb{J}_i\rangle$, and which is fully characterized by its reduced statistical tensors $\mathcal{A}_{kq}(\alpha_i \mathbb{J}_i)$, the angular distribution of the emitted electrons of a given Auger transition $|\alpha_i \mathbb{J}_i\rangle \to |\alpha_f \mathbb{J}_f\rangle$ can be written in the general form (Balashov *et al.* 2000, equation 3.10)

$$W(\vartheta, \varphi;\, \alpha_i \mathbb{J}_i \to \alpha_f \mathbb{J}_f) \;=\; \frac{A(i \to f)}{4\pi} \left[1 \,+\, \sum_{k\,=\,2,\,4,\,\ldots}^{k_{\max}} \sqrt{\frac{4\pi}{2k+1}}\; \alpha_k(\alpha_i \mathbb{J}_i \to \alpha_f \mathbb{J}_f) \sum_{q\,=\,-k}^{k} \mathcal{A}_{kq}(\alpha_i \mathbb{J}_i)\; Y_{kq}(\vartheta, \varphi) \right] ,$$

and where $\alpha_k(\alpha_i \mathbb{J}_i \to \alpha_f \mathbb{J}_f)$ are the (so-called) intrinsic anisotropy parameters of the electron emission

$$\begin{aligned} \alpha_k(\alpha_i \mathbb{J}_i \to \alpha_f \mathbb{J}_f) \;=\; & \left[\sum_{\kappa} \left\langle (\alpha_f \mathbb{J}_f,\, \varepsilon\, \kappa)\, \mathbb{J}_i \,\middle\|\, \mathbb{V}^{(\text{Auger})} \,\middle\|\, \alpha_i\, \mathbb{J}_i \right\rangle \right]^{-1} (-1)^{J_i + J_f + k - 1/2} \sqrt{2J_i + 1} \sum_{\kappa\kappa'} [\ell, \ell', j, j']^{1/2}\; \langle \ell 0,\, \ell' 0 \,|\, k 0 \rangle \\ & \times \begin{Bmatrix} J_i & j & J_f \\ j' & J_i & k \end{Bmatrix} \begin{Bmatrix} \ell & j & 1/2 \\ j' & \ell' & k \end{Bmatrix} \left\langle (\alpha_f \mathbb{J}_f,\, \varepsilon\, \kappa)\, \mathbb{J}_i \,\middle\|\, \mathbb{V}^{(\text{Auger})} \,\middle\|\, \alpha_i\, \mathbb{J}_i \right\rangle \left\langle (\alpha_f \mathbb{J}_f,\, \varepsilon\, \kappa')\, \mathbb{J}_i \,\middle\|\, \mathbb{V}^{(\text{Auger})} \,\middle\|\, \alpha_i\, \mathbb{J}_i \right\rangle^{*} \end{aligned}$$

➢ Here, the factor $A(i \to f)$ is the total probability of the Auger transition $|\alpha_i \mathbb{J}_i\rangle \to |\alpha_f \mathbb{J}_f\rangle$, integrated over the ejection angles. The anisotropy parameters $\alpha_k(\alpha_i \mathbb{J}_i \to \alpha_f \mathbb{J}_f)$ contain information about the dynamics of the decay, while the tensors $\mathcal{A}_{kq}(\alpha_i \mathbb{J}_i)$ just describe the polarization properties of the initial level.

➢ In JAC, the intrinsic anisotropy parameters are calculated and tabulated if the flag `calcAnisotropy = true` is set in `Auger.Settings`.

Two-electron single Auger emission (TESA):

➢ Non-resonant three-electron Auger transitions have been suggested several decades ago, though clear evidence for such TESA transition were found in Ar only with very low intensity relative to normal Auger.

➢ These TESA transitions usually start with the creation of a double vacancy in an inner shell, and which is filled simultaneously two outer-shell electrons, while the released energy is passed to a third emitted electron.

➢ Such inner-shell double vacancies are normally at energies above the minimum fourfold ionization energy and can easily be filled also by two separate successive two-electron Auger transitions involving four electrons in total.

Further information:

➢ While the Coulomb repulsion in the Auger amplitude above is typically sufficient in order to describe the autoionization of light and medium elements, the Breit interaction has been found important for electron emission and capture processes of highly-charged ions.

➢ The restriction to the electron-electron interaction in the computation (evaluation) of the Auger amplitudes is quite standard in all presently available Auger codes, even if the orbital functions of the resonant state $|\alpha_t \mathbb{J}_t\rangle$ and the final-ionic state $|\alpha_i \mathbb{J}_i\rangle$ are not taken orthogonal to each other.

➢ Often, the number of the possible scattering states $|(\alpha_f \mathbb{J}_f, \varepsilon\, \kappa)\, \alpha_t \mathbb{J}_t\rangle$ of a system increases rapidly since the free electrons may couple in quite different ways to the bound-state electrons from the final (Auger) ions.

➢ The AUGER component of the previous RATIP program (Fritzsche 2012) has been widely used for studying electron emission processes after inner-shell excitation and the ionization of atoms as well as for analyzing the coherence transfer through Auger cascades.

7.1.f. Dielectronic recombination (Dielectronic)

Process & notations:

➢ Dielectronic recombination (DR) of an atom or ion: $A^{q+} + e^- \longrightarrow A^{(q-1)+*} \longrightarrow A^{(q-1)+(*)} + \hbar\omega$

➢ Formal quantum notation: $|\alpha_i \mathbb{J}_i\rangle + |\varepsilon\,\kappa\rangle \longrightarrow |\alpha_d \mathbb{J}_d\rangle \longrightarrow |\alpha_f \mathbb{J}_f\rangle + \hbar\omega\,(\mathbb{M})$ or
$|\alpha_i \mathbb{J}_i\rangle + |\mathbf{p}_i\, m_i\rangle \longrightarrow |\alpha_d \mathbb{J}_d\rangle \longrightarrow |\alpha_f \mathbb{J}_f\rangle + \hbar\omega\,(\mathbb{M})$

➢ Using Jac: Perform an `Atomic.Computation(.., process=Jac.Dierec, processSettings=Dielectronic.Settings(..), ..)` or call directly functions from the module `Dielectronic`.

Motivation:

➢ In most computations, the dielectronic recombination of a N-electron target ion in the (initial) level $|\alpha_i \mathbb{J}_i\rangle$ is typically handled as a two-step process, in which first an electron is captured resonantly from the continuum into a [$(N+1)$-electron] resonance level $|\alpha_d \mathbb{J}_d\rangle$, embedded into the continuum of the initial ion and with often two or more electrons in some excited (one-electron) orbital. In a second step, then, this excited level $|\alpha_d \mathbb{J}_d\rangle$ either decays radiatively by the emission of photons to some (final) level $|\alpha_f \mathbb{J}_f\rangle$, below of the ionization threshold of the ion, or it returns by autoionization back to the ionization stage of the initial target ion.

➢ In practice, the number of the possible scattering states $|(\alpha_i\, \mathbb{J}_i,\, \varepsilon\,\kappa),\, \mathbb{J}_d M_d\rangle$ of the recombined ion often increases very rapidly since, the free electrons may couple in many different ways to the bound-state electrons of the initial ion.

Resonance strength of the dielectronic recombination:

➢ Partial resonance strength: If the interference between the radiative and dielectronic (nonradiative) capture of the electron is negligible in the field of the target, the integrated DR cross section for an isolated resonance level $|\alpha_d \mathbb{J}_d\rangle$, the (so-called) resonance strength, can be expressed in terms of the Auger and radiative rates of this level by

$$S(i \to d \to f) \;\equiv\; \int_{-\infty}^{\infty} dE\;\; \sigma^{(\mathrm{DR})}(E) \;=\; \frac{2\pi^2\,\hbar}{k_i^2}\;\; \frac{A_a(i \to d)\, A_r(d \to f)}{\Gamma_d}$$

where k_i denotes the wave number of the incident electron and Γ_d the half-widths of the resonance level $|\alpha_d \mathbb{J}_d\rangle$, embedded into the continuum. Since this resonance strength refers to the area under the DR cross sections, it is usually given in units of: $[S] = \mathrm{cm}^2\,\mathrm{eV}$.

➢ In the resonance strength above, $A_a(i \to d)$ is the rate for the inverse Auger capture from the initial into the (doubly-excited) resonance level $|\alpha_d \mathbb{J}_d\rangle$, while $A_r(d \to f)$ refers to the rate for the radiative stabilization to the final level $|\alpha_f \mathbb{J}_f\rangle$ of the $N+1$-electron ion.

➢ Total width of the resonance level $|\alpha_d \mathbb{J}_d\rangle$ The total width Γ_d is determined by all possible decay channels of the resonance level $|\alpha_d \mathbb{J}_d\rangle$ and is given in first-order perturbation theory by

$$\Gamma_d \;=\; \hbar \left(\sum_j A_a(d \to j) \;+\; \sum_{f'} A_r(d \to f') \right)$$

by taking the sum over all the individual Auger and radiative rates (widths) of the intermediate level $|\alpha_d \mathbb{J}_d\rangle$.

➢ The Auger and inverse capture rates $A_a(i \to d) = g_i/g_d \; A_a(d \to i)$ are proportional to each other owing to the principle of kinetic balance, and with the g's being the statistical factors of the initial and intermediate resonance levels.

➢ The use of the individual resonance strength $S(i \to d \to f)$ is appropriate especially, if the energy-dependent DR cross section has a Lorentzian profile

$$\sigma^{(\mathrm{DR})}(E) \;=\; \frac{S}{\pi} \frac{\Gamma/2}{(E_r - E)^2 + \Gamma^2/4}$$

around the resonance energy $E_r = E_d - E_i$ and also a natural width less or comparable to the energy spread of the electron beam. In general, this condition is well fulfilled for most $\Delta n \geq 1$ resonances (with an excitation of a bound electron from the shell $n_i \to n_f$, for which the total widths are small in most cases), but this condition can usually be utilized also for the $\Delta n = 0$ lines if the shape of the resonances is not to be analyzed in detail.

➢ Owing to the energy of the incident electron [cf. the factor $1/k_i^2$ above], the resonance strength increases rapidly towards the threshold of the dielectronic recombination and makes the process sensitive to low kinetic energies of the incoming electrons.

➢ Total resonance strength: At storage rings, the radiative stabilization of the ions in the intermediate resonance level $|\alpha_d \mathbb{J}_d\rangle$ is often not observed explicitly and, hence, the radiative rate for the individual transition $d \to f$ in the resonance strength above has to be replaced by the total radiative rate of the (doubly-excited) resonance level $|\alpha_d \mathbb{J}_d\rangle$:

$$A_r(d \to f) \quad \longrightarrow \quad \sum_{f'} A_r(d \to f') \qquad \Longrightarrow \qquad S(i \to d \to f) \quad \longrightarrow \quad S(i \to d) \;=\; \sum_{f'} S(i \to d \to f')$$

➢ In JAC, both the individual $S(i \to d \to f)$ and total resonance strengthes $S(i \to d)$ are calculated and tabulated by default for all selected pathways.

Statistical tensors of the resonance level $|\alpha_d \mathbb{J}_d\rangle$ and alignment:

➢ Statistical tensors of the resonance level $|\alpha_d \mathbb{J}_d\rangle$:

Capture rate:

➢ :

Further information

➢ Since, the radiative recombination often also increases close to the threshold, the isolated-resonance approach is formally no longer valid in this case and should be better replaced by some unified treatment of the radiative and non-radiative decay pathes for the capture of low-energy electrons.

➢ As seen from the (total) resonance strength above, the experimentally observed strength of the dielectronic recombination for a given resonance level $|\alpha_d \mathbb{J}_d\rangle$ is proportional to the capture rate $A_a(i \to d)$ as well as the (total) radiative rate.

7.1.g. Photoexcitation & fluorescence (PhotoExcitationFluores)

Process & notations:

➢ Photo excitation of an atom or ion with subsequent fluorescence emission: $A + \hbar\omega_i \longrightarrow A^* \longrightarrow A^{(*)} + \hbar\omega_f$

➢ Formal quantum notation: $|\alpha_i \mathbb{J}_i\rangle + \hbar\omega\,(\mathbf{k}\,||\,\mathbf{e}_z,\,\lambda;\,\{\mathbb{M}\}) \longrightarrow |\alpha_e \mathbb{J}_e\rangle \longrightarrow |\alpha_f \mathbb{J}_f\rangle + \hbar\omega_f\,(\Omega;\,\mathbf{P})$

➢ Using JAC: Perform an `Atomic.Computation(.., process=PhotoExcFluor, processSettings=PhotoExcitationFluores.Settings(..), ..)` or call directly functions from the module `PhotoExcitationFluores`.

Motivation:

➢ The photoexcitation and (subsequent) fluorescence emission from atoms and ions has been investigated in good detail for both, incident plane-wave radiation as well as for twisted Bessel and Laguerre-Gaussian beams.

➢ Since the properties of the photo-excited atoms can be calculated by the module `PhotoExcitation` and those for the radiative emission by the module `Radiative`, here we shall focus only upon properties that are related to the overall excitation-fluorescence process, such as the angular distribution or density matrix of the fluorescence photons.

➢ In JAC, the statistical tensors $\rho_{kq}(\alpha_e \mathbb{J}_e)$ can be calculated and tabulated by the module `PhotoExcitation`. These tensors are also required for describing the excitation-fluorescence process; they are calculated (but not tabulated here) if the flag `calcTensors = true` is set in `PhotoExcitationFluores.Settings`.

Density matrix of the fluorescence photon $\hbar\omega_f(\Omega)$:

➢ (Reduced) density matrix of the fluorescence photons for the photoemission from an aligned or oriented atom: For photons emitted under the angle $\Omega = (\vartheta, \varphi)$ with regard to the propagation direction of the incident plane-wave radiation $\mathbf{k}\,||\,\mathbf{e}_z$, the (reduced) density matrix

can be readily expressed in terms of the statistical tensors of the excited level $\rho_{kq}(\alpha_e \mathbb{J}_e)$ as

$$\langle \mathbf{k}_0\,\lambda \,|\, \rho_{\omega_f} \,|\, \mathbf{k}_0\,\lambda' \rangle \;=\; 2\pi \sum_{k,\,qq'} \sum_{\mathbb{M}\,\mathbb{M}'} D^{k}_{-qq'}(\varphi,\vartheta,0)\;\rho_{kq}(\alpha_e \mathbb{J}_e)\;i^{L'+p'-L-p}\;\lambda^{p}\;(\lambda')^{p'}\;\sqrt{2L+1}\,\sqrt{2L'+1}\;(-1)^{J_f+J_e+k+q+1}$$

$$\times\;\langle L\lambda,\, L'(-\lambda') \,|\, k-q' \rangle \begin{Bmatrix} L & L' & k \\ J_e & J_e & J_f \end{Bmatrix} \langle \alpha_f\, \mathbb{J}_f \,\|\, \mathbb{O}^{(\mathbb{M},\,\mathrm{emission})}(\omega_f) \,\|\, \alpha_e\, \mathbb{J}_e \rangle \left\langle \alpha_f\, \mathbb{J}_f \,\middle\|\, \mathbb{O}^{(\mathbb{M}',\,\mathrm{emission})}(\omega_f) \,\middle\|\, \alpha_e\, \mathbb{J}_e \right\rangle^{*}$$

➢ In Jac, the reduced density matrix of a fluorescence photon can be calculated and tabulated at selected angles $\{\Omega_1 = (\vartheta_1, \varphi_1),\, \Omega_2,\, ...\}$, if the flags `calcTensors = true` and `calcPhotonDm = true` is set in `PhotoExcitationFluores.Settings` and if the solid angles are specified explicitly by `PhotoExcitationFluores.Settings.Omegas`.

Angular distribution and Stokes parameters of the fluorescence photon $\hbar\,\omega_f(\Omega;\,\mathbf{P})$:

➢ Angular distribution of the fluorescence light for the photoemission from a aligned or oriented atom: Most generally, the angular distribution can be obtained from the photon density matrix above by a summation over the polarization states:

$$W(\vartheta,\varphi) \;=\; \sum_{\lambda} \langle \mathbf{k}_0\,\lambda \,|\rho_{\omega_f}|\, \mathbf{k}_0\,\lambda \rangle \;.$$

➢ Using the expressions from above, this angular distribution could be calculated for selected angles $\{\Omega_1 = (\vartheta_1, \varphi_1),\, \Omega_2,\, ...\}$. However, the computation of this angular distribution is currently not (yet) implemented, although this could be readily done.

➢ Angular distribution of the fluorescence light: For initially unpolarized atoms and unpolarized photons in the photo-excitation process, in particular, this distribution is given by the same formulas as for the photoemission (alone), if the alignment parameters $\mathcal{A}_{k0}(\alpha_e \mathbb{J}_e)$ are known for the excited level $|\alpha_e \mathbb{J}_e\rangle$.

$$W(\vartheta) \;=\; \frac{W_o}{4\pi} \left(1 + \sum_{k=2,4,..} f_k(\alpha_e \mathbb{J}_e, \alpha_f \mathbb{J}_f)\, \mathcal{A}_{k0}(\alpha_e \mathbb{J}_e)\, P_k(cos\vartheta) \right) .$$

➢ In Jac, the alignment parameters of the (intermediate) excited level $\mathcal{A}_{kq}(\alpha_e \mathbb{J}_e)$ can be calculated and tabulated by the module `PhotoExcitation`, while the structure functions $f_k(\alpha_e \mathbb{J}_e,\, \alpha_f \mathbb{J}_f)$ can be obtained by using the module `Radiative`.

7.1.h. Photoexcitation & autoionization (PhotoExcitationAutoion)

Process & notations:

➢ Photo-excitation & autoionization of an atom or ion: $A + \hbar\omega \longrightarrow A^* \longrightarrow A^{(*)} + e_a^-$

➢ Formal quantum notation: $|\alpha_i \mathbb{J}_i\rangle + \hbar\omega\,(\mathbb{M}) \longrightarrow |\alpha_r \mathbb{J}_r\rangle \longrightarrow |\alpha_f \mathbb{J}_f\rangle + |\varepsilon\kappa\rangle$

➢ Using JAC: Perform an `Atomic.Computation(.., process=PhotoExcAuto, processSettings=PhotoExcitationAutoion.Settings(..), ..)` or call directly functions from the module `PhotoExcitationAutoion`.

Motivation:

➢ The photoexcitation and (subsequent) autoionization of atoms and ions has been explored in good detail, either as the dominant (photo-) ionization process within the vincinity of certain (photoionization) resonances or simply as competitive process to atomic photoionization.

➢ Often, the photoexcitation-autoionization can be considered independently of the *direct* photoionization and then leads to partial and total photoexcitation-autoionization cross sections.

➢ If the direct photoionization is negligible, the photoexcitation-autoionization is the time-reversed process to the dielectronic recombination.

➢ In JAC, partial resonance strength $S(i \to r \to f)$ and total resonance strength $S(i \to r)$ are calculated an tabulated by default. Further implementations are required to obtain also Fano profiles, total photoioniozation cross sections, etc.

Fano profiles in photo-ionization cross sections:

➢ For an isolated resonance, the total photoionization cross section can be (formally) parametrized in the vincinity of the resonant level $|\alpha_r \mathbb{J}_r\rangle$ by the energy-dependent cross section

$$\sigma(\mathcal{E}) \;=\; \sigma^{(\mathrm{EA})}\,\frac{(q+\mathcal{E})^2}{1+\mathcal{E}^2} + \sigma^{(\mathrm{D})}$$

where $\sigma^{(\mathrm{D})}$ is the direct photoionization cross section and $\sigma^{(\mathrm{EA})}$ the cross section due to the photo-excitation and autoionization of the resonance. Moreover, $\mathcal{E} = (E_\omega - E_r)/(\Gamma/2)$ indicates the departure of the incident photon energy E_ω from the resonance energy E_r, in units of the half-width $(\Gamma/2)$ of the resonance.

➢ The Fano q parameter determines the overall profile of the cross section, ranging from a near-Lorentzian $(q \to \infty)$, to a window-like $(q \to 0)$, and up to a completely asymmetric resonance $(q \to \pm 1)$.

➢ In JAC, no attempt has (yet) been made to calculate the Fano profiles explicitly for selected resonances, although this would be possible by combining proper calls to functions from the modules `PhotoIonization`, `PhotoExcitation` as well as `Auger`.

Total photoionization amplitudes and cross sections across the resonance level $|\alpha_r \mathbb{J}_r\rangle$:

➢ The photoexcitation and (subsequent) autoionization of atoms and ions obviously contributes to the photoionization and, hence, to its amplitudes and cross sections.

➢ Total photoionization amplitudes across the resonance level $|\alpha_r \mathbb{J}_r\rangle$:

$$\mathcal{M}\,(\omega;\, (\alpha_f \mathbb{J}_f,\, \varepsilon\kappa)\, \mathbb{J}_t,\, \alpha_r \mathbb{J}_r,\, \alpha_i \mathbb{J}_i)$$

$$= \left\langle (\alpha_f \mathbb{J}_f,\, \varepsilon\kappa)\, \mathbb{J}_t \,\middle\|\, \mathbb{O}^{(\mathbb{M},\,\text{photoionzation})} \,\middle\|\, \alpha_i \mathbb{J}_i \right\rangle + \frac{\left\langle (\alpha_f \mathbb{J}_f,\, \varepsilon\kappa)\, \mathbb{J}_t \,\middle\|\, \mathbb{O}^{(\text{Auger})} \,\middle\|\, \alpha_r \mathbb{J}_r \right\rangle \left\langle \alpha_r \mathbb{J}_r \,\middle\|\, \mathbb{O}^{(\mathbb{M},\,\text{absorption})} \,\middle\|\, \alpha_i \mathbb{J}_i \right\rangle}{E_i \,+\, \omega \,-\, E_r \,+\, i\,\Gamma_r/2}$$

In this notation of the resonant photoionization, we assume the photoelectron to escape by means of the partial wave $|\varepsilon\,\kappa\rangle$ with kinetic energy $\varepsilon = E_i + \omega - E_f$ and with well-defined angular momentum and parity.

➢ Apart from the *direct* photoionization amplitude (first term), the total photoionization amplitude now also contains the photoexcitation-autoionization amplitudes (second term).

Angular distribution of Auger electrons:

➢ Of course, the angular distribution of the emitted Auger electrons always critically depend on the (properties of the) prior excitation process; in this `ImpactExcitationAutoIon` module, we typically assume a photoexcitation of the atoms or ions for calculating subsequent properties of Auger electrons. We also assume that the direct photoionization is negligible near to the considered resonance level $|\alpha_r \mathbb{J}_r\rangle$.

➢ If the initial level $|\alpha_i \mathbb{J}_i\rangle$ is axially symmetric along the z-axis, $\mathcal{A}_{kq}(\alpha_i \mathbb{J}_i) \sim \delta_{q0}$, the angular distribution only depends on the angle ϑ between the symmetry (z-) axis and the linear momentum of the ejected electron, and the angular distribution then simplifies to

$$W(\vartheta;\, \alpha_i \mathbb{J}_i \to \alpha_f \mathbb{J}_f) \;=\; \frac{A_a(i \to f)}{4\pi} \left[1 + \sum_{k\,=\,2,\,4\,,\ldots}^{k_{\max}} \alpha_k(\alpha_i \mathbb{J}_i \to \alpha_f \mathbb{J}_f)\; \mathcal{A}_{k0}(\alpha_i \mathbb{J}_i)\; P_k(\cos\vartheta) \right] .$$

➢ In JAC, no attempt has (yet) been made to tabulate the angular distribution $W(\vartheta;\, \alpha_i \mathbb{J}_i \rightarrow \alpha_f \mathbb{J}_f)$ explicitly for selected scenarios; cf. section 7.1.e.

Further information:

➢ Resonances in atomic photoionization cross sections have been investigated for a (very) long time as function of the frequency of the incoming light. Such resonances in the total cross sections are of particular interest since they are a clear signature of the internal structure of many-electron atoms and ions. Apart from the *direct* photoionization, inner-shell excitation enable the atom to emit electrons along different 'pathes'.

➢ A special type of these 'resonances' in the photoionization cross sections are used in resonant Auger spectroscopy. In this spectroscopy, an inner-shell electron is first excited to some (unoccupied) valence shell, leaving the atom in a well-defined hole state. In a second step, these hole states then autoionize, and this completes the photoionization process.

7.1.i. Rayleigh & Compton scattering of light `(RayleighCompton)`

Process &amplitude:

➢ Rayleigh or Compton scattering of photons at an atom or ion: $A + \hbar\omega_i \longrightarrow A^{(*)} + \hbar\omega_f$ ... including $\omega_i = \omega_f$

➢ Formal quantum notation: $|\alpha_i \mathbb{J}_i M_i\rangle + \hbar\omega_i(\mathbf{k}_i, \lambda_i;\, \{\mathbb{M}_i\}) \longrightarrow |\alpha_f \mathbb{J}_f M_f\rangle + \hbar\omega_f(\mathbf{k}_f, \lambda_f;\, \{\mathbb{M}_f\})$

$\omega_i = \omega_f$ ... for elastic Rayleigh scattering

➢ Using JAC: Perform an `Atomic.Computation(.., process=Compton, processSettings=RayleighCompton.Settings(..), ..)` or call directly functions from the module `RayleighCompton`.

Motivation:

➢ The elastic scattering of light by the bound electrons of an atom or ion is commonly known as Rayleigh scattering and has been found a versatile tool in the past for studying the electronic structure of atoms and their (chemical) environment.

➢ The inelastic (Compton or Raman) scattering of light on atoms, ions or molecules is associated in contrast with an excitation of the target and has also been explored since the 1920s, both experimentally and theoretically.

Second-order scattering amplitude

➢ Compton scattering amplitude: In second-order perturbation theory, the elastic Rayleigh and inelastic Compton process can be described in terms of the two-photon transition amplitudes for a transition from substates $|\alpha_i \mathbb{J}_i M_i\rangle \rightarrow |\alpha_f \mathbb{J}_f M_f\rangle$ owing to the absorption and emission of photons with well-defined wave vectors $\mathbf{k}_{i,f}$ and polarization vectors $\boldsymbol{\epsilon}_{i,f}$. This amplitude is given in terms of the electron-photon interaction operator by (Jahrsetz *et al.*, 2015)

$$\mathcal{M}_{fi}^{(\text{Compton})}(\alpha_f \mathbb{J}_f M_f,\, \alpha_i \mathbb{J}_i M_i; \mathbf{k}_f, \boldsymbol{\epsilon}_f,\, \mathbf{k}_i, \boldsymbol{\epsilon}_i) = \sum_{\alpha_\nu \mathbb{J}_\nu M_\nu} \left[\frac{\left\langle \alpha_f \mathbb{J}_f M_f \left| \hat{R}^\dagger(\boldsymbol{k}_f, \boldsymbol{\epsilon}_f) \right| \alpha_\nu \mathbb{J}_\nu M_\nu \right\rangle \left\langle \alpha_\nu \mathbb{J}_\nu M_\nu \left| \hat{R}(\boldsymbol{k}_i, \boldsymbol{\epsilon}_i) \right| \alpha_i \mathbb{J}_i M_i \right\rangle}{E_i + \omega_i - E_\nu} \right.$$
$$\left. + \frac{\left\langle \alpha_f \mathbb{J}_f M_f \left| \hat{R}(\boldsymbol{k}_i, \boldsymbol{\epsilon}_i) \right| \alpha_\nu \mathbb{J}_\nu M_\nu \right\rangle \left\langle \alpha_\nu \mathbb{J}_\nu M_\nu \left| \hat{R}^\dagger(\boldsymbol{k}_f, \boldsymbol{\epsilon}_f) \right| \alpha_i \mathbb{J}_i M_i \right\rangle}{E_i - \omega_f - E_\nu} \right] .$$

Here, the energies of the photons involved are related by $\omega_f = \omega_i - E_f + E_i$ to each other and to the energies of the initial and final states of the atoms or ions.

➢ Owing to the time-ordering in (time-dependent) perturbation theory, there are obviously two contributions to this second-order amplitude for the *absorption-emission* and *emission-absorption* of the two photons involved.

➢ Although these second-order amplitudes can be readily written down, they are less useful for practical computations as they are based on different representations of the atomic and photon state(s); we therefore first need to perform a multipole expansion of the electron-photon interaction operators and to do all neccessary simplifications.

➢ Compton (scattering) amplitude for the scattering of photons with well-defined helicity and multipolarity:

$$\mathcal{M}_{fi}^{(\text{Compton})}(\alpha_f \mathbb{J}_f M_f,\, \alpha_i \mathbb{J}_i M_i;\, \mathbb{M}_f, \lambda_f,\, \mathbb{M}_i, \lambda_i) = \ldots \frac{\left\langle \alpha_f \mathbb{J}_f \left\| \mathbb{O}^{(\mathbb{M}_f,\, \text{emission})} \right\| \alpha_\nu \mathbb{J}_\nu \right\rangle \left\langle \alpha_\nu \mathbb{J}_\nu \left\| \mathbb{O}^{(\mathbb{M}_i,\, \text{absorption})} \right\| \alpha_i \mathbb{J}_i \right\rangle}{E_i + \omega_f - E_\nu} + \ldots$$

Angle-differential and total cross sections:

➢ Angle-differential cross section for the Compton scattering of unpolarized light by initially unpolarized atoms: For unpolarized incident plane-wave photons and if the polarization of the scattered photons as well as the magnetic sublevel population of the residual ions both remain unobserved, the angle-differential cross section is given by

$$\frac{d\sigma^{\,(\mathrm{Compton})}}{d\Omega}\,(\vartheta;\,\omega_i)$$

$$= \frac{1}{2}\,\frac{\omega_f}{\omega_i}\,\frac{1}{2J_i+1}\sum_{\lambda_i\,\lambda_i'\,\lambda_f\lambda_f'}\sum_{M_i,\,M_f} c_{\lambda_i\,\lambda_i'}\;\mathcal{M}_{fi}^{(\mathrm{Compton})}(\alpha_f\mathbb{J}_f M_f,\,\alpha_i\mathbb{J}_i M_i;\,\mathbb{M}_f,\lambda_f,\,\mathbb{M}_i,\lambda_i)\;\mathcal{M}_{fi}^{(\mathrm{Compton})}(\alpha_f\mathbb{J}_f M_f,\,\alpha_i\mathbb{J}_i M_i;\,\mathbb{M}_f,\lambda_f',\,\mathbb{M}_i,\lambda_i')$$

Unfortunately, there is no simple parametrization of this angle-differential cross section $\frac{d\sigma^{\,(\mathrm{Compton})}}{d\Omega}\,(\vartheta;\,\omega_i)$.

➢ The angle-differential Rayleigh cross sections can be obtained from the formulas above by using $|\alpha_f\mathbb{J}_f\rangle = |\alpha_i\mathbb{J}_i\rangle$ in the two-photon amplitudes and irreducible tensors.

➢ In Jac, the angle-differential Rayleigh and Compton scattering cross sections are calculated by default for all selected initial levels and $(i \to f)$ lines, if a proper spectrum is specified in `RayleighCompton.Settings.spectrum`.

Further information:

➢

7.1.j. Multi-photon excitation and decay (`MultiPhotonDeExcitation`)

Process & notations:

➢ Multi-photon excitation of an atom or ion: $A + n\,\hbar\omega \longrightarrow A^*$

➢ Multi-photon decay of an atom or ion: $A^* \longrightarrow A^* + n\,\hbar\omega$

➢ Formal quantum notation: $|\alpha_i \mathbb{J}_i\rangle + \hbar\omega_1(\mathbf{k}_1, \lambda_1; \{\mathbb{M}_1\}) + \hbar\omega_2(\mathbf{k}_2, \lambda_2; \{\mathbb{M}_2\}) + ... + \hbar\omega_n(\mathbf{k}_n, \lambda_n; \{\mathbb{M}_n\}) \longrightarrow |\alpha_f \mathbb{J}_f\rangle$ or

$$|\alpha_i \mathbb{J}_i\rangle \longrightarrow |\alpha_f \mathbb{J}_f\rangle + \hbar\omega_1(\mathbf{k}_1, \lambda_1; \{\mathbb{M}_1\}) + \hbar\omega_2(\mathbf{k}_2, \lambda_2; \{\mathbb{M}_2\}) + ... + \hbar\omega_n(\mathbf{k}_n, \lambda_n; \{\mathbb{M}_n\})$$

➢ Using JAC: Perform an `Atomic.Computation(.., process=MultiPhoton, processSettings=MultiPhotonDeExcitation.Settings(..), ..)` or call directly functions from the module `MultiPhotonDeExcitation`.

Motivation:

➢ The two-photon decay of few-electron ions $|\alpha_i \mathbb{J}_i\rangle \longrightarrow |\alpha_f \mathbb{J}_f\rangle + \hbar\omega_1 + \hbar\omega_2$ has often been considered, both experimentally and theoretically. For this two-photon decay, the total decay rate as well as the spectral (energy) distribution of the emittedvphotons have been explored.

➢ In JAC, only the inital and final levels are tabulated by default, together with their symmetry and total transition energy, while the proper flags must be set in `MultiPhotonDeExcitation.Settings` for all further cross section information.

Two-photon decay amplitude and total rate:

➢ Two-photon amplitude for the emission of photons with well-defined helicity and multipolarity:

$$\mathcal{M}_{fi}^{(2-\text{emission})}(\alpha_f \mathbb{J}_f M_f,\, \alpha_i \mathbb{J}_i M_i;\, \mathbb{M}_2, \lambda_2,\, \mathbb{M}_1, \lambda_1;\, \omega) = \frac{\langle \alpha_f \mathbb{J}_f \| \mathbb{O}^{(\mathbb{M}_2, \text{emission})} \| \alpha_\nu \mathbb{J}_\nu \rangle \langle \alpha_\nu \mathbb{J}_\nu \| \mathbb{O}^{(\mathbb{M}_1, \text{emission})} \| \alpha_i \mathbb{J}_i \rangle}{E_i - \omega - E_\nu}$$

➢ Two-photon energy-differential emission rate: For the transition of the atom from level $|\alpha_i \mathbb{J}_i\rangle \rightarrow |\alpha_f \mathbb{J}_f\rangle$ can be written as (Goldman

and Drake, 1988; Surzhykov 2005)

$$\frac{dW}{d\omega_1}(\omega_1;\, \alpha_i\, \mathbb{J}_i \rightarrow \alpha_f\, \mathbb{J}_f) = \frac{4\pi}{2J_i\, +\, 1}\, \frac{\omega_1\, \omega_2}{(2\pi)^3\, c^2} \sum_{M_i\, M_f} \sum_{\lambda_1,\, \lambda_2} |\, \mathcal{M}_{fi}(\alpha_f \mathbb{J}_f M_f,\, \alpha_i \mathbb{J}_i M_i;\, \mathbb{M}_2, \lambda_2,\, \mathbb{M}_1, \lambda_1;\, \omega)\, |^2\, d\,\Omega_1\, d\,\Omega_2$$

$$= \frac{(4\pi)^5}{2J_i\, +\, 1}\, \frac{\omega_1\, \omega_2}{(2\pi)^3\, c^2} \sum_{\mathbb{M}_1,\, \mathbb{M}_2} \sum_{\mathbb{J}_\nu} \left\{ \frac{1}{2J_\nu\, +\, 1} \left(|S^{(2-\text{emission})}_{\mathbb{J}_\nu}(\omega_1;\, \mathbb{M}_2, \mathbb{M}_1;\, fi)|^2 \, +\, |S^{(2-\text{emission})}_{\mathbb{J}_\nu}(\omega_2;\, \mathbb{M}_1, \mathbb{M}_2;\, fi)|^2 \right) \right.$$

$$\left. + 2 \sum_{\mathbb{J}'_\nu} (-1)^{J_\nu\, +\, J'_\nu\, +\, L_1\, +\, L_2} \begin{Bmatrix} J_f & J'_\nu & L_1 \\ J_i & J_\nu & L_2 \end{Bmatrix} S^{(2-\text{emission})}_{\mathbb{J}_\nu}(\omega_2;\, \mathbb{M}_1, \mathbb{M}_2;\, fi)^*\; S^{(2-\text{emission})}_{\mathbb{J}_\nu}(\omega_1;\, \mathbb{M}_2, \mathbb{M}_1;\, fi) \right\}$$

Here, the summations over $\mathbb{J}_\nu$ and $\mathbb{J}'_\nu$ are restricted, and their allowed values can be quite easily read-off from the standard selection rules for the multipole matrix elements.

➢ Reduced two-photon (emission) amplitude:

$$S^{(2-\text{emission})}_{\mathbb{J}_\nu}(\omega;\, \mathbb{M}_2, \mathbb{M}_1;\, \alpha_f\, \mathbb{J}_f,\, \alpha_i\, \mathbb{J}_i) \equiv S^{(2-\text{emission})}_{\mathbb{J}_\nu}(\omega;\, \mathbb{M}_2, \mathbb{M}_1;\, fi)$$

$$= \sum_{\alpha_\nu} \frac{\left\langle \alpha_f \mathbb{J}_f \left\| \mathcal{O}^{(\mathbb{M}_2,\, \text{emission})} \right\| \alpha_\nu \mathbb{J}_\nu \right\rangle \left\langle \alpha_\nu \mathbb{J}_\nu \left\| \mathcal{O}^{(\mathbb{M}_1,\, \text{emission})} \right\| \alpha_i \mathbb{J}_i \right\rangle}{E_i\, -\, \omega\, -\, E_\nu}$$

$$= S^{(2-\text{absorption})}_{\mathbb{J}_\nu}(???\ \omega;\, \mathbb{M}_2, \mathbb{M}_1;\, fi\ ???) \;=\; S^{(2-\text{Compton})}_{\mathbb{J}_\nu}(???\ \omega;\, \mathbb{M}_2, \mathbb{M}_1;\, fi\ ???)$$

➢ In JAC, the two-photon energy-differential emission rate are calculated and tabulated if ...

7.1.k. Coulomb excitation (CoulombExcitation)

Process & notations:

➢ Coulomb excitation of an atom or ion by fast, heavy ions: $A + Z_p \longrightarrow A^* + Z_p$ (projectile remains unaffected)

➢ Formal quantum notation: $|\alpha_i \mathbb{J}_i\rangle + Z_p(\beta_p) \longrightarrow |\alpha_f \mathbb{J}_f\rangle\,, \qquad \beta_p = \frac{v_p}{c}$

➢ Using JAC: Perform an `Atomic.Computation(.., process=CoulExc, processSettings=CoulombExcitation.Settings(..), ..)` or call directly functions from the module `CoulombExcitation`.

Motivation

➢ In Coulomb excitation processes, one often assumes that a single electron from a (fast-moving) projectile ion with relative velocity $\beta_p = v_p/c$ (with regard to the target) is excited by a target nucleus at rest.

➢ Of course, an analogue process occurs also when we consider the excitation of the target that may occur due to a fast-moving (bare) projectile ion, and in which case the role of the projectile and target need simply to be interchanged in all formulas below.

Coulomb excitation amplitude of few-electron projectile ions in position space

➢ Coulomb (excitation) amplitude for the excitation of a (single) projectile electron: If a one-electron projectile moves at a trajectory with impact parameter b, the amplitude for an excitation from level $i \to f$ is given by Eichler & Meyerhof (1995, Eq. 6.2)

$$\mathcal{M}_{fi}^{(\mathrm{Coulex})}(b) = i\,\frac{\gamma\, Z_t\, e^2}{\hbar} \int dt\, \exp\left(\frac{i}{\hbar}\,(E_f - E_i)\,t\right) \int d^3r\, \psi_f^\dagger(\mathbf{r})\, \frac{(1 - \beta_p\,\alpha_z)}{r'(t)}\, \psi_i(\mathbf{r}),$$

$$r'(t) = \sqrt{(x-b)^2 + y^2 + \gamma^2\,(z - v\,t)^2}, \qquad \beta_p = \frac{v_p}{c}\,,$$

where $\mathbf{r}$ is the coordinate of the projectile electron, $r'(t)$ its (time-dependent) distance from the target nucleus, and where $\psi_f(\mathbf{r})$ and $\psi_i(\mathbf{r})$ denote the final- and initial-state eigenfunctions of the projectile electron with energies E_f and E_i.

➢ Coulomb (excitation) amplitude for the excitation of a many-electron projectile (ion): For an Coulomb excitation of a many-electron projectile from the sublevel $|\alpha_i\, \mathbb{J}_i M_i\rangle \;\rightarrow\; |\alpha_f\, \mathbb{J}_f M_f\rangle$, the excitation amplitude for given impact parameter b can then be written in first-order perturbation theory and natural units ($\hbar = m_e = c = 1$) as:

$$\mathcal{M}_{fi}^{(\mathrm{Coulex})}(b;\, \alpha_f\, \mathbb{J}_f M_f,\, \alpha_i\, \mathbb{J}_i M_i) \;=\; i\,\gamma\,\alpha\,Z_t \int dt\; e^{i\,(E_f - E_i)t} \left\langle \alpha_f \mathbb{J}_f M_f \left| \sum_{k=1}^{N} \frac{1 - \beta_p\, \hat{\alpha}_z(k)}{r'_k(t)} \right| \alpha_i \mathbb{J}_i M_i \right\rangle .$$

➢ From this transition amplitude, the cross section for an excitation of the projectile from (sub-) level $|\alpha_i\, \mathbb{J}_i\rangle \rightarrow |\alpha_f \mathbb{J}_f M_f\rangle$ can be obtained by integrating over all the impact parameters b and by taking the average over the initial magnetic sublevels M_i.

➢ In JAC, we do not use the Coulomb excitation amplitude in position space but make use of a representation of this amplitude in momentum space instead, see below.

Coulomb excitation amplitude of few-electron projectile ions in momentum space:

➢ Coulomb (excitation) amplitude for the excitation of a (single) projectile electron: To evaluate Coulomb excitation cross sections for one- and many-electron atoms, it is often more convinient to work in momentum space and to express all properties in terms of the Fourier transform of the Coulomb excitation amplitude in position space. If we make use of the momentum transfer $\mathbf{q} = (\mathbf{q}_b, q_z)$, the time-integration in this Coulomb (excitation) amplitude can be carried out explicitly (Eichler & Meyerhof 1995, Eq. 6.4)

$$\mathcal{M}_{fi}^{(\mathrm{Coulex})}(b) \;=\; \frac{i\,\nu_p}{\pi} \int \frac{d^2\, q_b}{q_b^2 + (1-\beta^2)\, q_0^2}\; e^{-i\,\mathbf{q}_0\cdot\mathbf{b}}\; \mathcal{K}_{fi}^{(\mathrm{Coulex})}(\mathbf{q})\,; \qquad \mathcal{K}_{fi}^{(\mathrm{Coulex})}(\mathbf{q}) \;=\; \left\langle \psi_f(\mathbf{r}) \left| (1 - \beta\,\alpha_z)\; e^{i\,\mathbf{q}\cdot\mathbf{r}} \right| \psi_i(\mathbf{r}) \right\rangle .$$

This formula removes the complicated time dependence in $r'(t)$ and replaces it instead by an explicit wave number (momentum transfer) dependence.

➢ Note, that in momentum space, the (momentum-space) Coulomb excitation amplitude $\mathcal{K}_{fi}^{(\mathrm{Coulex})}(\mathbf{q})$ does no longer depend on the impact parameter b but now simply contains an integration over the momentum transfer $\mathbf{q}$, and which starts from the minimum momentum transfer for the excitation of the initial ion from level $|i\rangle \;\rightarrow\; |f\rangle$: $q_0 = (E_f - E_i)/v_p$.

➢ In momentum space, indeed, most Coulomb excitation cross sections can be expressed directly in terms of the momentum-space Coulomb excitation amplitude $\mathcal{K}_{fi}^{(\mathrm{Coulex})}(\mathbf{q})$.

➢ (Momentum-space) Coulomb excitation amplitude for many-electron projectiles: This amplitude can be further simplified by using the Wigner-Eckert theorem (Surzhykov and Fritzsche, 2008)

$$\mathcal{K}_{fi}^{(\mathrm{Coulex})}(\mathbf{q};\, \alpha_f\, \mathbb{J}_f M_f,\, \alpha_i\, \mathbb{J}_i M_i) \;=\; \left\langle \alpha_f\, \mathbb{J}_f M_f \left| \sum_k^N (1 - \beta\, \alpha_z(k))\, e^{i\,\mathbf{q}\cdot\mathbf{r}_k} \right| \alpha_i\, \mathbb{J}_i M_i \right\rangle$$

$$= \sum_{LM} i^L\, Y^*_{LM}(\arccos(q_0/q), 0) \left\langle \alpha_f \mathbb{J}_f M_f \left| \sum_{k=1}^N (1 - \beta_p\, \hat{\alpha}_z(k))\, j_L(q\, r_k)\, Y_{LM}(\vartheta_k, \varphi_k) \right| \alpha_i \mathbb{J}_i M_i \right\rangle ,$$

$$= \sum_t \frac{1}{\sqrt{2J_f + 1}} \langle J_i M_i,\, t\,(M_f - M_i) \,|\, J_f M_f \rangle \sum_L i^L\, Y^*_{L,\, M_f - M_i}(\arccos(q_0/q), 0) \left\langle \alpha_f \mathbb{J}_f \left\| H_{tL}^{(\mathrm{Coulex})}(q) \right\| \alpha_i \mathbb{J}_i \right\rangle$$

$$= \sum_t \frac{1}{\sqrt{2J_f + 1}} \langle J_i M_i,\, t\,(M_f - M_i) \,|\, J_f M_f \rangle \sum_L i^L\, Y^*_{L,\, M_f - M_i}(\arccos(q_0/q), 0)$$

$$\times \left(\delta_{t\,L} \left\langle \alpha_f \mathbb{J}_f \left\| \mathbb{K}^{(\mathrm{L,\,Coulex,\,jY})} \right\| \alpha_i \mathbb{J}_i \right\rangle - \beta_p \langle LM,\, 10 \,|\, tM \rangle \left\langle \alpha_f \mathbb{J}_f \left\| \mathbb{K}^{(\mathrm{t,\,Coulex,\,jT})} \right\| \alpha_i \mathbb{J}_i \right\rangle \right)$$

In Jac, these (momentum-space) Coulomb excitation amplitudes $\mathcal{K}_{fi}^{(\mathrm{Coulex})}(\mathbf{q};\, \alpha_f\, \mathbb{J}_f M_f,\, \alpha_i\, \mathbb{J}_i M_i)$ are implemented explicitly and the integration over q is typically performed by a Gauß-Legendre integration.

Coulomb excitation operators and interaction strength:

➢ Coulomb excitation (interaction) strength: The (full) Coulomb excitation amplitude in momentum space above combines two kinds of reduced (many-electron) matrix elements due to the two interaction operators: $\sum_{k=1}^N j_L(q\, r_k) Y_L(\vartheta_k, \varphi_k)$ of rank L as well as $\sum_{k=1}^N j_L(q\, r_k)\, \hat{\boldsymbol{\alpha}}(k) \cdot \mathrm{T}_{tL}(\vartheta_k, \varphi_k)$ of rank t, respectively. These two reduced matrix elements are the actual building blocks that are needed in order to represent and to explore the properties of the target or projectile excitation process.

➢ Coulomb excitation (interaction) strength: The building blocks for the computation of the Coulomb excitation and ionization amplitudes

are given by the reduced matrix elements

$$\left\langle \alpha_f \mathbb{J}_f \left\| \mathbb{K}^{(\mathrm{L,\,Coulex,\,jY})} \right\| \alpha_i \mathbb{J}_i \right\rangle = \left\langle \alpha_f \mathbb{J}_f \left\| \sum_{k=1}^{N} j_L(q\,r_k)\, Y_L(\vartheta_k, \varphi_k) \right\| \alpha_i \mathbb{J}_i \right\rangle$$

$$\left\langle \alpha_f \mathbb{J}_f \left\| \mathbb{K}^{(\mathrm{t,\,Coulex,\,jT})} \right\| \alpha_i \mathbb{J}_i \right\rangle = \left\langle \alpha_f \mathbb{J}_f \left\| \sum_{k=1}^{N} j_L(q\,r_k)\, \hat{\boldsymbol{\alpha}}(k) \cdot \boldsymbol{T}_{tL}(\vartheta_k, \varphi_k) \right\| \alpha_i \mathbb{J}_i \right\rangle$$

Energie-differential, partial and total Coulomb excitation cross sections:

➢ Partial Coulomb excitation cross section: If the Fourier transformation from the position to momentum coordinates is performed, the integrals over the time t and the impact parameter b can be evaluated *analytically*. Then, the partial (excitation) cross section for the Coulomb excitation from (sub-) levels $|\alpha_i \mathbb{J}_i\rangle \to |\alpha_f \mathbb{J}_f M_f\rangle$ can be written as (Surzhykov and Fritzsche, 2008)

$$\sigma(\alpha_i \mathbb{J}_i \to \alpha_f \mathbb{J}_f M_f) = \frac{2\pi}{2J_i+1} \sum_{M_i} \int_0^\infty \mathrm{d}b\, b \left| \mathcal{M}_{fi}^{(\mathrm{Coulex})}(b;\, \alpha_f\, \mathbb{J}_f M_f,\, \alpha_i\, \mathbb{J}_i M_i) \right|^2$$

$$= 2\pi \left(\frac{8\,\pi\, Z_t\, \alpha}{\beta_p} \right)^2 \frac{1}{2J_i+1} \sum_{M_i} \int_{q_0}^\infty dq\, \frac{q}{\left(q^2 - q_0^2 \beta_p^2\right)^2} \left| \mathcal{K}_{fi}^{(\mathrm{Coulex})}(\mathbf{q};\, \alpha_f\, \mathbb{J}_f M_f,\, \alpha_i\, \mathbb{J}_i M_i) \right|^2 .$$

Alignment of Coulomb-excited ions:

➢ Alignment of Coulomb-excited ions in level $|\alpha_f \mathbb{J}_f\rangle$: For a well-defined ion-atom collision axis, a Coulomb-excited ion in level $|\alpha_f \mathbb{J}_f\rangle$ is generally aligned; this alignment depends on the partial Coulomb cross sections $\sigma(\alpha_f\, \mathbb{J}_f M_f)$ can be described in terms of one (or several)

parameters $\mathcal{A}_k(\alpha_f \mathbb{J}_f)$:

$$\mathcal{A}_k(\alpha_i \mathbb{J}_i \to \alpha_f \mathbb{J}_f) \;=\; \frac{\sqrt{2J_f+1}}{\sigma(\alpha_i \mathbb{J}_i \to \alpha_f \mathbb{J}_f)} \sum_{M_f} (-1)^{J_f - M_f} \langle J_f M_f \, J_f - M_f \,|\, k0 \rangle \;\; \sigma(\alpha_i \mathbb{J}_i \to \alpha_f \mathbb{J}_f M_f) \,,$$

7.2. In JAC partly-implemented processes

7.2.a. Photoionization & fluorescence (PhotoIonizationFluores)

Density operator of the fluorescence photon $\hbar\omega_f(\mathbb{M})$:

➢ After the inner-shell photoionization, the photoion appears to be in an excited level $|\alpha_e \mathbb{J}_e\rangle$ that decays subsequently to some energetically lower level $|\alpha_F \mathbb{J}_f\rangle$ by the emission of a characteristic photon.

➢ Characteristic photon density matrix in the helicity representation: For this characteristic photon, the density matrix can be expressed in the form $\langle \mathbf{k}_0 \, \lambda \,|\, \hat{\rho}_\gamma \,|\, \mathbf{k}_0 \, \lambda' \rangle$, in which $\mathbf{k}_0 \equiv (\vartheta_0, \varphi_0)$ denotes the wave vector along the propagation direction of the fluorescence photon and $\lambda = \pm 1$ its helicity. Note that the helicity representation of this density matrix also describes the photon polarization.

Stokes parameter of the fluorescence photon $\hbar\omega_f(\mathbb{M})$:

➢ The density matrix of the fluorescence photon $\hbar\omega_f(\mathbb{M})$ is usually parametrized in terms of the so-called Stokes parameters (Blum 1981; Balashov *et al.*, 2001)

$$\left\langle \mathbf{k}_0 \lambda \,\middle|\, \hat{\rho}_{\omega_f} \,\middle|\, \mathbf{k}_0 \lambda' \right\rangle \;\equiv\; c_{\lambda,\lambda'} \;=\; \frac{1}{2} \begin{pmatrix} 1+P_3 & -P_1 + iP_2 \\ -P_1 - iP_2 & 1-P_3 \end{pmatrix} ,$$

and which are utilized to characterize both the degree of linear (P_1 and P_2) and circular (P_3) polarization of the light.

7.2.b. Photoionization & autoionization (PhotoIonizationAutoion)

Process & notations:

- Photo ionization of an atom or ion with subsequent autoionization: $A + \hbar\omega \longrightarrow A^* \longrightarrow A^{(*)} + e_a^-$
- Formal quantum notation: $|\alpha_i \mathbb{J}_i\rangle + \hbar\omega(\mathbb{M}) \longrightarrow |\alpha_r \mathbb{J}_r\rangle + |\varepsilon_p \kappa_p\rangle \longrightarrow |\alpha_f \mathbb{J}_f\rangle + |\varepsilon_p \kappa_p\rangle + |\varepsilon_a \kappa_a\rangle$
- Using JAC: Perform an `Atomic.Computation(..., process = Jac.xxx, processSettings = PhotoIonizationAutoion.Settings(), ...` or call directly functions from the module `PhotoIonizationAutoion`.

Process & notations:

- Dielectrocnic recombination of an atom or ion with subsequent fluorescence: $xxx \quad A + \hbar\omega \longrightarrow A^* \longrightarrow A^{(*)} + e_a^-$
- Formal quantum notation: $|\alpha_i \mathbb{J}_i\rangle + \hbar\omega(\mathbb{M}) \longrightarrow |\alpha_r \mathbb{J}_r\rangle + |\varepsilon_p \kappa_p\rangle \longrightarrow |\alpha_f \mathbb{J}_f\rangle + |\varepsilon_p \kappa_p\rangle + |\varepsilon_a \kappa_a\rangle$
- Using JAC: Perform an `Atomic.Computation(..., process=DierecFluor, processSettings=DielectronicFluores.Settings(), ..=` or call directly functions from the module `DielectronicFluores`.

7.2.c. Electron-impact (de-) excitation (ImpactExcitation)

Process & notations:

- Electron-impact excitation of an atom or ion: $e_s^- + A \longrightarrow A^* + e_s^{-'}$
- Formal quantum notation: $|\alpha_i \mathbb{J}_i\rangle + |\varepsilon_i \kappa_i\rangle \longrightarrow |\alpha_f \mathbb{J}_f\rangle + |\varepsilon_f \kappa_f\rangle$ or $|\alpha_i \mathbb{J}_i\rangle + |\mathbf{p}_i\, m_i\rangle \longrightarrow |\alpha_f \mathbb{J}_f\rangle + |\mathbf{p}_f\, m_f\rangle$
-
- Using JAC: Perform an `Atomic.Computation(..., process = Jac.xxx, processSettings = ImpactExcitation.Settings(), ...` or call directly functions from the module `ImpactExcitation`.

Motivation:

- The electron-impact excitation of atoms is often described in first-order Born approximation, in which one can easily distinguish individual excitation channels. This approximation neglects however the coupling of *closed channels* but which can later be incorperated perturbatively.
- We here make use of the distorted-wave Born approximation (DWBA) that accounts for the distortion of the continuum orbitals due to (local) potential of the nucleus and all remaining electrons. The DWBA typically gives better results than the pure Born or the Coulomb-Born approximation. The current implementation is similar to the codes by Zhang *et al.*(1989) as well as to the FAC code (Gu 2008).
- Electron-impact ionization cross sections are required, for example, for calculating level populations and spectral line intensities of non-local-thermodynamic-equilibrium (non-LTE) plasmas.

Collision strength and cross sections:

- The name collision strength was first suggested by Seaton (1953). For a given transition $\alpha_i \mathbb{J}_i \rightarrow \alpha_f \mathbb{J}_f$, the collision strength is related to the cross section Q by

$$\Omega(\alpha_i \mathbb{J}_i,\, \alpha_f \mathbb{J}_f) \;=\; \frac{4\pi\, g_i}{\lambda_i^2}\, Q(\alpha_i \mathbb{J}_i,\, \alpha_f \mathbb{J}_f)$$

  The statistical weight g_i of level $|\alpha_i \mathbb{J}_i\rangle$ ensures the relation $\Omega(\alpha_i \mathbb{J}_i,\, \alpha_f \mathbb{J}_f) = \Omega(\alpha_f \mathbb{J}_f,\, \alpha_i \mathbb{J}_i)$ by detailed balance.

➢ Collision strength:

$$\Omega_{if} \;=\; 2 \sum_{\kappa_i,\,\kappa_f} \sum_{\mathbb{J}_t} [J_t] \; \Big| \big\langle (\mathbb{J}_f,\, \epsilon_f, \kappa_f)\; \mathbb{J}_t M_t \,\big|\, V^{\,\mathrm{e-e}} \,\big|\, (\mathbb{J}_i,\, \epsilon_i, \kappa_i)\; \mathbb{J}_t M_t \big\rangle \Big|^2$$

where $|\varepsilon_i, \kappa_i\rangle$ and $|\varepsilon_f, \kappa_f\rangle$ denote the partial waves of the incident and scattered electron.

➢ A continuum orbital is said to be normalized per unit energy if it has an asymptotic amplitude $\sqrt{k/\epsilon}$ (or, $\sqrt{2/k}$ in the non-relativistic limit) or if it fullfills, equivalently,

$$\int dr \;\; [P_\epsilon(r)\; P_{\epsilon'}(r) \;+\; Q_\epsilon(r)\; Q_{\epsilon'}(r)] \;\;=\;\; \pi\, \delta(\epsilon \,-\, \epsilon')\,.$$

➢ Electron-impact excitation cross section: If the continuum orbitals are normalized *per unit energy*, the electron-impact ionization cross section is obtained from the collision strength Ω_{if} by

$$\sigma_{if} \;\;=\;\; \frac{\pi}{k_i^2\; g_i}\, \Omega_{if}$$

where g_i is the statistical weight of the initial state and k_i is the wavenumber or initial momentum of the incident (scattered) electron. The wavenumber of the incident electron is related to its energy ε_i by $k_i^2 \;=\; 2\,\varepsilon_i \,\big(1 \,+\, \frac{\cdot\cdot}{\cdot\cdot}\,\epsilon_i\big)$.

➢ In the JAC program, the standard decomposition of the electron-electron interaction matrix elements is utilized to compute the collision strength.

7.2.d. Electron-impact excitation & autoionization (`ImpactExcitationAutoIon`)

Process & notations:

➢ Electron-impact excitation & autoionization of an atom or ion: ... $A \,+\, e_s^- \;\;\longrightarrow\;\; A^* \,+\, e_s^{-'} \;\;\longrightarrow\;\; A^{+(*)} \,+\, e_s^{-'} \,+\, e_a^-$

➢ Formal quantum notation: $|\alpha_i \mathbb{J}_i\rangle \,+\, |\varepsilon_i \kappa_i\rangle \;\;\longrightarrow\;\; |\alpha_r \mathbb{J}_r\rangle \,+\, |\varepsilon_r \kappa_r\rangle \;\;\longrightarrow\;\; |\alpha_f \mathbb{J}_f\rangle \,+\, |\varepsilon_r \kappa_r\rangle \,+\, |\varepsilon_a \kappa_a\rangle$

➢ Using JAC: Perform an `Atomic.Computation(..., process = Jac.xxx, processSettings = ImpactExcitationAutoIon.Settings(), ...` or call directly functions from the module `ImpactExcitationAutoIon`.

7.2.e. Radiative-Auger decay (RadiativeAuger)

Process & notations:

- Radiative-Auger (autoionization) of an atom or ion: $A^{q+*} \longrightarrow A^{(q+1)+(*)} + (e_a^- + \hbar\omega)$
- Formal quantum notation: $|\alpha_i \mathbb{J}_i\rangle \longrightarrow |\alpha_f \mathbb{J}_f\rangle + \hbar\omega(\mathbb{M}) + |\varepsilon_a\, \kappa_a\rangle$
- Using Jac: Perform an `Atomic.Computation(..., process = Jac.xxx, processSettings = RadiativeAuger.Settings(), ...` or call directly functions from the module `RadiativeAuger`.

7.2.f. Multi-photon ionization (MultiPhotonIonization)

Process & notations:

- Multi-photon ionization: of an atom or ion $A + n\,\hbar\omega \longrightarrow A^{(*)} + e_p^-$
- Formal quantum notation: $|\alpha_i \mathbb{J}_i\rangle + \hbar\omega_1(\mathbb{M}_1) + \hbar\omega_2(\mathbb{M}_2) + ... + \hbar\omega_n(\mathbb{M}_n) \longrightarrow |\alpha_f \mathbb{J}_f\rangle + |\varepsilon\, \kappa\rangle$
- Using Jac: Perform an `Atomic.Computation(..., process = Jac.xxx, processSettings = MultiPhotonIonization.Settings(), ...` or call directly functions from the module `MultiPhotonIonization`.

Further information:

- The standard models for multi-photon ionization are typically based on a semiclassical time-dependent description of the laser field and on scattering-theoretical arguments. In these models, the photons and electrons are thus not treated as particles of a truly closed system to which formal scattering theory would be applicable.

7.2.g. Multi-photon double ionization (MultiPhotonDoubleIon)

Process & notations:

➢ Multi-photon double ionization: of an atom or ion $A + n\,\hbar\omega \longrightarrow A^{(*)} + e^-_{p_1} + e^-_{p_1}$

➢ Formal quantum notation: $|\alpha_i \mathbb{J}_i\rangle + \hbar\omega_1(\mathbb{M}_1) + \hbar\omega_2(\mathbb{M}_2) + ... + \hbar\omega_n(\mathbb{M}_n) \longrightarrow |\alpha_f \mathbb{J}_f\rangle + |\varepsilon_1\,\kappa_1\rangle + |\varepsilon_2\,\kappa_2\rangle$

➢ Using JAC: Perform an `Atomic.Computation(..., process = Jac.xxx, processSettings = MultiPhotonDoubleIon.Settings(), ...` or call directly functions from the module `MultiPhotonDoubleIon`.

7.2.h. Internal conversion (InternalConversion)

Process & notations:

➢ Internal conversion of an atom or ion: $A^{q+} + \text{nucleus}^* \longrightarrow A^{(q+1)+*} + e^-_c$

➢ Formal quantum notation: $|\alpha_i \mathbb{J}_i\rangle + \text{nucleus}^*(\{\mathbb{M}\}, \mathcal{E}) \longrightarrow |\alpha_f \mathbb{J}_f\rangle + e^-_c(\mathbf{p}, m_s)$ or
$|\alpha_i \mathbb{J}_i\rangle + \text{nucleus}^*(\{\mathbb{M}\}, \mathcal{E}) \longrightarrow |\alpha_f \mathbb{J}_f\rangle + |\varepsilon\,\kappa\rangle\,,$ $\varepsilon = \mathcal{E} - (E_i - E - f)$

➢ Here, the excited nucleus decays by (several) multipoles $\{\mathbb{M}\}$ and releases the energy $\mathcal{E}$, leading to an emitted electron with kinetic energy ε.

➢ Using JAC: Perform an `Atomic.Computation(.., process=Jac.Conversion, processSettings=InternalConversion.Settings(..), ..)` or call directly functions from the module `InternalConversion`.

Motivation:

- Internal conversion: refers to the (decay) process in which an excited nucleus undergoes a transition to its ground or some lower-lying level and in which the excitation energy is given to an electron, leading to an ionization of the atom or ion. In general, this internal (energy) conversion, gamma-ray emission as well as electron-positron pair formation (for nucear excitation energies above 1.022 MeV) are competing processes.
- However, internal conversion does not constitute a simple photoionization process in which an emitted γ photon leads to the emission of electrons but it refers to an alternate de-excitation pathway of excited nuclei.
- The internal conversion process (ICP) has been found a versatile tool for studying nuclear structure. The measurement and analysis of conversion electron spectra reveal possible transitions between nuclear levels. By comparing these spectra with calculated internal conversion coefficients, it is often possible to assign a unique multipolarity to the nuclear gamma radiation and, hence, a total angular momentum and parity to the excited nuclear states.
- The internal conversion coefficients can provide detailed information about the atomic nucleus, if theoretical and experimental values are compared for transitions of different multipolarity and mixing ratios. A detailed knowledge of these coefficients is needed for determining absolute transition rates and for the normalization of decay schemes, for Mössbauer spectrocopy, for nuclear reaction computations as well as for the calculation of the decay heat of the fuell cells of nuclear reactors.

General theory:

- The internal conversion process can be described by means of the quantum theory of retarded charge interactions.
- In particular, the internal conversion is a second-order quantum electrodynamical process in which a virtual photon is exchanged between the nucleus (proton) and an electron.
- Internal conversion amplitude: The (single-electron) matrix element of the conversion transition can be written as (Listengarten ...; Band *et al.*, 2002)

$$\left\langle f \left| \, \mathbb{H}^{(\text{conversion})} \, \right| i \right\rangle \;=\; -e \int d^3\mathbf{r}\; \psi_f^*(\mathbf{r}) \;\; [\, \Phi(\mathbf{r}) \;+\; \boldsymbol{\alpha} \cdot \mathbf{A}(\mathbf{r}) \,] \;\; \psi_i(\mathbf{r}),$$

where $\Phi(\mathbf{r})$ and $\mathbf{A}(\mathbf{r})$ are the time-independent parts of the scalar and vector potentials of the electromagnetic field that arise due to the nuclear transition charges and currents, and by including the retardation of these interactions.

➢ The retarded potentials in the internal conversion amplitude above are

$$\Phi(\mathbf{r},t) \;=\; e^{-i\,\omega\,t}\,\Phi(\mathbf{r}), \qquad \Phi(\mathbf{r}) \;=\; \int d^3\mathbf{R}\,\frac{\rho\mathbf{R}}{|\mathbf{r}\,-\,\mathbf{R}|}\,e^{i\,k\,|\mathbf{R}\,-\,\mathbf{R}|} \;=\; \sum_{LQ}\,\Phi_{LQ}(\mathbf{r})$$

$$\mathbf{A}(\mathbf{r},t) \;=\; e^{-i\,\omega\,t}\,\mathbf{A}(\mathbf{r}), \qquad \mathbf{A}(\mathbf{r}) \;=\; \frac{1}{c}\int d^3\mathbf{R}\,\frac{\mathbf{Jr}}{|\mathbf{R}\,-\,\mathbf{R}|}\,e^{i\,k\,|\mathbf{R}\,-\,\mathbf{R}|} \;=\; \sum_{LQ}\,\mathbf{A}_{LQ}(\mathbf{r})$$

with the wavenumber $k = \omega/c = \mathcal{E}/\hbar\,c$, and where $\mathbf{r} = (r,\vartheta,\varphi)$ and $\mathbf{R}$ are the coordinates of the electron and nucleus (proton), respectively.

➢ Here, we shall not go into the details for the representation of these potentials but just note that these interaction potentials can be written as sum over multipole contributions as well as in terms of the nuclear charge density $\rho\mathbf{R}$ and current density $\mathbf{Jr}$, respectively.

Internal conversion coefficients:

➢ The internal conversion coefficient is defined as the ratio of the number of electrons N_e ejected from the i-th atomic shell to the number of gamma quanta N_γ leaving the atom during the same time:

$$\alpha^{\,(\mathrm{conversion})}(\alpha_i\mathbb{J}_i \;\rightarrow\; \alpha_f\mathbb{J}_f) \;=\; \frac{N_e}{N_\gamma}, \qquad \alpha^{\,(\mathrm{conversion})}(\alpha_i\mathbb{J}_i) \;=\; \sum_f\,\alpha^{\,(\mathrm{conversion})}(\alpha_i\mathbb{J}_i \;\rightarrow\; \alpha_f\mathbb{J}_f)$$

The total internal conversion coefficient of a given (initial) level $\alpha^{\,(\mathrm{conversion})}(\alpha_i\mathbb{J}_i)$ is the sum of partial conversion coefficient associated with all possible ionization channels (lines) of the atom or ion.

Further information:

➢ Internal conversion coefficients have been tabulated in a larger number of tables and compilations; in these tabulations, the screening of the nuclear electric field by the atomic electrons was often treated in the framework of either some statistical Thomas-Fermi-Dirac or Dirac-Fock-Slater models.

➢ For different x_α pre-factors in the Dirac-Fock-Slater (type) potentials, the differences in the calculated conversion coefficients are typically small ~ 1 % for K-shell electrons but may increase to ~ 70 % for outer electrons and even larger when the kinetic energy of the conversion

electron is low ($\leq$ 1 keV). The question of whether the hole should be incorporated into the potential or not has been explored previously and lead to a slight preference for noninclusion.

7.2.i. Electron capture with nuclear decay

Process & notations:

- Electron capture of an atom or ion by nuclear decay: $A(Z+1) + e^- \longrightarrow A(Z) + \nu_e$
- Formal quantum notation: $E_\nu = Q^+ - E_f - E_b > 0$
- Here, the nucleus decays by capturing an atomic electron (often from the K-shell) and under the emission of an electron. Q^+ is the energy difference due to the rest masses of the parent and daughter nucleus, E_f the energy of the final nuclear state of the daughter nucleus and E_b the binding energy of the captured electron. The release energy E_ν will be shared between the emitted neutron and, possible, some bremsstrahlungs photon or some shaked valence electron.
- Using JAC: Perform an `Atomic.Computation(.., process=Jac.Conversion, processSettings=InternalConversion.Settings(..), ..)` or call directly functions from the module `InternalConversion`.

Motivation:

- For allowed transitions, nearly all vacancies occur in the ns shells, mainly for the K, L_1 , M_1 , etc.

7.3. Further processes, not yet considered in JAC

7.3.a. Electron-impact ionization (ImpactIonization)

Process & notations:

➢ Electron-impact ionization of an atom or ion: $e_s^- + A \longrightarrow A^* + e_s^{-\prime} + e^-$

➢ Formal quantum notation: $|\alpha_i \mathbb{J}_i\rangle + |\varepsilon_i\, \kappa_i\rangle \longrightarrow |\alpha_f \mathbb{J}_f\rangle + |\varepsilon_f\, \kappa_f\rangle + |\varepsilon_a\, \kappa_a\rangle$ where $|\varepsilon_c\, \kappa_c\rangle$ is the initially bound *atomic* electron.

➢ Using JAC: Perform an `Atomic.Computation(..., process = Jac.xxx, processSettings = ImpactIonization.Settings(), ...` or call directly functions from the module `ImpactIonization`.

Motivation:

➢ The electron-impact ionization process is important in all (high-temperature) plasma.

➢ We refer to the three *free* electrons, that are involved in this process, as incident, (final-) scattered and additional (-ly released) electron, and with the corresponding indices above.

Cross sections:

➢ Electron-impact ionization cross section: These cross sections are obtained similarly as the electron-impact excitation cross section but by allowing an ionizing transition between fine-structure levels $\alpha_i \mathbb{J}_i(N) \rightarrow \alpha_f \mathbb{J}_f(N-1)$ (Fontes *et al.* 2015)

$$\sigma\,(\text{ionization})(\alpha_i \mathbb{J}_i, \alpha_f \mathbb{J}_f) \;=\; \frac{8}{k_i^2\, g_i} \sum_{\mathbb{J}_s,\, \mathbb{J}_t} (2J_s + 1) \sum_{\kappa_i \kappa_f \kappa_e} \int_0^{\varepsilon_i - I_p} \varepsilon' \left| \left\langle (\alpha_f \mathbb{J}_f,\, \epsilon_a \kappa_a)\, \mathbb{J}_t \,\middle\|\, \mathbb{V}^{(\mathrm{e-e})} \,\middle\|\, \alpha_i \mathbb{J}_i \right\rangle \right|^2$$

➢ This cross section contains a summation over all possible values $\mathbb{J}_t$ of the final ion and the (additionally) released electron due to the impact of the incident electron $\varepsilon_i \kappa_i$

7.3.b. Coulomb ionization (CoulombIonization)

Process & notations:

- Coulomb ionization by fast, heavy ions: $A^{(q+1)+} + Z_p \longrightarrow A^{(q+1)+(*)} + e^- + Z'_p$
- Formal quantum notation: $|\alpha_i \mathbb{J}_i\rangle + Z_p(...) \longrightarrow |\alpha_f \mathbb{J}_f\rangle + e^-$

7.3.c. Double-Auger decay (DoubleAuger)

Process & notations:

- Simultaneous double Auger (autoionization) of an atom or ion:
- Formal quantum notation: $|\alpha_i \mathbb{J}_i\rangle \longrightarrow |\alpha_f \mathbb{J}_f\rangle + |\varepsilon_1\, \kappa_1\rangle + |\varepsilon_2\, \kappa_2\rangle$

7.3.d. Radiative double electron capture

Process & notations:

- Radiative double electron capture (RDEC) of an ion:
- Formal quantum notation: $|\alpha_i \mathbb{J}_i\rangle + ... \longrightarrow$

Motivation:

- Double photoionization of atoms has attracted much interest during the last decades as the emission of a second electron is caused by the electron-electron interaction.

7.3.e. Interference of multi-photon ionization channels (MultiPhotonInterference)

Process & notations:

- ➢ Interference of non-resonant one-photon (2ω) and resonant two-photon (ω) ionization of an atom or ion:
- ➢ Formal quantum notation: $|\alpha_i \mathbb{J}_i\rangle + ... \longrightarrow$

Motivation:

- ➢ Two-pathway quantum interference process has been manipulated in order to obtain quantum control.
- ➢ Such quantum control studies were initially stimulated by the small fraction of the second harmonic that typically arise at XFEL and which is often difficult to be filtered out, though it can strongly influence the experimental from two-photon ionization experiments. Despite the rather small intensity of the second harmonic, the ionization by photons with frequency $2\,\omega$ (second harmonic, first-order process) can readily compete with, or even dominate, the two-photon ionization by photons with frequency ω.

Interference of non-res. one-photon (2ω) and resonant two-photon (ω) ionization:

- ➢ For a linearly-polarized bichromatic beam, the interference due to different quantum pathes manifests itself in an asymmetry of the photoelectron angular distributions (PAD) with respect to the plane that is perpendicular to the electric field of the incident radiation; cf. Grum-Grzhimailo *et al.*(2015).
- ➢ Photoelectron angular distribution (PAD): In the dipole approximation and for an isotropic target, this angular distribution must be axially symmetric with regard to the polarization direction

$$\frac{dW}{d\Omega} = \frac{W_o}{4\pi}\left[1 + \sum_{k=1}^{K} \beta_k\, P_k(\cos\vartheta)\right]$$

where ϑ is the angle of the photoelectron with regard to the polarization direction (E-field). The β_k denote the anisotropy parameters, which can expressed in terms of the photoionization amplitudes.

- ➢ For a combination of one-photon and two-photon ionization paths, all terms with $k = 1, 2, 3, 4$ should be accounted for in the equation above. The odd polynomials appear due to coherent creation of photoelectron partial waves with opposite parities by the fundamental and the second harmonic of the radiation.

Scattering cross sections:

➢ Möller cross section for free electron-electron scattering: In Born approximation, this electron-electron scattering cross sections is given by (Rohrlich and Carlson, 1954)

$$\left(\frac{d\sigma}{d\varepsilon}\right)^{(\mathrm{e-e})} = \frac{\chi}{T}\left[\frac{1}{\varepsilon^2} + \frac{1}{(1+\varepsilon)^2} + \left(\frac{\gamma-1}{\gamma}\right)^2 - \frac{2\gamma-1}{\gamma^2}\cdot\frac{1}{\varepsilon\,(1-\varepsilon)}\right], \qquad \gamma = \frac{2\pi\,e^4}{mv^2} = \frac{2\pi\,r_o^2\,mc^2}{\beta^2}, \qquad r_o = \frac{e^2}{mc^2}$$

Here, the incident total energy is $E = \gamma\,mc^2$, the kinetic energy is $T = (\gamma-1)\,mc^2$ and ε is the energy transfer in units of T.

➢ Bhabha cross section for free electron-positron scattering: In Born approximation, this electron-electron scattering cross sections is given by (Rohrlich and Carlson, 1954)

$$\left(\frac{d\sigma}{d\varepsilon}\right)^{(\mathrm{e-p})} = \frac{\chi}{T}\left\{\frac{1}{\varepsilon^2} - \frac{\gamma^2-1}{\gamma^2}\cdot\frac{1}{\varepsilon} + \frac{1}{2}\left(\frac{\gamma-1}{\gamma}\right)^2 - \left(\frac{\gamma-1}{\gamma+1}\right)\left[\frac{\gamma+2}{\gamma}\cdot\frac{1}{\varepsilon} - 2\,\frac{\gamma^2-1}{\gamma} + \varepsilon\left(\frac{\gamma-1}{\gamma}\right)^2\right]\right.$$
$$\left. + \left(\frac{\gamma-1}{\gamma+1}\right)^2\cdot\left[\frac{1}{2} + \frac{1}{\gamma} + \frac{3}{2\gamma^2} - \left(\frac{\gamma-1}{\gamma}\right)^2\varepsilon\,(1-\varepsilon)\right]\right\}$$

Process & notations:

➢ Non-radiative electron capture of an ion: $\ldots\ |\alpha_i \mathbb{J}_i\rangle + |\epsilon\kappa_c\rangle \longrightarrow |\alpha_f \mathbb{J}_f\rangle + \ldots$

➢ Formal quantum notation: $|\alpha_i \mathbb{J}_i\rangle + \ldots$

Process & notations:

➢ Vacuum electron capture of an ion: $\ldots\ |\alpha_i \mathbb{J}_i\rangle + |\epsilon\kappa_c\rangle \longrightarrow |\alpha_f \mathbb{J}_f\rangle + \ldots$

- Formal quantum notation: $|\alpha_i \mathbb{J}_i\rangle + ...$
- For vacuum capture, the target is considered to act as an perturbing potential that excites an electron-positron pair in the field of the projectile nucleus. While the electron is captured in one of the bound states (predominantly into $1s$), the positron is emitted.

7.4. Other topics closely related to atomic processes

7.4.a. Atomic databases

CHIANTI: A database for emission lines:

- CHIANTI is a database of assessed atomic parameters and transition rates needed for the calculation of the line and continuum emission of optically thin, collisionally-dominated plasma.
- CHIANTI was first released in 1996 and since then various new releases have been made available in order to expand the database and improve the quality of the data. Emphasis has been given especially to the line identifications and improvement of the reference wavelengths.
- For several ions, the wavelengths and identifications are different from and more accurate than those of the NIST database. Therefore, CHIANTI is now often used as a reference atomic database for ions and has been included in several other atomic codes and packages.
- In its last version (Del Zanna *et al.*, 2015), the CHIANTI database includes a large amount of new data and ions which improvement the soft X-ray, extreme UV (EUV) and UV spectral regions, which several space missions currently cover.

NIST-XCOM:

- The XCOM database provides photon scattering data and attenuation coefficients between 1 keV and 100 GeV for all the elements of the periodic table. It also lists total cross sections, attenuation coefficients and partial interaction coefficients for selected processes, such as Compton and Rayleigh scattering, photoelectric absorption as well as pair production (Amako *et al.*, 2005).

NIST-ESTAR:

➢ The ESTAR database provides stopping powers and ranges of electrons as a function of energy between 10 keV and 1 GeV, derived from the so-called ICRU Report (Amako *et al.*, 2005).

NIST-PSTAR:

➢ The PSTAR and ASTAR databases provide stopping powers and ranges of protons and in the energy intervals 1 keV – 10 GeV and 1 keV – 1 GeV, respectively, and were derived from the so-called ICRU Report 49.

7.4.b. Other codes with atomic data input

Codes from astro and plasma physics:

➢ Radiative-Collisional code based on FAC, RCF: This code has been used to simulate steady-state plasmas under non-local thermodynamic equilibrium condition, especially photoinization-dominated plasmas. RCF takes almost all of the radiative and collisional atomic processes into a rate equation to interpret the plasmas systematically. The Flexible Atomic Code (FAC) supplies all the atomic data needed for RCF, which insures calculating completeness and consistency of atomic data.

➢ RCF is a steady-state, collisionalradiative, optically thin model. Its rate-equation

$$\frac{dN_{i,j}}{ddt} = \text{populating process} - \text{depopulating process} = 0$$

where $N_{i,j}$ is the density of the j-th level of the i-th charge state. The processes included are the ionization and recombination between neighboring charge states as well as the excitation and de-excitation within the same charge state. Their inverse processes are typically taken into account by the detailed balance principle.

7.4.c. Radiative opacity

Motivation:

➢ The radiative opacity of a plasma is of great significance for various research fields, such as inertial confinement fusion, stellar physics as well as the development of x-ray lasers. The (so-called) Opacity Project calculated the atomic data for most astrophysically abundant elements and set a database of opacities.

➢ Knowing the opacity of a plasma, the fraction of transmitted radiation with regard to some incident radiation of given intensity can be expressed as:

$$F(h\nu) \;=\; \exp\left(-\rho\,\eta'(h\nu)\,L\right)$$

where L is the path length of the light through the plasma, ρ the mass density and $\eta'(h\nu)$ the radiative opacity. This fraction can be readily determined experimentally and can be obtained theoretically by taking the integral over a Gaussian function, and where the full width corresponds to the spectrometer resolution.

Definition of detailed and mean radiative opacities:

➢ For a plasma in a local thermodynamic equilibirum at temperature T and mass density ρ, the radiative opacity $\eta(\hbar\omega)$ is given by (Cheng and Jiaolong, 2008)

$$\rho\,\eta(\hbar\omega)... \;=\; \left[\mu^{(\text{bound}-\text{bound})}(\hbar\omega) \;+\; \mu^{(\text{bound}-\text{free})}(\hbar\omega) \;+\; \mu^{(\text{free}-\text{free})}(\hbar\omega)\right] \;\left(1 \;-\; \exp\left(\frac{\hbar\omega}{k_B\,T}\right)\right) \;+\; \mu^{(\text{scattering})}(\hbar\omega)$$

where $\mu^{(\text{bound}-\text{bound})}$, $\mu^{(\text{bound}-\text{free})}$, $\mu^{(\text{free}-\text{free})}$ and $\mu^{(\text{scattering})}$ are the absorption coefficients due to bound-boud, bound-free, free-free and well as scattering processes, respectively.

➢ Cheng and Jiaolong (2008) provides a brief description how the various absorption coefficients can be computed from the excitation and photoionization cross sections.

➢ The Rosseland and Planck mean opacities are required for many practical applications such as radiative transfer.

➢ Rosseland mean opacity: With $u \;=\; \frac{\hbar\omega}{k_B\,T}$, the Rosseland opacity is defined by

$$\frac{1}{K^{(\text{Rosseland})}} \;=\; \int_0^\infty du\;\frac{W^{(\text{Rosseland})}}{\eta(u)}\,; \qquad\qquad W^{(\text{Rosseland})} \;=\; \frac{15}{4\,\pi^4}\;\frac{u^4\,e^{-u}}{(1\;-\;e^{-u})^2}$$

➢ Planck mean opacity:

$$\frac{1}{K^{\,(\mathrm{Planck})}} \;=\; \int_0^\infty du\, W^{\,(\mathrm{Planck})}\,[\eta(u) \;-\; \eta^{\,(\mathrm{scattering})}(u)]\,; \qquad\qquad W^{\,(\mathrm{Planck})} \;=\; \frac{15}{\pi^4}\,\frac{u^3\,e^{-u}}{(1\;-\;e^{-u})}$$

7.4.d. Opacities for astrophysical matter clouds

Neutron star mergers:

➢ Neutron stars: Neutron star have been postulated already short after the discovery of the neutron as the ultimate fate of massive stars, ending in supernova. The existence of neutron stars was later shown in the 1960s due to the observation of first pulsars.

➢ Today, the equation of state and the distribution of neutron star masses are believed to be known reasonably well.

➢ Modern simulations of neutron star mergers take into account both, the (elemental) composition of the ejecta as well as the neutrino wind along the poles.

➢ A current question is whether the mergers lead to a robust r-process environment that can produces heavy neutron-rich isotopes with mass $A \geq 130$, and in proportions similar to solar abundance (Thielemann *et al.*, 2017).

Gravitational-wave astronomy:

➢ The discovery of gravitational waves (GW) from the inspiral and coalescence of binary black holes (BH) and/or neutron stars (NS) by the Laser Interferometer Gravitational Wave Observatory (LIGO) has opened a new window on the cosmos.

➢ In the neutron-rich ejecta from double neutron star (NS-NS) and BH-NS binaries, in particular, the so-called r-process nucleosynthesis (rapid neutron capture) is expected to proceed rapidly, leading to many heavy elements like gold, platinum and many others.

➢ Kilonova Kilonovae are day to week-long thermal, supernova-like transients, which are powered by the radioactive decay of heavy, neutron-rich elements synthesized in the expanding merger ejecta. The radioactive decay of such unstable neutron-rich nuclei powers a rapid evolution of a supernova-like transition of stellar matter that is known as kilonova or macronov in the literature. These kilonovae can be understood also as roughly isotropic electromagnetic counterpart to the GW signal and, thusm provide a unique and direct probe of such r-process sites (Metzger 2017).

- ➢ In practice, however, it is not easy to precisely locate the sky positions of the GW sources which need to be determined by triangulating the arrival times of the GW signals by different detectors. At present, the uncertainties in this triangulation are quite large (initially $\approx$ 850 deg^2 for GW15091 and with a later improvement to $\approx$ 250 deg^2), though these uncertainties will be reduced to $\approx$ $10-100$ deg^2 , once Virgo in Italy and, eventually, KAGRA in Japan and LIGO-India will join the network (Metzger 2017).
- ➢ Nevertheless, even an localisation of the GW signals within $10-100$ deg^2 greatly exceed the fields of view of most radio, optical and x-ray telescopes, and in particular those telescopes that are sensitive enough to detect the electro-magnetic counterparts of NS-NS and BH-NS mergers.
- ➢ The discovery of electromagnetic signals in coincidence with chirp at the graviational-wave detectors leads to a better location and a much richer picture about the merger process. This may allow to extract directly information on the binary formation channels, the age of the stellar population as well as the dynamics of binary mergers.

r-process:

- ➢ Burbidge *et al.* (1957) and Cameron (1957) realized already more than 60 years ago that approximately half of the elements heavier than iron are synthesized via the capture of neutrons onto lighter seed nuclei like iron in a dense neutron-rich environment in which the timescale for neutron capture is shorter than the lifetimes for β-decay.

Astrophysical opacities models:

- ➢ A new astrophysical opacity model (called OPAL) has been developed at the Lawrence Livermore National Laboratory (LLNL) with which it was shown that $\Delta n = 0$ transitions results in overlapping lines. This overlap significantly increase the opacity of the iron component of the mixture and which was suggested also by observation of stellar pulsations

Opacities for ejecta from neutron-star mergers:

- ➢ In general, the merger of stellar mass BH-BH binaries is not expected to produce luminous electro-magnetic emission because there is not enough baryonic matter in these systems.
- ➢ Despite of a rather large number of the expected BH-BH mergers during the next few years, a better synthesis and analysis of GW and the associated electro-magnetic signals will probably come from NS-NS or BH-NS mergers, i.e. if neutron stars are involved.
- ➢ The ejecta from NS-NS binaries is hot immediately after the merger; however, this thermal energy can initially not escape so easily as radiation owing to its high optical depth just after the merger (Metzger 2017)

$$\tau \;=\; \rho\,\kappa\,R \;=\; \frac{3M\,\kappa}{4\pi\,R^2} \;\propto\; 70\,\left(\frac{M}{10^{-2}\,M_\odot}\right)\,\left(\frac{\kappa}{\mathrm{cm}^2\,\mathrm{g}^{-1}}\right)\,\left(\frac{v}{0.1\,c}\right)^{-2}\,\left(\frac{t}{\mathrm{day}}\right)^{-2}$$

where $\rho = 3M/(4\pi R^3)$ is the mean density and κ the opacity, i.e. the cross section per unit mass. When the ejecta expands, the diffusion time of the photons decreases with $t^{\,(\mathrm{diffusion})} \propto 3M\,\kappa/4\pi\,c\,vt$ until the radiation can escape eventually, once we have $t^{\,(\mathrm{diffusion})} = t$.

Opacity calculations:

- ➢ Radiative opacities are required for the modeling of astrophysically relevant plasmas under local thermodynamic equilibrium (LTE) conditions. For the computation of these opacities, the atomic structure calculations should be carried out for all fine-structure levels and by including configuration interactions.
- ➢ Three typical example applications for opacity calculations are: (i) iron opacities at conditions of the solar convection zone, (ii) nickel opacities for modeling various stellar envelopes and (iii) the samarium opacities for the modeling of light curves as produced by neutron star mergers.
- ➢ In recent work, the frequency-dependent LTE opacity of iron has been studied for the conditions of the base of the solar convection zone. These studied revealed rather large (30-400%) differences between experiment and theory for the monochromatic opacity of an neon-like iron plasma (or nearby charge states). Until the present, the source of this not yet understood and remains an active area of research.

Opacity measurements for homogeneous plasma with uniform density:

➢ Uniform plasma density: For a uniform density, the transmisison of the sample

$$T(\omega) \;=\; \frac{I(\omega)}{I_o} \;=\; \exp\left(-\,\rho\,L\,\kappa(\omega)\right)$$

is measured where $I(\omega)$ is the attenuated intensity of the probe (backlighter) radiation and I_o the reference intensity. This transmission is related also to opacity by the Beer-Lambert law if the reabsorption can be neglected in the homogeneous plasma. Here, ρ is the density of the material and L its thickness.

7.4.e. Ionization equilibria in astrophysical sources

Astrophysical observation of EUV spectra:

➢ High-quality EUV spectra: The Solar EUV Rocket Telescope and Spectrograph (SERTS, 1992) and the Extreme Ultraviolet Explorer (EUVE, 1990) spectrometers provided high-quality EUV spectra and helped improve the diagnostics of high temperature plasmas.

➢ The ability to resolve a large number of individual emission lines and to measure accurate intensities over a wide wavelength range have allowed to analyze the temperatures, densities and abundances of elements in a variety of astrophysical sources (Brickhouse *et al.*, 1995).

➢ The fine structure of (line) multiplets nowadays allow to solve the full rate equations for several atoms in the plasma, including collisions among all levels and cascades. This enables one to calculate also the emissivities of weak lines that were previously omitted from the investigation.

7.4.f. Synthetic spectra for laser-induced breakdown spectroscopy (LIBS)

Laser-induced breakdown spectroscopy:

➢ The laser-induced breakdown spectroscopy (LIBS) has been found a versatile analytical tool with various applications.

- In this technique, a high-power laser beam is typically focused onto the surface of a sample for analysis and, if the laser power exceeds a certain threshold, an optical breakdown occurs. In practice, the breakdown threshold depends on the wavelength and duration of the laser pulses as well as the analyzed media.
- For a nanosecond laser ablation, for example, the threshold varies from $1.9 \cdot 10^8$ W cm^{-2} for copper up to $10^{10\,..\,11}$ W cm^{-2} for aqueous solutions (Yaroshchyk *et al.* 2006).
- A plasma, i.e. a gas of highly-ionized atoms, is formed during the breakdown with an electron density of $10^{16\,..\,20}$ cm^{-3} for typical Nd:YAG laser-induced plasmas.

Computation of LIBS spectra:

- Ciucci *et al.* (1999) first estimated within a certain accuracy the composition of a laser-induced plasma by using computational methods instead of calibration standards. Their computation were based on the assumption that the plasma and sample compositions are the same and that the plasma is optically thin and in local thermal equilibrium (LTE) during the observation.
- The code by Yaroshchyk *et al.* (2006) is also based on the assumption of a LTE and a well-defined plasma temperature and electron density; it takes a number of characteristics atomic emission lines as input to create a synthesized theoretical emission spectrum of selected elements which are compared to the spectra of four separate compact spectrometers covering the spectral region 185–950 nm.

7.4.g. Plasma light sources for nanolithography

EUV light sources:

- Ions with several open shells: The (correlated) electronic structure of medium and heavvy ions with several open shells is both, tedious and difficult to calculate, and their complex level structure often hampers a straightforward experimental assignment.
- EUV light at 13.5-nm wavelength: In order to generate extreme ultraviolet (EUV) light at 13.5-nm wavelength by laser-produced plasmas, the emission of multiply-charged tin ions have been found promising for nanolithographic applications. For these ions, the EUV light is generated by thousands of transitions that form so-called unresolved transition arrays (UTA) with rather little dependence on the particular charge state (Winderberger *et al.*, 2016).
- For multiply charged tin ions with a [Kr] $4d^m$ $m = 6..0$ configuration, the upper configurations for an EUV emission are [Kr] $(4p^6 4d^{m-1} 4f + 4p^6 4d^{m-1} 5p + 4p^5 4d^{m1})$ (Winderberger *et al.*, 2016).

7.4.h. Decay of medical radioisotopes

Radioisotopes used in clinical therapy:

- Most radioisotopes that are used in clinical therapy emit β particles, i.e. ionizing radiation. The biological effect of this radiation is often characterized by the so-called linear energy transfer (LET) and measured in units of [keV/μm] for the deposited energy along the particle track.
- A new class of radionuclides including ^{149}Tb, ^{213}Bi, ^{211}Po, ^{211}A, ^{223}Ra, ^{225}Ac, ^{227}Ac, ^{226}Th and ^{230}U, which all emit α, have been considered for therapy. The LET for most therapeutic α emitters ranges from 25 to 230 [keV/μm].
- In addition, electrons and positrons emitted in the nuclear β decay and the internal conversion processes have kinetic energies ranging from tens of keV to several MeV and their LET is much lower, typically 0.2 [keV/μm].

7.4.i. X-ray absorption of solid-state materials

Motivation:

- X-ray near-edge absorption (XANES): XANES as well as the related spectroscopies such as the resonant x-ray scattering (RXS) and x-ray magnetic circular dichroism (XMCD), are powerful spectroscopic techniques for probing the electronic structure around the absorbing atom (Bunau and Joly, 2009).
- In the near-edge region, one is very sensitive to the surroundings of the absorbing atom. This makes absorption spectroscopies a very useful tool to investigate geometric and electronic structure.
- In x-ray absorption spectroscopy, there has been a great need for codes that help reproduce the near-edge structure within a reasonable calculation time.
- These codes can be classified into two major categories: i) multi-electronic but monoatomic codes which are based on some multiplet theory and which give rise to a proper parametrized description of the localized electronic state, while the delocalized states can often not be decribed correctly. ii) multi-atomic but mono-electronic codes which provide correct description of the extended states but fail to account for the highly correlated state that interact with the core hole (for example, for the calculation of the L2 and L3 edges of the 3d elements).

7.4.j. Configuration-averaged energies and cross sections

Configuration-averaged energies:

➢ Cowan (1981)provides a non-relativistic expression for the configuration-averaged energy as it often occurs in the computation of radiative and collisional rates (Peyrusse, 1999)

$$E_c \;=\; \sum_a N_a \,\langle a\rangle \;+\; \sum_{ab} N_a\,(N_b \;-\; \delta_{ab})\;\langle a,b\rangle$$

$$\langle a\rangle \;=\; \varepsilon_a \;+\; \left\langle a\,\middle|\, -V^{\,(\mathrm{SCF})}(r) \;-\; \frac{2\,Z}{r}\,\middle|\, a\right\rangle, \qquad\qquad \langle a,b\rangle \;=\; \frac{1}{2}\,\frac{g_a}{g_a \;-\; \delta_{ab}}\left[R^{(0)}(ab,ab) \;-\; \frac{1}{2}\sum_k \begin{pmatrix} \ell_a & k & \ell_b \\ 0 & 0 & 0 \end{pmatrix}^2 R^{(k)}(ab,ba)\right].$$

Here, $g_a \;=\; 2(2\ell_a + 1)$ is the degeneracy of subshell a, $V^{\,(\mathrm{SCF})}(r))$ is the self-consistent atomic potential and R is the non-relativistic Slater integral.

Configuration-averaged cross sections:

➢ Peyrusse (1999) also provides non-relativistic expressions for the configuration-average radiative rates as well as for the configuration-average excitation strengths.

7.4.k. Mass attenuation coefficients

Attenuation coefficients:

- xxxxx The photon mass attenuation coefficient is calculated as This coefficient is related to the cross section of that process ac- cording to the equation (1) where represents the density of the target material, is the thickness of the slab along the incident photon direction, is the number of incident photons, is the number of photons traversing the target without interacting.
- A partial interaction coefficient can be calculated con- sidering only a single interaction process (Rayleigh scattering, Compton scattering, pair production, and photoelectric effect). This coefficient is related to the cross section of that process ac- cording to the equation where represents the atomic mass of the target material and is Avogadro number.

$$C_6 \;=\; \frac{3}{\pi}\int_0^\infty d\omega\,[\alpha^{(\mathrm{E1})}(i\,\omega;\;\beta_o \mathbb{J}_o M_o)]^2\;.$$

-

-

8. Atomic cascades

Cascades approaches

- Average singe-configuration approach (averageSCA): ... only one 'common set of orbitals' for all ionization stages of the atom and of 'configuration-averaged' data throughout the simulations.
- Singe-configuration approach (SCA): ... applies a common set of orbitals for each ionization stage of the atom.
- Multiple-configuration approach (MCA): ... incorporates also electron-electron correlations by configuration mixing contributions with closeby-lying configurations; it 'groups' the configurations together by using physical insight into the cascade process.

8.1. In JAC implemented cascade approximations

Average singe-configuration approach (averageSCA):

- ... only partly implemented yet.
- This approach makes use of only one "common set of orbitals" for all ionization stages of the atom and of "configuration-averaged" data throughout the simulations; we here use the orbital set from the singly-charged ion to compute all necessary cross sections and rates.
- Approximate configuration averaged and decay rates are applied throughout by simply averaging over all fine-structure levels, rates and cross sections.
- For dealing with continuum electrons, we use approximate orbitals without exchange and without any relaxation of the electron density and by only using the first 3-4 (non-vanishing) partial waves in the computation of all photo- and autoionization amplitudes.

8.2. In JAC partly-implemented cascade approximations

Singe-configuration approach (SCA):

- ... not yet implemented.
- This approach applies a common set of orbitals for each given ionization stage of the atom.
- However, all fine-structure (many-electron) transitions amplitudes are calculated explicitly for the selected atomic processes.

9. Field- and collision-induced atomic responses

Atoms in intense laser pulses

- ➢ Atoms, which are irradiated by intense laser pulses, can emit radiation at multiples of the laser frequency, the (high) so-called harmonics.
- ➢ Such high-order harmonics, i.e. highly-energetic photons, can be produced by focusing either a high-frequency (excimer) laser or some low-frequency laser (Nd:glass, Ti:sapphire) into an atomic gas.
- ➢ Especially for low-frequency lasers, the harmonic spectrum is known to exhibit a characteristic behaviour: A rapid decrease of the yield for the first few harmonics, followed by a plateau and a rather abrupt cut-off.

9.1. Floquet theory

Motivation:

- ➢ Many time-dependent problems in physics are periodic to a good approximation. For such physical systems, the (time) evolution can be solved either directly by numerical integration of the (time-dependent) Schrödinger, and making use of the time-dependent Hamiltonian.
- ➢ Floquet formalism: For a periodic evolution, time-dependent problems can be transformed also into a time-independent problem by applying the Floquet formalism, a very desirable transformation as iime-independent problems can often be solved more efficiently.
- ➢ While, in applying the Floquet formalism, often the Lindblad and Bloch-Redfield master equations are adapted, we note that these equations are derived for a time-independent Hamiltonian. In many cases, however, these standard master equations have still been found useful for solving time-dependent problems.

Floquet ansatz:

➢ Vector potential of a linearly-polarized electric field:

$$\mathbf{A}(t) \;=\; \boldsymbol{\epsilon}\, A_o\, \sin(\omega t); \qquad A_o \;=\; -\frac{c\, E_o}{\omega} \qquad \rightsquigarrow \qquad \mathbf{E}(t) \;=\; \boldsymbol{\epsilon}\, E_o\, \cos(\omega t).$$

➢ Floquet ansatz for the wave function:

$$\psi(t) \;=\; \exp(-i\, E t) \sum_{n=-\infty}^{\infty} \exp(-i\, n\, \omega t)\, \psi_n, \qquad E \;=\; \Re(E) \;-\; i\Gamma/2$$

where the functions ψ_n are often called the harmonic components, while E is the complex quasi-energy of the Siegert state $\psi(t)$ and Γ the total ionization rate of this state.

9.2. In JAC implemented responses

None.

9.3. In JAC partly-implemented responses

None.

9.4. Further responses not yet considered in JAC

9.4.a. Collisional-radiative (CR) models

Basic CR models:

- Collisional radiative models are sometimes called zero-dimensional plasma models. They are often applied in order to calculate atomic state distribution functions for one or more atomic species as function of the particle densities and temperatures. Most CR models assume that the radiative absorption and emission as well as electron-collision processes dominate the plasma and that all other (ion-atom, three-atom, ...) processes are negligible.
- A CR model can be used to calculate the effective emissivity or the effective ionization and recombination rates as function of electron temperature and density. These rates and results can then be applied in plasma transport model for determining local ionization, recombination and radiation effects.
- CR models help determine atomic level population densities of atoms in different plasma environments. Calculations are typically based on the CR recombination and ionization rate coefficients, radiative energy losses as well as on various individual rate coefficients.
- Different CR models can be distinguished due to the – analytic or numerical – treatment of the rate coefficients as well as the number and type of processes, for which such rate coefficients are taken into account.

Approximations:

- CR models are typically built on the level densities $n(p)$ for a serious of levels p_1, p_2, ..., p_N. In general, the relation between the temporal and spatial distribution of the level density $n(p)$ is given by the diffusion equation

$$\left(\frac{\partial\, n(p)}{\partial t}\right)_{\rm CR} \;=\; \frac{\partial\, n(p)}{\partial t} \;+\; \boldsymbol{\nabla}\cdot\left(n(p)\,\boldsymbol{\omega}(p)\right)$$

  Often, several atomic levels are simply combined into a single (effective) level p_e, and where an equal distribution is assumed for all of its physical levels: $n(p) = n(p_e)/g(p_e)$ with $g(p_e)$ being the statistical weight of the effective level p_e.
- If changes in the level density are dominated by radiative and collisional (de-) excitation processes, most CR models simply assume

$$\left(\frac{\partial\, n(p)}{\partial t}\right)_{\rm CR} \;=\; 0 \;=\; P(p) \;-\; n(p)\,D(p)$$

and just solve a matrix equation. Here, $P(p)$ is the collisional and radiative production rate, and $D(p)$ the (so-called) *destructive* factor. The two functions $P(p)$, $D(p)$ can be written in terms of different rate coefficients for electron-impact excitation, ionization as well as for radiative and three-body recombination.

10. Time-evoluation of many-electron atomic state functions and density matrices

10.1. Time-dependent approximations of many-electron states

Time-evolution of ASF:

- ➢ A reliable description of the time-dependent (TD) many-electron dynamics has attracted recent interest in order to theoretically support a real-time analysis and control of the ultrafast electronic and nuclear dynamics of atoms and molecules in intense laser pulses.
- ➢ A computational and conceptual simple approach to the many-electron dynamics is the TD configuration-interaction singles (TD-CIS) method in which only singly excited configurations, relative to the Hartree-Fock ground state, are taken into account in the configuration interaction expansion.
- ➢ Miyagi and Madsen (2013) make use of the TD-CIS method by performing an optimization of the orbitals as well as the expansion coefficients at each time step in the evolution. This separate optimization makes it possible to construct a reasonable accurate wave function with just a relatively small number of electronic configurations. For the optimization, Miyagi and Madsen (2013) utilized the Dirac-Frenkel-McLachlan TD variational principle.

10.2. Time-dependent statistical tensors

Motivation:

- ➢ In physics, Liouville's theorem is known from classical statistical and Hamiltonian mechanics, and it asserts that the phase-space distribution function is constant along the trajectory of the system.

➢ Similarly, the quantum-mechanical analog of Liouville equation describes the time evolution of a mixed state. The quantum form can be obtained by the standard replacements of classical variables with quantum operators and Poisson brackets with commutators.

➢ The Liouville equation for the atomic density matrix ρ reads

$$\frac{\partial \rho}{\partial t} \;=\; -\frac{i}{\hbar}\,[\mathbb{H},\,\rho\,] \;-\; \Gamma\,\rho, \qquad\qquad \mathbb{H} \;=\; \mathbb{H}^{(\mathrm{atom})} \;+\; \mathbb{H}^{(e-\gamma)}$$

where the first term in the Hamiltonian describes the (inner-) atomic and the atom-photon interactions, and the second term the relaxation matrix Γ. This relaxation matrix accounts for the atomic spontaneous decay due to either radiative or nonradiative (Auger) processes of the atom.

10.3. Time-integration of statistical tensors

Motivation:

➢ Various methods can be applies to solve the coupled first-order odg's for the time-evolution of the statistical tensors. Apart from those methods which solve the equations with given accuracy (but typically require the evaluation of the rhs at any given time t), we are mainly interested in *shooting* or *predictor-corrector* methods which makes only use of previous solutions of ρ and $d\rho/dt \;=\; f$ on a equidistant time grid.

Numerical methods:

➢ If we use a step-size h and define $\rho(t_j) \;=\; \rho_j$, $\frac{d\rho}{dt}(t_j) \;=\; f_j$, the following integration formulas can be applied.

➢ Euler's methods:

$$\rho_{j+1} \;=\; \rho_j \;+\; h\,f_j$$

➢ Adams-Bashford methods:

$$\rho_{j+1} = \rho_j + h\left[\frac{3}{2}f_j - \frac{1}{2}f_{j-1}\right]$$

$$\rho_{j+1} = \rho_j + h\left[\frac{23}{12}f_j - \frac{16}{12}f_{j-1} + \frac{5}{12}f_{j-2}\right]$$

$$\rho_{j+1} = \rho_j + h\left[\frac{55}{24}f_j - \frac{59}{24}f_{j-1} + \frac{37}{24}f_{j-2} - \frac{9}{24}f_{j-3}\right]$$

10.4. Time evolution of statistical tensors. Formalism

10.4.a. Liouville equation for the atomic density matrix

Vector potential and state multipoles:

➢ In the electron-photon interaction, the vector potential of the electromagnetic field is typically chosen to fulfill $\mathrm{div}\mathbf{A}(\mathbf{r}_i, t) = 0$.

➢ When the electron-photon interaction Hamiltonian $\mathbb{H}^{(e-\gamma)}$ is applied upon the density operator ρ, we shall consider only processes with one photon.

➢ Moreover, we assume a vector potential for a monochromatio field with frequency ω and wave vector $\mathbf{k} = (\vartheta_k, \varphi_k)$ $(|\mathbf{k}| = \frac{\omega}{c})$ with regard to the coordinates in the laboratory system.

➢ Envelope of the vector potential: For a pulse with (real) envelope $f(t)$, the vector potential then includes two terms

$$\mathbf{A}(\boldsymbol{r}, t) = \mathbf{A}(\mathbf{r})\, f(t)\, e^{-i\omega t} + \mathbf{A}^*(\mathbf{r})\, f^*(t)\, e^{i\omega t}.$$

Liouville equation in the representation of well-defined angular momenta:

➢ Liouville equation: In an atomic basis with well-defined total angular momenta and parity, the Liouville equation can be re-written as

$$\frac{\partial}{\partial t}\,\langle \alpha \mathbb{J}_\alpha M_\alpha \,|\, \rho \,|\, \beta \mathbb{J}_\beta M_\beta \rangle \;=\; -\frac{i}{\hbar}\,(E_\alpha \,-\, E_\beta)\,\langle \alpha \mathbb{J}_\alpha M_\alpha \,|\, \rho \,|\, \beta \mathbb{J}_\beta M_\beta \rangle$$

$$-\,\frac{i}{\hbar}\sum_{\nu \mathbb{J}_\nu M_\nu}\Big(\big\langle \alpha \mathbb{J}_\alpha M_\alpha \,\big|\, \mathbb{H}^{(\mathrm{e}-\gamma)} \,\big|\, \nu \mathbb{J}_\nu M_\nu \big\rangle\,\langle \nu \mathbb{J}_\nu M_\nu \,|\, \rho \,|\, \beta \mathbb{J}_\beta M_\beta \rangle \,-\, \langle \alpha \mathbb{J}_\alpha M_\alpha \,|\, \rho \,|\, \nu \mathbb{J}_\nu M_\nu \rangle \big\langle \nu \mathbb{J}_\nu M_\nu \,\big|\, \mathbb{H}^{(\mathrm{e}-\gamma)} \,\big|\, \beta \mathbb{J}_\beta M_\beta \big\rangle\Big)$$

$$-\sum_{\gamma \mathbb{J}_\gamma M_\gamma}\langle \alpha \mathbb{J}_\alpha M_\alpha \,|\, \Gamma \,|\, \gamma \mathbb{J}_\gamma M_\gamma \rangle\,\langle \gamma \mathbb{J}_\gamma M_\gamma \,|\, \rho \,|\, \beta \mathbb{J}_\beta M_\beta \rangle$$

10.4.b. Time-dependent statistical tensors of atomic lines

Time-dependent statistical tensors:

➢ Statistical tensors: With the substitutions of the statistical tensors from above and the notations $[ab...c] \equiv (2a+1)(2b+1)...(2c+1)$, the

Liouville equation can be written as Grum-Grzhimailo, 2012)

$$
\begin{aligned}
i\hbar\dot{\tilde{\rho}}_{kq}(\alpha\mathbb{J}_\alpha,\beta\mathbb{J}_\beta) \;=\; & -2\pi\sqrt{\frac{\hbar}{c\,k}}\sum_{\nu\mathbb{J}_\nu\,KQ}\\
& \Big[f(t)\,e^{-i(\omega-\omega_{\alpha\nu})t}\sum_{LM\lambda} g_\lambda(-1)^{J_\alpha+J_\beta+K+L}[LK]^{1/2}\,\langle KQ,\,LM\,|\,kq\rangle \begin{Bmatrix} J_\alpha & J_\beta & k\\ K & L & J_\nu\end{Bmatrix} D^L_{M\lambda}(\varphi_k,\vartheta_k,0)\,\Big(\Big\langle\alpha\mathbb{J}_\alpha\Big\|\,\mathbb{T}^{(m)}_L\,\Big\|\nu\mathbb{J}_\nu\Big\rangle + i\lambda\,\Big\langle\alpha\mathbb{J}_\alpha\Big\|\,\mathbb{T}^{(e)}_L\,\Big\|\nu\mathbb{J}_\nu\Big\rangle\Big)\,\tilde\rho_{KQ}(\nu\mathbb{J}_\nu,\beta\mathbb{J}_\beta)\\
& - f^*(t)\,e^{i(\omega-\omega_{\nu\alpha})t}\sum_{LM\lambda} g^*_\lambda(-1)^{J_\beta+k+J_\nu+L}[Lk]^{1/2}\,\langle kq,\,LM\,|\,KQ\rangle \begin{Bmatrix} J_\alpha & J_\beta & k\\ K & L & J_\nu\end{Bmatrix} D^{L\,*}_{M\lambda}(\varphi_k,\vartheta_k,0)\,\Big(\Big\langle\nu\mathbb{J}_\nu\Big\|\,\mathbb{T}^{(m)}_L\,\Big\|\alpha\mathbb{J}_\alpha\Big\rangle - i\lambda\,\Big\langle\nu\mathbb{J}_\nu\Big\|\,\mathbb{T}^{(e)}_L\,\Big\|\alpha\mathbb{J}_\alpha\Big\rangle\Big)\,\tilde\rho_{KQ}(\nu\mathbb{J}_\nu,\beta\mathbb{J}_\beta)\\
& + f(t)\,e^{-i(\omega-\omega_{\nu\beta})t}\sum_{LM\lambda} g_\lambda(-1)^{J_\alpha+J_\beta+K}[LK]^{1/2}\,\langle KQ,\,LM\,|\,kq\rangle \begin{Bmatrix} J_\alpha & J\_beta & k\\ L & K & J_\nu\end{Bmatrix} D^L_{M\lambda}(\varphi_k,\vartheta_k,0)\,\Big(\Big\langle\nu\mathbb{J}_\nu\Big\|\,\mathbb{T}^{(m)}_L\,\Big\|\beta\mathbb{J}_\beta\Big\rangle + i\lambda\,\Big\langle\nu\mathbb{J}_\nu\Big\|\,\mathbb{T}^{(e)}_L\,\Big\|\beta\mathbb{J}_\beta\Big\rangle\Big)\,\tilde\rho_{KQ}(\alpha\mathbb{J}_\alpha\,\nu\mathbb{J}_\nu)\\
& - f^*(t)\,e^{i(\omega-\omega_{\beta\nu})t}\sum_{LM\lambda} g^*_\lambda(-1)^{J_\alpha+K+J_\nu}[Lk]^{1/2}\,\langle kq,\,LM\,|\,KQ\rangle \begin{Bmatrix} J_\alpha & J_\beta & k\\ L & K & J_\nu\end{Bmatrix} D^{L\,*}_{M\lambda}(\varphi_k,\vartheta_k,0)\,\Big(\Big\langle\beta\mathbb{J}_\beta\Big\|\,\mathbb{T}^{(m)}_L\,\Big\|\nu\mathbb{J}_\nu\Big\rangle - i\lambda\,\Big\langle\beta\mathbb{J}_\beta\Big\|\,\mathbb{T}^{(e)}_L\,\Big\|\nu\mathbb{J}_\nu\Big\rangle\Big)\,\tilde\rho_{KQ}(\alpha\mathbb{J}_\alpha,\nu\mathbb{J}_\nu)\Big]\\
& - i\hbar\sum_{\gamma\mathbb{J}_\gamma} G^{KQ}_{kq}(\alpha\mathbb{J}_\alpha,\beta\mathbb{J}_\beta,\gamma\mathbb{J}_\gamma)\,e^{i\omega_{\alpha\gamma}t}\,\tilde\rho_{KQ}(\gamma\mathbb{J}\gamma,\beta\mathbb{J}_\beta)
\end{aligned}
$$

10.5. Observables to be derived from time-dependent statistical tensors

Motivation:

➢ If we solve the set of time-dependent (Liouville) equations for the state multipoles, we can obtain the atomic statistical tensors for
(a) discrete atomic states $\rho_{kq}(\alpha\mathbb{J}_\alpha;\beta\mathbb{J}_\beta)$ (b) for atomic states with one electron in continuum $\rho_{kq}(\alpha_f\mathbb{J}_f,\varepsilon\kappa:\alpha\mathbb{J}_\alpha,\alpha'_f\mathbb{J}'_f,\varepsilon'\kappa':\alpha\mathbb{J}_\alpha)$,
(c) *nondiagonal* elements $\rho_{kq}(\alpha_f\mathbb{J}_f,\varepsilon\kappa:\alpha\mathbb{J}_\alpha,\,\beta\mathbb{J}_\beta)$ and $\rho_{kq}(\alpha_f\mathbb{J}_f,\varepsilon\kappa:\alpha\mathbb{J}_\alpha,\alpha'_f\mathbb{J}'_f,\varepsilon'\kappa':\beta\mathbb{J}_\beta)$.

11. Semiempirical estimates

11.1. In JAC implemented estimates for atomic properties and data

None.

11.2. In JAC partly-implemented estimates for atomic properties and data

11.2.a. Ionization energies

- Their are numerous tabulations for the first and second ionization potentials of (almost) all elements from the periodic table.
- A simple parametrization for the ionization of inner-shell electrons has been worked out by Thayer Watkins for elements from the $n\ell$-shell, although it seems not to be very reliable

$$E_b \;=\; 10.42924\,\left[(Z/n)^2 \,+\, 1.371650145\right]^2 \,-\, 16.76869944 \;=\; -11.0053 \,+\, 10.31048\,(Z/n)^2 \,+\, 28.83251\,(Z/n) \,-\, 2.88439\,\ell$$

- In JAC, an estimate for the binding energy of an $n\ell$-electron in the neutral atom can be obtained from `JAC.estimate("ionization potential: inner-shell", shell::Shell, Z::Int64)`.

11.2.b. Weak-field ionization of effective one-electron atoms

Property & notations:

- Field ionization: by a quasi-static external field: $A^{(*)} + F\,\mathbf{e}_z \longrightarrow A^+ * e^-$.
- Formal quantum notation: $|\alpha\mathbb{J}\rangle \longrightarrow$ ...
- Not yet implemented.
- In Jac, all estimates on the field-ionization rates of atoms are always based on a non-relativistic, single-electron approach. No attempt has (yet) been made to generalize this approximation towards real many-electron atoms and ions with their fine-structure.

Motivation:

- Ionization of atoms by an external electric field is a fundamental atomic process that plays an important role, for instance, in the formation of charge-state distributions in (dilute) plasma under strong fields.
- Vice versa: The observations of temporal variations in the line intensities of ions, that are produced by field ionization, can help determine spectroscopically the macroscopic-field distribution in plasma.
- Since the field-ionization probability grows (very) rapidly with the electric field strength F, the field strength can be derived from accurate measurements of the ionization probabilities.

Further information:

- Ionization probabilities are often calculated within the WKB approximation, i.e. in the weak-field limit. In general, field ionization probability depends critically on the projection of the total orbital angular momentum upon the direction of the field.
- In most field-ionization probability computations, a quasi-static and homogeneous electric field is assumed as it occurs, for example, for macroscopic-scale fields in plasma. This assumption is in contrast to many local fields that may occur at the atomic scale.

➢ For the case of a single electron with binding energy E in the valence shell $(n\,\ell)$ and outside of closed shells otherwise, the quasi-classical escape rate is given by (Fisher *et al.*, 1998)

$$\Gamma(E,\ell,m) \;=\; B_{n\ell}^2\,\frac{(2\ell+1)\,(\ell+m)!}{2^{m+1}\,k^m\,m!\,(\ell-m)!}\;\left(\frac{2\,k^2}{F}\right)^{2Z/k\,-\,m\,-\,1}\;\exp\left(-\frac{2\,k^3}{3\,F}\right)$$

where Z is the charge of the parent ion as seen by the electron are large r, $k = \sqrt{2\,|E|}$ is the modulus of the (electron's) wave vector and $B_{n\ell}$ is the amplitude that characterizes the outgoing electron wave.

11.2.c. Electron-impact ionization. Cross sections

Kolbenstvedt model for the electron-impact ionization:

➢ Haque and coworkers (2010) explored a so-called Kolbenstvedt model for the electron-impact ionization of the K-, L- and M-shells of neutral atoms and ions.

11.3. Further estimates on atomic properties, not yet considered in JAC

11.3.a. Electron and positron stopping powers `(StoppingPower)`

Property & notations:

➢ Stopping power: due to the penetration of electrons and positrons through matter: $A^{(*)}$ .. .

Motivation:

➢ Stopping powers of matter for electrons are important for many applications involving energy deposition. In radiation physics, chemistry, biology and medicine, it is important to have simple but accurate estimates about the stopping power of energetic electrons in various media for (Gümüs, 2005).

➢ Until the present, no simple and practical model exists for the stopping power of electrons with energies below 10 keV.

Approximate stopping power formulas:

➢ The stopping power of materials arise from two types of processes, namely collisional and radiative processes. The collisions of the incident particles with the target material is most important and mainly arises from collisions between the incident particles and the atomic electrons.

$$\frac{dE}{dx} = \left(\frac{dE}{dx}\right)^{(\text{collision})} + \left(\frac{dE}{dx}\right)^{(\text{radiative})}$$

➢ For incoming electrons, a modified collisional stopping power formula for incoming electrons can be written as given by Sugiyama (1985) or Rohrlich and Carlson (1954)

➢ Full Bethe-Bloch formula:

$$-\frac{dE}{dx} = \left(\frac{e^2}{4\pi\,\epsilon_o}\right) \frac{4\pi\,z^2\,N_A\,Z\,\rho}{mc^2\,\beta^2\,A} \left[\ln\left(\frac{2mc^2\,\beta^2}{I}\right) - \ln(1-\beta^2) - \beta^2\right]$$

11.3.b. Plasma Stark broadening of spectral lines

Motivation:

➢ Stark broadening of spectral lines: This broadening has been found very important in (so-called) DA and DB white dwarf atmospheres.

➢ Apart from white dwarfs, Stark broadening of spectra is also an important pressure-broadening mechanism for arious types of other stars.

➢ Various semi-empirical calculations of the Stark widths and shifts have been performed in the impact approximation by using Griems (1968) formula.

➢ For selected lines, it was shown that Stark broadening can change the observed widths by 10-45 %.

Semi-empirical approximations:

➢ Lorentzian profile of isolated lines: For isolated lines $|\alpha_i \mathbb{J}_i\rangle \rightarrow |\alpha_f \mathbb{J}_f\rangle$ with level energies E_i and E_f, the line profile is often assumed to be Lorentzian, shifted by the energy d and with the (total) line widths Γ due to the (plasma) Stark broadening.

$$F(\omega) \;=\; \frac{(\Gamma/2\pi)}{(\omega \,-\, \omega_{if} \,-\, d)^2 \,+\, (\Gamma/2)^2}, \qquad\qquad \omega_{if} \;=\; \frac{E_i \,-\, E_f}{\hbar} \,.$$

where

➢ Energy shift and (total) widths of the Stard-broadened line: Both, the energy shift d as well as the (total) widths Γ can be expressed in terms of the velocity distribution $f(v)$ of the electrons in the plasma, its density $N^{(\mathrm{elec})}$, the impact parameter b of the incident electrons as well as the elastic and inelastic (electron-impact excitation) cross sections for excitations of the initial and final levels to neighboured levels.

$$\Gamma \;=\; N^{(\mathrm{elec})} \int dv\, v\, f(v) \;\left(\sigma^{(\mathrm{elastic}} \,+\, \sigma^{(\mathrm{inelastic}}\right); \qquad\qquad d \;=\; N^{(\mathrm{elec})} \int dv\, v\, f(v) \;\int_{R_1}^{R_{\mathrm{Debye}}} db\, 2\pi\, b\, \sin(\phi_p)$$

and where ϕ_p is a plasma-specific phase shift. Further details on the Stark broadening of spectral lines are given by Dimitrijevich and Sahel-Brechot (1996).

➢ In 1968, Griem suggested simple semiempirical formulas for the Stark line shift and widths in impact approximation which is based on some original formular by Baranger (1958) as well as an effective Gaunt factor by Seaton (1962) and Regemorter (1962). With these formulas, the Stark linewidths and Stark line shifts can be obtained by:

$$\frac{\Gamma}{[a.u.]} \;=\; 8 \left(\frac{\pi}{3}\right)^{3/2} \frac{\hbar}{m\, a_o}\, N_e \left(\frac{E_H}{k\,T}\right)^{1/2} \left[\sum_{i'} |\,\langle i'\,|\mathrm{r}|\,i\rangle\,|^2\, g_{se}\left(\frac{E}{\Delta\, E_{i'i}}\right) \,+\, \sum_{f'} |\,\langle f'\,|\mathrm{r}|\,f\rangle\,|^2\, g_{se}\left(\frac{E}{\Delta\, E_{f'f}}\right)\right]$$

$$\frac{d}{[a.u.]} \;=\; -8 \left(\frac{\pi}{3}\right)^{3/2} \frac{\hbar}{m\, a_o}\, N_e \left(\frac{E_H}{k\,T}\right)^{1/2} \left[\sum_{i'} \left(\frac{\Delta\, E_{i'i}}{|\Delta\, E_{i'i}|}\right) |\,\langle i'\,|\mathrm{r}|\,i\rangle\,|^2\, g_{sh}\left(\frac{E}{\Delta\, E_{i'i}}\right) \,+\, \sum_{f'} \left(\frac{\Delta\, E_{f'f}}{|\Delta\, E_{f'f}|}\right) |\,\langle f'\,|\mathrm{r}|\,f\rangle\,|^2\, g_{sh}\left(\frac{E}{\Delta\, E_{f'f}}\right)\right]$$

In these formulae, E_H is the hydrogen ionization energy, N_e is the free-electron density of the perturber levels, T is the electron temperature, $E \;=\; 3/2\, kT$ the mean energy of the perturbing electron and g_{se}, g_{sh} are the effective Gaunt factors which are calculated

and tabulated by Griem. These Gaunt factors are slowly varying functions of $x_{j'j}$ where $x_{j'j} = E/\Delta E_{j'j}$ is the energy difference between a perturbing level j' and the perturbed initial/upper (final/lower) level j.

➢ The atomic matrix elements need often to be obtained from *ab-initio* Hartree-Dirac-Fock computations, and the summation over the levels is obtained by making use of the table by Moore (1958).

11.3.c. Atomic electron-momentum densities

Definition & notations:

➢ For a given atomic level $|\alpha\mathbb{J}\rangle$, the (radial electron) momentum density $I(p;\,\alpha\mathbb{J})$ and the one-electron momentum density $\Pi_{n\kappa}(p;\,\alpha\mathbb{J})$ and is given by (Koga and Thakkar, 1996)

$$I(p;\,\alpha\mathbb{J}) \;=\; 4\pi\,p^2\,\Pi(p;\,\alpha\mathbb{J}), \qquad\qquad \Pi(p;\,\alpha\mathbb{J}) \;=\; \frac{1}{4\pi\,p^2}\,\sum_{i=1}^{N}\,\langle\psi_\alpha\,|\,\delta(p\,-\,p_i|\,\psi_\alpha\rangle\,.$$

➢ The radial one-electron momentum density I is used to calculate the corresponding moments of the momentum density

$$\langle p^k\rangle \;=\; \int_0^\infty dp\,p^k\,I(p;\,\alpha\mathbb{J}), \qquad\qquad -2\;\le\;k\;\le\;4$$

➢ These moments are often applied in:

- density functional theory: since $\langle p\rangle\,/\,\pi$ is close to the Dirac-Slater exchange energy;
- x-ray cristallography: since $\langle p^3\rangle$ is roughly proportional to the initial value of the so-called Patterson function
- Compton profiles: since $J(q) \;=\; \frac{1}{2}\,\int_{|q|}^\infty dp\,p^{-1}\,I(p)$ is twice the peak height of the isotropic Compton profile.

12. Beams of light and particles

12.1. Helmholtz wave equation

Propagation of light in free space:

➢ Helmholtz wave equation: If we consider the propagation of light in free space, the Maxwell equations simplify and the spatial structure of their solution satisfy the Helmholtz wave equation (an elliptic partial differential equation)

$$\nabla^2 u(\mathbf{r}) \; + \; k^2 \, u(\mathbf{r}) \;\; = \;\; 0 \, .$$

It follows from the time-dependent wave equations by trying a separation of variables and by splitting away the time dependence.

➢ Harmonic solution of the Helmholtz equation:

$$u(\mathbf{r}) \;\; = \;\; C_1 \, e^{i \, \mathbf{k} \cdot \mathbf{r}} \; + \; C_2 \, e^{-i \, \mathbf{k} \cdot \mathbf{r}} k \;\; = \;\; |\mathbf{k}| \;\; = \;\; \frac{\omega}{c} \, .$$

Paraxial approximation to the Helmholtz equation:

➢ The Helmholtz equation still represents a complicated partial differential equation; in the science of optics, one often has well-defined paraboloidal waves or Gaussian beams in which the field change along the propagation direction is small compared to the change in perpendicular direction; $\partial u / \partial z \ll \partial u / \partial x$, $\partial u / \partial y$. Under this circumstances, the paraxial approximation to the Helmholtz equation applies

$$\nabla_\perp^2 \, u(\mathbf{r}) \; + \; 2ik \, \frac{\partial u}{\partial z}(\mathbf{r}) \;\; = \;\; 0 \, ,$$

a restrictions upon the variation of the amplitude function u that is often also written in the form

$$\left|\frac{\partial u}{\partial z}\right| \ll |k\,u| \qquad \text{and} \qquad \left|\frac{\partial^2 u}{\partial z^2}\right| \ll |k^2\,u|\,.$$

12.2. Light beams

Light beams:

➢ In studying light-matter interaction, light beams play a major practical role, and there characterization and properties are important to understand the details of the interaction.

➢ These beams are usually formed when the em field from a given source is projected by filters and blends into a beam. In many lighting devices, for example, a lamp and a parabolic reflector is used to produce an artificially light beam with a more or less large divergence (car headlights, spotlights, ...).

12.2.a. Gaussian beams

Motivation:

➢ Planes waves (as well as Gaussian beams) are solutions of Maxwell's solution and the homogenous wave equation; they general posses a **polarization** which can be readily described in terms of complex amplitudes and by selecting the real or imaginary part eventually. So far, perhaps, a very quick reminder to a lecture on classical electro dynamics.

➢ In optics, a Gaussian beam is a beam of electromagnetic radiation whose transverse electric field amplitude and, hence, its intensity distributions are approximately described by some Gaussian distribution. In fact, many laser emit beams with roughly a Gaussian profile; these beams are often called the TEM_{00} fundamental modes of the laser's optical resonator. Gaussian beams form a widespread model in laser physics.

Characterization of Gaussian beams:

➢ Complex-valued electric field amplitude $u(\mathbf{r})$: In a Gaussian beam, the electric field amplitude

$$u(\rho, z) \;=\; u_0 \frac{w_0}{w(z)} \exp\left(\frac{-\rho^2}{w^2(z)}\right) \exp\left(-ikz \,-\, ik\frac{\rho^2}{2R(z)} \,+\, i\zeta(z)\right)$$

obeys the paraxial Helmholtz equation. This amplitude is sufficient in order to describe the properties of the beam since the electric field and magnetic field propagate together and obey the same wave equation.

➢ Characteristic parameters: In the definition above, we have

- ρ ... radial distance from the center axis of the beam;
- z is the axial distance from the beam's narrowest point (the 'waist'),
- i is the imaginary unit (for which $i^2 = -1$),
- $k = \frac{2\pi}{\lambda}$ is the wave number (in radians per meter), $E0 = |E(0,0)|$
- w(z) is the radius at which the field amplitude and intensity drop to 1/e and 1/e2 of their axial values, respectively, w0 = w(0) is the waist size,
- $w0 = w(0)$ is the waist size,
- $R(z)$ is the radius of curvature of the beam's wavefronts, and ...(z) is the Gouy phase shift, an extra contribution to the phase that is seen in Gaussian beams.

➢ For plane waves, $u(\mathbf{r})$ = constant; the electric and magnetic field is always perpendicular to the propagation direction and the linear momentum (density) $\mathbf{p}(\mathbf{r})$ = constant and parallel to the propagation axis.

12.2.b. Vortex beams. Characterization, properties and generation

General remarks:

- The recent years have seen a tremendous effort in generating and manipulating such vortex beams with a good number of new or promising applications, including the capture, manipulation and transport of nanoscopic particles (optical tweezer), high-resolution microsocopy or for data transmission.
- For example, beams that have m intertwined helical wavefronts are also solutions of the wave equation. The structure of these complicated beams is difficult to visualize, but their form is familiar to us all in the guise of the $m = 3$ fusilli pasta.

Characterization of vortex beams:

- Orbital angular momentum (OAM) of light is related to the spatial distribution of the em field and is accompanied by a phase dependence of the vector potential of the
field.
- a vortex state is a wave with helical wave front that carries orbital angular momentum (OAM) with respect to the beam axis.
- Wave functions: $\sim e^{im\varphi}$ are eigenfunctions of $\ell_z = \frac{\partial}{\partial \varphi}$.

Properties of vortex beams:

- For all points in the beam, the ratio between the azimuthal and z components of the momentum is found to be l/kr. The linear momentum of each photon is given by $\hbar k$, so if we take the cross-product of its azimuthal component with the radius vector, r, we get an orbital angular momentum per photon of $m\hbar$. Note also that the azimuthal component of the wavevector is m/r, independent of the wavelength.

$$p = \hbar k \longrightarrow p_\varphi = ... \longrightarrow \quad l = r p_\varphi = m\hbar$$

- However, OAM $\neq$ spin, despite the rather similar illustrations in the literatur; in particular, there exist vortex states for spinless waves (e.g. acoustic vortex waves).

Fourier expansions of light and particle beams:

- ... General remark about such basis ...
- Twisted beams, for instance, Bessel beams: ω, k_z, $\kappa = |\mathbf{k}_\perp|$, m ,
  m ... new degree of freedom.
- Spherical waves: ω, $|\mathbf{k}|$, L, M
- Plane waves: ω, $\mathbf{k} = (k_x, k_y, k_z)$

Generation of vortex beams in different frequency regions:

- For intense, short-wavelength FEL radiation, the damage threshold of optical elements, that are placed into the beam path, and difficulties in the fabrications of optical surfaces impose strong limitations in applying optical methods in the (soft) x-ray region (Terhalle *et al.* 2011, Peele *et al.* 2002).
- For high-brightness and short-wavelength FEL radiation, the damage threshold of optical elements and the difficulties in the fabrication of high-quality optical surfaces impose strong limitations on the use of optical methods for generating soft x-ray vortex beams.

Generation of vortex beams by pitch-fork holograms:

- The superposition of a regular phase profile with some proper grating results in a fork hologram that can be used for the generation of vortex beams.
- A more convenient approach for generating beams with OAM is based on the diffraction of light upon a fork-like or pitch-fork hologram (see figure). Such holograms can be generated also dynamically under the control of a computer by using a spatial light modulator.

Generation of vortex beams by spiral phase plates:

- Beijersbergen *et al.* (1994) ; figure shows the transformation of a TEM_{00} mode into a helical beam.
- In the paraxial limit, the OAM of a light beam can be exchanged with material media that have a transverse spatial inhomogeneity.

Generation of vortex beams by q-plates:

➢ The so-called (so-called) q-plate is a device that is realized by using liquid crystals, polymers or sub-wavelength gratings; this device exploits a change of sign if the polarization of the incoming light is modified.

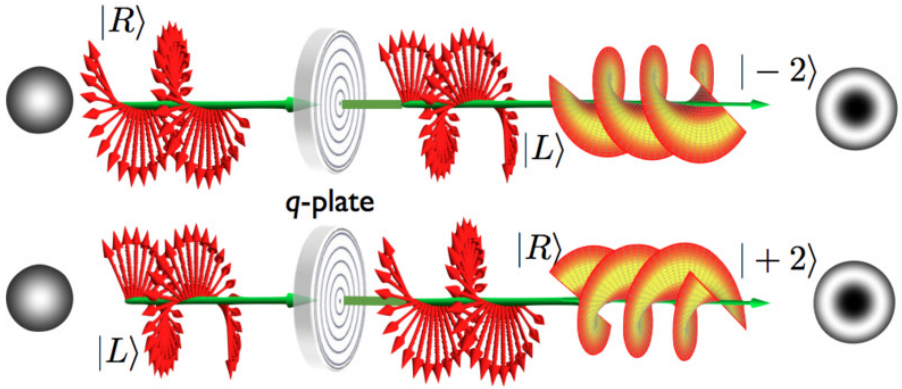

Figure 12.1.: The q-plate effect for left and right-hand circular polarizations.

Generation of vortex beams by spatial light modulators:

➢

Generation of vortex beams by cylcindrical mode converters:

➢ OAM can also be generated by converting a Hermite-Gaussian beam into a Laguerre-Gaussian beam by using an astigmatic system with two well-aligned cylindrical lenses.

➢ These lenses are placed at a specific distance, cf. figure in order to introduce a well-defined relative phase between the horizontal and the vertical Hermite-Gaussian beams.

Generation of vortex beams by helical undulators:

➢ X-ray vortex beams with E ≈ 100 eV have been generated in a helical undulator by Bahrdt *et al.* (2013) and Hemsing *et al.* (2013).

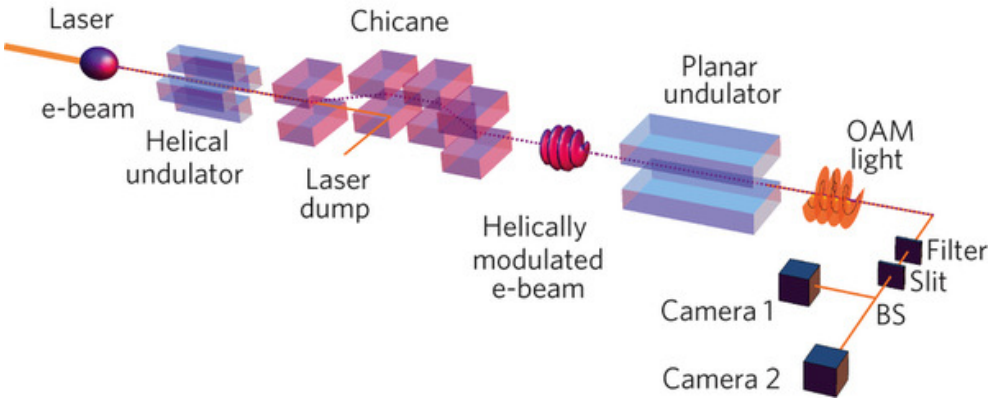

Figure 12.2.: An unmodulated relativistic electron beam interacts with a linearly polarized laser in a helical undulator, which gives the electrons an energy kick that depends on their position in the focused laser beam.

➢ When compared with helical modulators, the approach by Ribic and coworkers (2014) is considered to be more general since, by modifying the phase mask, the seed laser can be readily manipulated in order to change the transverse properties of the FEL light.

12.2.c. Hermite-Gaussian beams

Motivation:

➢ Hermite-Gaussian modes are a convenient description for the output of lasers whose cavity design is not radially symmetric, but rather has a distinction between horizontal and vertical. In terms of the previously defined complex q parameter, the intensity distribution in the x-plane is proportional to

➢ Ordinary laser beams, with planar wavefronts are usually characterized in terms of Hermite-Gaussian modes. These modes have rectangular symmetry and are described in terms of two mode indices m and n, which give the number of nodes in the x and y directions respectively; the modes are labelled HG_{mn}.

Characterization of Hermite-Gaussian beams:

➢

12.2.d. Laguere-Gauss beams

Motivation:

➢ the Laguerre-Gaussian (LG) beams carry OAM (Allen *et al.* 1992, 2003) that appears to be intrinsic, like any SAM associated with circular polarization. This is surprising as the OAM of LG beams is due to their helical phase distribution about the beam axis which coincides also with a phase singularity (Nye and Berry, 1974).

Characterization of Laguerre-Gauss beams:

➢ For a Laguerre-Gaussian beam with well-defined quantum numbers m, p, the complex amplitude of the light field in the waist of the beam is defined as

$$u_{lp}^{\mathrm{LG}}(r,\varphi) \;=\; \langle r,\varphi \,|\, m,p\rangle \;=$$

➢ In the polar represenation, the LG basis is often written as

$$u_{lp}^{\mathrm{LG}}(r,\varphi) \;=\; R_{mp}(r)\,\Phi_m(\varphi) \qquad \text{with} \qquad \Phi_m(\varphi) \;=\; \frac{e^{im\,\varphi}}{\sqrt{2\pi}}$$

➢ Especially, a Laguerre-Gaussian beam in the fundamental mode is

$$u_{00}^{\mathrm{LG}}(r,\varphi) \;=\; R_{00}(r)/\sqrt{2\pi}$$

➢ Poyting vector of Laguerre-Gaussian beams: A careful calculation of the Poynting vector for Laguerre-Gaussian models leads to a physically understandable interpretation of orbital angular momentum. In particular, there is an azimuthal component of the Poynting vector at each point on the wavefront and non-zero resultant when integrated over the beam cross-section.

12.2.e. Bessel beams

Motivation:

➢ Beams with well-defined OAM, monochromatic and non-diffractive.

➢ Bessel beams have usually three components of the topological charge.

Characterization of Bessel beams:

➢ Bessel states $|\kappa, m\rangle$: Bessel beams can be interpreted as a superposition over plane waves with fixed transverse momentum , longitudinal momentum and circular polarization

$$\psi(\mathbf{r}) \;=\; e^{-i\,\omega t + i\,k_z\,z}\;|\kappa, m\rangle\;, \qquad |\kappa, m\rangle \;\propto\; e^{i\,m\varphi}\;J_m(\kappa\,\rho)$$

➢ Vector potential: The vector potential of the Bessel beams is often written as Fourierintegral over Bessel states of different projections of

the orbital angular momentum.

$$\mathbf{A} \;=\; e^{-i\,\omega t}\,\frac{1}{(2\pi)^2}\int d\mathbf{k}_\perp\, e^{-i\,\mathbf{k}\cdot\mathbf{r}}\, a_{\kappa\,m}(\mathbf{k}_\perp)\,\mathbf{e}_{\mathbf{k},\lambda}$$

$$a_{\kappa\,m}(\mathbf{k}_\perp) \;=\; \sqrt{\frac{2\pi}{\kappa}}\,(-i)^m\, e^{-i\,m\,\varphi_{\mathbf{k}}}\,\delta(k_\perp\,-\,\kappa)$$

$$\mathbf{e}_{\mathbf{k},\lambda} \;=\; \frac{1}{\sqrt{2}}\begin{pmatrix}\cos\vartheta_k\,\cos\varphi_k\,-\,i\lambda\,\sin\varphi_k\\ \cos\vartheta_k\,\sin\varphi_k\,+\,i\lambda\,\cos\varphi_k\\ -\,\sin\vartheta_k\end{pmatrix}\qquad\text{polarization vector}$$

$$\tan\vartheta_k \;=\; \frac{\kappa}{k_z}\qquad\text{opening angle}$$

➢ Bessel beams are superpositions of OAM components with three different topological charges, $m' \,=\, m-1,\; m,\; m+1$

$$\mathbf{A} \;=\; \begin{pmatrix}a_1\\ a_2\\ 0\end{pmatrix}\,e^{i\,(m-1)\,\varphi}\,J_{m-1}(\kappa\,\rho)\;+\;\begin{pmatrix}0\\ 0\\ a_3\end{pmatrix}\,e^{i\,m\,\varphi}\,J_m(\kappa\,\rho)\;+\;\begin{pmatrix}a_4\\ a_4\\ 0\end{pmatrix}\,e^{i\,(m+1)\,\varphi}\,J_{m+1}(\kappa\,\rho)$$

➢ Bessel beams possess a well-defined z-component of the total angular momentum (TAM)

$$j_z\,\mathbf{A} \;=\; (l_z\,+\,s_z)\,\mathbf{A} \;=\; m\,\mathbf{A}$$

➢ Probabilities to find the individual OAM components:

$$P_{m-1} \;=\; \frac{1}{4}\,(\cos\vartheta_k\,+\,\lambda)^2\,,\qquad P_m \;=\; \frac{1}{2}\,(\sin\vartheta_k)^2\qquad P_{m+1} \;=\; \frac{1}{4}\,(\cos\vartheta_k\,-\,\lambda)^2$$

12.2.f. Airy beams

Motivation:

➢

Characterization of Airy beams:

➢ The Airy and Bessel beams are the two (known) major optical solutions to the wave equation which are immune to diffraction in the sense that they do not expand upon propagation (Durnin 1987; Berry and Balazs, 1979).

➢ An Airy beam preserves its shape of intensity during propagation and forms a parabolic curve, quite analogue to the trajectory of a free projectile as seen in a plane perpendicular to the propagation. The Airy beams are also known as accelerating beam (Berry and Balazs, 1979; Siviloglou *et al.*, 2007), although the linear momentum remains conserved for these beams since the intensity centroid of an Airy beam forms a straight line.

➢ Airy and Bessel beams are both self-healing, that is they recover their intensity profiles even if they are partially obstructed by an obstacle. This remarkable feature exhibits makes these beams very robust with regard to perturbations, such as scattering and turbulence.

➢ Voloch-Bloch *et al.* (2013) generated Airy electron beams by using a holographic approach in a transmission electron microscope; for this, they transformed an electron wave function into an Airy pattern by means of a cubic phase modulation in the transverse plane. Both, self-bending and self-healing features were observed if the beam was obstructed by a small object during its propagation.

Further information:

➢

12.2.g. Necklace ring beams

Motivation:

➢

Characterization of necklace ring beams beams:

➢

Further information:

➢

12.2.h. Light beams with non-integer OAM beams

Motivation:

➢

Characterization of non-integer OAM beams:

➢

Further information:

➢

12.2.i. Vector beams

Motivation:

➢ The VV beams form a direct product space between the optical SAM and OAM subspaces and therefore their experimental measurement through the higher-order SP requires their decomposition into these parts.

Characterization of non-integer OAM beams:

➢ Higher-order Stokes parameters:

Further information:

➢

12.2.j. Traktor beams

Motivation:

➢ Tractor beam are defined to use (a negative) nonconservative radiation pressure, that differs from a gradient force, and which is directed towards the source. This generally requires a continuous redirection of momentum flux (Sukhov and Dogariu, 2010, 2011; Chen *et al.* 2011).

➢ Therefore, time-evolving potential energy wells such as rotating anisotropic traps (Paterson *et al.*, 2001) or optical conveyors that move trapped particles are not considered as tractor beams.

Characterization of traktor beams:

➢

Further information:

➢

12.2.k. Polarization radiation

Motivation:

- ➢ EM radiation can be emitted not only by accelerated charges but also due to the motion of magnetic moments and higher multipoles. Until now, however, this (so-called) polarization radiation has never been verified experimentally for any frequency of light.
- ➢ The main reason for not yet proving this radiation is that the current of the magnetic moment is suppressed by $\sim 10^{-5}$ w.r.t. the charge current.
- ➢ In addition, the quasiclassical theory and calculations become inconsistent because quantum corrections are of the same order fr these phenomena.

Characterization of polarization radiation:

➢

Further information:

- ➢ In particular, the magnetic moment contribution has never been observed in any form of polarization radiation. Ivanov and Karlovets (2013) propose to detect it using vortex electrons carrying large orbital angular momenta m. For electrons with $E \approx 300$ keV and $m = 100-1000$, they predicted an asymmetry of the order of 0.1 %–1 %, which could be measured with existing technology. In particular, they showed that the magnetic-moment contribution manifests itself as a left-right asymmetry of the emitted radiation with respect to the incidence plane, and we predict for electrons with $E \approx 300$ keV $m \sim 1000$ an asymmetry of the order of 1 %.

➢ In general, there exist two broad classes of radiation: bremsstrahlung and polarization radiation (PR). The former is produced by accelerating charges, while the latter can be emitted by a uniformly moving charge but only in the presence of a medium. Depending on the medium or target geometry, one distinguishes different forms of PR: Cherenkov radiation, transition radiation, diffraction radiation, Smith-Purcell radiation.

12.2.I. Manipulation of optical beams

Optical elements:

➢

➢ spatial light modulator

Mach-Zehnder interferometers:

➢

12.2.m. Application of optical (vortex) beams

Motivation:

➢ Different applications of vortex beams and the angular momentum of light is envisaged and currently explored. In particular, several applications have been already demonstrated in research laboratories, although they have not yet reached the stage of commercialization.

➢ Applications are numerous: cold atoms, trapped nanoparticles, remote measurement of rotation, entanglement and quantum information, interaction with matter, applications in microscopy, in astrophysics.

Optical tweezer:

- ➢ Optical tweezer: ('single-beam gradient force trap') are realized by some highly focused laser beam in order to provide an attractive or repulsive force on nano- or mesoscopic dielectric objects.
- ➢ Orientational manipulation of particles or particle aggregates.

Optical phasors:

- ➢ Phase sensitive amplification and regeneration.

Applications in quantum information theory:

- ➢ quantum information encoding, Higher-dimensional quantum information encoding, for possible future quantum cryptography or quantum computation applications.
- ➢ The orbital-angular momentum (OAM) of light has recently emerged as a promising candidate for quantum and classical information systems.

12.3. Electron beams

12.3.a. Gaussian electron beams

Motivation:

- ➢

12.3.b. Twisted electron beams

Motivation:

➢

Generation of electron beams:

➢ Electron vortex beams were realized experimentally by three groups in 2010-2011: Uchida & Tonomura [Nature **464** (2010) 737], Verbeeck, Tian & Schattschneider [Nature **467** (2010) 301] and McMorran *et al.* [Science **331** (2011) 192].

➢ They realized electron vortex beams with parameters: $E = 300$ keV, a projection of the OAM with $m \lesssim 100$ and by focusing the electron beam to 1.2 Å spot size.

Representation of electron beams:

➢ Although it is not possible to generate ideal Bessel beams, because they are not power normalizable, quasi-Bessel beams can be obtained within a good approximation.

➢ Bessel beams represent a coherent superposition of conical plane waves along a closed ring (circle).

➢ In cylindrical coordinates r, φ, z, the wave function of electrons in a Bessel beam is given by

$$\psi(r,\varphi,z;t) \;=\; J_m(k_r\, r)\, e^{im\varphi}\, e^{-i(\omega t - k_z z)}$$

where $J_m(x)$ is the m-th order Bessel function of the first kind and k_r and k_z denote the transverse and longitudinal components of the wave vector, respectively.

➢ The energy of the electron $E = \hbar omega$ defines the de-Broglie wave length and the modulus of the wave vector by

$$k^2 \;=\; k_r^2 \,+\, k_z^2 \;=\; \frac{2m\omega}{\hbar} \;=\; \left(\frac{2\pi}{\lambda_d B}\right)^2 .$$

➢ The wave function above give rise to a probability-density distribution $\mathcal{P} :\equiv \psi\,\psi^+$ which is independent of z and t:

$$\mathcal{P}((r,\varphi,z;t) \;=\; \mathcal{P}((r,\varphi,0;0) \;=\; [J_m(k_r\, r)]^2 .$$

This shows that the probability-density distribution of the electrons in the transverse plane is stationary and independent of where this plane is taken.

- For Bessel beams with a nonzero m value, the electrons possess a nonuniform phase front which forms a helical shape with m dislocations in the phase and where the handedness of the phase front is defined by the sign of m.
- The current density of electron Bessel beam circulates azimuthally in the transverse plane and, thus, introduces an orbital angular momentum of $m\hbar$ per electron. The magnetic moment that is associated with an orbital amgular momentum is sometimes refered to as 'Bohr magneton'. This Bohr magneton comes in addition to the known dipole moment due to the spin of the electron. Unlike the electron spin, the orbital angular momentum of the electrons can take values much higher than $\hbar/2$, and even up to several hundred $|\hbar|$.
- An electron Bessel beam with a nonzero m value possess exhibit a shape with multiple rings and with a null probability density at the origin.

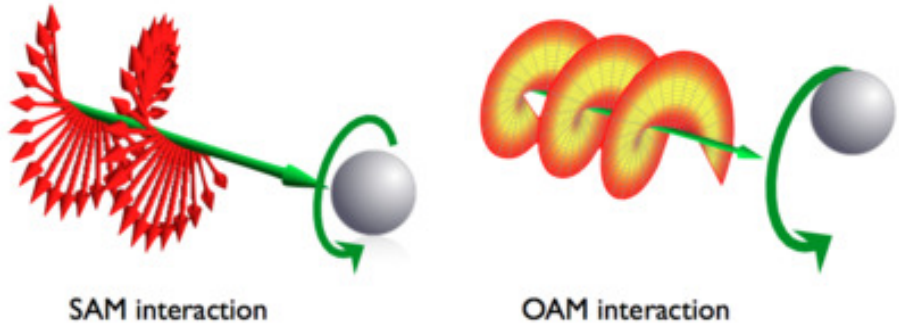

Figure 12.3.: If the particle is not at the beam center the two angular momenta will give rise to different kinds of rotation of the particle. SAM will give rise to a rotation of the particle around its own center, i.e., to a particle spinning. The OAM, instead, will generate a revolution of the particle around the beam axis.

13. References

1992 *Phys. Rev.*

Åberg and Howat 1982 *Corpuscles and Radiation in Matter I*, ed Mehlhorn W (in: Encyclopedia of Physics, vol XXXI; Springer, Berlin, p 469)

Agostinelli S and Geant 4 collaboration 2003 *Nuc. Instr. Meth.* **A506** 250 *Geant4a simulation toolkit*

Allen L, Beijersbergen M W, Spreeuw R J C and Woerdman J P 1992 *Phys. Rev.* **A45** 8185 *Orbital angular momentum of light and the transformation of Laguerre-Gaussian laser modes*

Allen L, Barnett S M and Padgett M J 2003 *Optical Angular Momentum* (Institute of Physics Publishing, Bristol)

Avgoustoglou E, Johnson W R, Plante D R, Sapirstein J, Sheinerman S and Blundell S A 1992 *Phys. Rev.* **A46** 5478 *Many-body perturbation theory formulas for the energy levels of excited states of closed-shell atoms*

Avgoustoglou E, Johnson W R, Liu Z W und Sapirstein J 1995 *Phys. Rev.* **A51** 1196 *Relativistic many-body calculations of* $[\,2p^5 3s\,]$ *excited state energy levels for neon-like ions*

Balashov V V, Grum-Grzhimailo A N and Kabachnik N M 2000 *Polarization and Correlation Phenomena in Atomic Collisions* (Kluwer Academic Plenum Publishers, New York)

Band I M, Trzhaskovskaya M B, Nestor Jr N W, Tikkanen P O and Raman S 2002 *Atom. Data NUcl. Data Tables* **81** 1 *DiracFock internal conversion coefficients*

Beth R A 1936 *Phys. Rev.* **50** 115 *Mechanical detection and measurement of the angular momentum of light*

Bethe H A and Salpeter E E 1957 *Quantum Mechanics of One- and Two-Electron Systems* (Springer-Verlag, Berlin, Gttingen, Heidelberg)

Beiersdorfer P, Clementson J and Safronova U I 2015 *Atoms* **3** 260 *Tungsten data for current and future uses in fusion and plasma science*

Bezanson J, Edelman A, Karpinski S and Shah V B 2017 *SIAM Review* **59** 65 *Julia: A fresh approach to numerical computing*

Bliokh K Y, Bliokh Y P, Savelev S and Bliokh F N 2007 *Phys. Rev. Lett.* **99** 190404 *Semiclassical dynamics of electron wave packet states with phase vortices*

Canton-Rogan S E, Wills A A, Gorczyca T W, Wiedenhoeft M, Nayandin O, Liu C-N and Berrah N 2000 *Phys. Rev. Lett.* **85** 3113 *Mirroring doubly excited resonances in argon*

Cheng G and Jiaolong Z 2008 *Phys. Rev.* **E78** 046407 *Spectrally resolved and Rosseland and Planck mean opacities of iron plasmas at temperatures above 100 eV: A systematic study*

Cowan R D 1981 *The Theory of Atomic Structure and Spectra* (University of California Press, 1981, 731 pages)

Da Pieve F, Fritzsche S, Stefani G and Kabachnik N M 2007 *J. Phys.* **B40** 329 *Linear magnetic and alignment dichroism in Augerphotoelectron coincidence spectroscopy*

Derevianko A, Johnson W R, Safronova M S and Babb J F 1999 Phys. Rev. Lett. **82** 3589 *High-precision calculations of dispersion coefficients, static dipole polarizabilities and atom-wall interaction constants for alkali-metal atoms*

Eichler J and Meyerhof W 1995 *Relativistic Atomic Collisions* ((Academic Press, San Diego)

Fisher D, Maron Y and Pitaevskii L P 1998 *Phys. Rev.* **A58** 2214 *Ionization of many-electron atoms by a quasistatic electric field*

Fontes C J, Zhang H L, Abdallah Jr J, Clark R E H, Kilcrease D P, Colgan J, Cunningham R T, Hakel P, Magee N H and Sherrill M E 2015 *J. Phys.* **B48** 144014 *The Los Alamos suite of relativistic atomic physics codes*

Fritzsche S 2001 *J. Electron Spectrosc. Relat. Phenom.* **114116** 1155 *A toolbox for studying the properties of openshell atoms and ions*

Fritzsche S 2002 *Phys. Scr.* **T100** 37 *Largescale accurate structure calculations for openshell atoms and ions*

Fritzsche S, Nikkinen J, Huttula S-M, Aksela H, Huttula M and Aksela S 2007 *Phys. Rev.* **A75** 012501 *Interferences in the $3p^4nl$ satellite emission following the excitation of argon across the $2p^5_{1/2}4s$ and $2p^5_{3/2}3d$ $J = 1$ resonances*

Fritzsche S, Fricke B and Sepp W-D 1992 *Phys. Rev.* **A45** 1465 *Reduced L_1 level-width and Coster-Kronig yields by relaxation and continuum interactions in atomic zinc*

Furukawa H and Nishihara K 1992 *Phys. Rev.* **A46** 6596 *Fermi-degeneracy and discrete-ion effects in the spherical-cell model and electron-electron correlation effects in hot dense plasma*

Gaidamauskas E, Naze C, Rynkun P, Gaigalas G, Jönsson P and Godefroid M 2011 *J. Phys.* **B44** 175003 *Tensorial form and matrix elements of the relativistic nuclear recoil operator*

Gebarowski R, Burke P G, Taylor K T, Dörr M, Bensaid M and Joachain C J 1992 *J. Phys.***B30** 1837 *R-matrixFloquet theory of multiphoton processes: X. Theory of harmonic generation*

Gaunt 1929 *Proc. R. Soc.* **A122** 513 *IV. The triplets of helium*

Goldman S P and Drake G W F 1992 *Phys. Rev. Lett.* **68** 1683 *Asymptotic Lamb shifts for helium Rydberg states*

Gordon R G and Kim Y S 1972 *J. Chem. Phys.* **56** 3122 *Theory for the forces between closed-shell atoms and molecules*

Grant I P 1988 *in: Methods in Computational Chemistry* ed Wilson S, vol 2 (Plenum, New York, p 1) *Relativistic effects in atoms and molecules*

Grant I P and Pyper N C 1976 *J. Phys.* **B9** 761 *Breit interaction in multiconfiguration relativistic atomic calculations*

Grant I P and Quiney H M 1988 *in: Advances in Atomic and Molecular Physics* **23** eds D Bates and B Bederson (Academic, New York, p 37) *Foundation of Relativistic Theory of Atomic and Molecular Structure*

Griem H 1974 *Spectral Line Broadening by Plasmas* (Academic Press, New York, London)

Grum-Grzhimailo A N, Gryzlova E V, Staroselskaya E I, Venzke J and Bartschat K 2015 *Phys. Rev.* **A91** 063418 *Interfering one-photon and two-photon ionization by femtosecond VUV pulses in the region of an intermediate resonance*

Guo D-S, Åber T and Crasemann B 1989 *Phys. Rev* **A40** 4997 *Scattering theory of multiphoton ionization in strong fields*

Guo D-S and Drake G W F 1992 *Phys. Rev* **A45** 6622 *Multiphoton ionization in circularly polarized standing waves*

Guzzinati G, Schattschneider P, Bliokh Y K, Nori F and Verbeeck J 2013 *Phys. Rev. Lett.* **110** 093601 *Observation of the Larmor and Gouy rotations with electron vortex beams*

Haque A K F, Shahjahan M, Uddin M A, Patoary M A R, Basak A K, SahaB C and Malik F B 2010 *Phys. Scr.* **81** 045301 *Generalized Kolbenstvedt model for electron impact ionization of the K-, L- and M-shell ions*

Hartgers A, van Dijk J, Jonkers J, van der Mullen J A M 2001 *Comp. Phys. Commun.* **135** 199 *CRModel: A general collisional radiative modeling code*

Hou Y, Bredow R, Yuan J and Redmer R 2015 *Phys. Rev.* **E91** 033114 *Average-atom model combined with the hypernetted chain approximation applied to warm dense matter*

Hou Y and Yuan J 2009 *Phys. Rev.* **E79** 016402 *Alternative ion-ion pair-potential model applied to molecular dynamics simulations of hot and dense plasmas: Al and Fe as examples*

Hubbell J H, Veigele W J, Briggs E A, Brown R T, Cromer D T and Howerton R J 1992 *J. Phys. Chem. Ref. Data* **4** 471 *Atomic form factors, incoherent scattering functions, and photon scattering cross sections*

Huntemann N, Sanner C, Lipphardt B, Tamm C and Peik E 2016 *Phys. Rev. Lett.* **116** 063001 *Single-ion atomic clock with* 3×10^{18} *systematic uncertainty*

Inal M K, Surzhykov A and Fritzsche S 2005 *Phys. Rev.* **A72** 042720 *Linear polarization of the* $2p^5 3s \rightarrow 2p^6$ *lines following the inner-shell photoionization of sodiumlike ions*

Inhester L, Burmeister C F, Groenhof G and Grubm"uller H 1992 *J. Chem. Phys.* **136** 144304 *Auger spectrum of a water molecule after single and double core ionization*

Jahrsetz T, Fritzsche S and Surzhykov A 2015 *Phys. Rev.* **A89** 042501 *Inelastic Raman scattering of light by hydrogenlike ions*

Johnson W R 1995 *in: Physics with Multiply Charged Ions* ed D Liesen (NATO ASI Series 348, Plenum Press, New York London, p 1 *Correlation and QED for highly-charged ions*

Johnson W R 2007 *Atomic Structure Theory: Lectures on Atomic Physics* (Springer)

Johnson W R, Guo D S, Idrees M and Sapirstein J 1985 *Phys. Rev.* **A32** 2093 *Weak-interaction effects in heavy atomic systems*

Jönsson P, Gaigalas G, Bieron J, Froese Fischer C and Grant I P 2013 *Comp. Phys. Commun.* **184** 2197 *New version: Grasp2K relativistic atomic structure package*

Kabachnik N M 1981 *J. Phys.* **B14** L337

Kabachnik N M, Fritzsche S, Grum-Grzhimailo A N, Meyer M and Ueda K 2007 *Phys. Rep.* **451** 155 *Coherence and correlations in photoinduced Auger and fluorescence cascades in atoms*

Karlovets D V 2012 *Phys. Rev.* **A86** 062102 *Electron with orbital angular momentum in a strong laser wave*

Kibeedia T, Burrows T W, Trzhaskovskayac M B, Davidsona P M and Nestor Jr C W 2008 *Nucl. Instr. Meth.* **A589** 202 *Evaluation of theoretical conversion coefficients using BrIcc*

Kim Y S and Gordon R G 1974 *Phys. Rev.* **B9** 3548 *Theory of binding of ionic crystals: Application to alkali-halide and alkane-earth-dihalide crystals*

Klar H 1980 *J. Phys.* **B13** 4741

Krause M O 1979 *J. Phys. Chem. Ref. Data* **8** 329 *Atomic radiative and radiationless yields for K and L shells*

Koga T and Thakkar A J1996 J. Phys. **B 29** 2973Moments and expansion coefficients of atomic electron momentum densities: numerical Hartree-Fock calculations for hydrogen to lawrencium 2

Libermann D A 1979 *Phys. Rev.* **B20** 4981 *Self-consistent field model for condensed matter*

Lindgren I and Rosen A 1974 *Case Studies in Atomic Physics* **5** *Relativistic self-consistent-field calculations with application to atomic hyperfine interaction. Part I: Relativistic selfconsistent fields*

Listengarten M A 1961 in *Gamma Rays*, ed Sliv L A (Acad. Sci. USSR, Moscow-Leningrad, 1961), p 271 (in Russian)

Liu C-N and Starace A F 1999 *Phys. Rev. A***59** R1731 *Mirroring behavior of partial photodetachment and photoionization cross sections in the neighborhood of a resonance*

Marxer H 1991 *Phys. Rev. A* **44** 1543 *Exact correspondence relationship for the expectation values of* r^{-k} *for hydrogenlike states*

Marxer H 1995 *J. Phys.* **B28** 341 *Off-diagonal matrix elements* $\langle n\ell \,|\, r^k \,|\, n\ell' \rangle$ *for hydrogen-like states: an exact correspondence relationship in terms of orthogonal polynomials and the WKB approximation*

Matula O, Hayrapetyan A G, Serbo V G, Surzhykov A and Fritzsche S 2013 *J. Phys.* **B46** 205002 *Atomic ionization of hydrogen-like ions by twisted photons: angular distribution of emitted electrons*

Matula O, Hayrapetyan A G, Serbo V G, Surzhykov A and Fritzsche S 2014 *New J. Phys.* **16** 053016 *Radiative capture of twisted electrons by bare ions*

Mazevet S and Abdallah Jr J 2006 *J. Phys.* **B39** 3419 *Mixed UTA and detailed line treatment for mid-Z opacity and spectral calculations*

Metzger B D 2017 *Living Rev. Relativ.* **20** 3 *Kilonovae*

Milione G, Sztul H I, Nolan D A and Alfano R R 2011 *Phys. Rev. Lett.* **107** 053601 *Higher-order Poincare sphere, Stokes parameters and the angular momentum of light*

Miyagi H and Madsen L B 1992 *Phys. Rev.* **A87** 062511 *Time-dependent restricted-active-space self-consistent-field theory for laser-driven many-electron dynamics*

Nye J F and Berry M V 1974 *Proc. R. Soc. London Ser.* **A336** 165 *Dislocations in wave trains*

Pachucki K and Grotch H 1995 *Phys. Rev.* **A51** 1854 *Pure recoil corrections to hydrogen energy levels*

Pan L, Taylor K T and Clark C W 1988 *Phys. Rev. Lett.* **61** 2673 *Computation of the ac Stark effect in the ground state of atomic hydrogen*

Parpia F, Froese Fischer C and Grant I P 1996 *Comput. Phys. Commun.* **94** 249 *GRASP92: A package for largescale relativistic atomic structure calculations*

Porsev S G, Kozlov M G and Reimers D 2009 *Phys. Rev.* **A79** 032519 *Transition frequency shifts with fine-structure constant variation for Fe I and isotope-shift calculations in Fe I and Fe II*

Porsev S G and Derevianko A 2006 *J. Exp. Theo. Phys.* **102** 195 *High-accuracy calculations of dipole, quadrupole and octupole electric-dynamic polarizabilities and van-der-Waals coefficients* C_6, C_8 *and* C_{10} *for alkaline-earth dimers*

Post D E and Kendall R P 2004 *Int. J. HPC Applications* **18** 399 *Software project management and quality engineering practices for complex, coupled ...*

Potvliege R M 1998 *Comput. Phys. Commun.* **114** 42 *STRFLO: a program for time-independent calculations of multiphoton processes in one-electron atomic systems: I. Quasienergy spectra and angular distributions*

Radtke T, Fritzsche S and Surzhykov A 2006 *Phys. Rev. A* **74** 032709 *Density-matrix formalism for the photoion-electron entanglement in atomic photoionization*

Ribic P R, Guathier D and De Ninno G 2014 *Phys. Rev. Lett.* **112** 203602 *Generation of coherent extreme-ultraviolet radiation carrying orbital angular momentum*

Rohrlich F and Carlson B C 1954 *Phys. Rev.* **93** 38 *Positron-electron differences in energy loss and multiple scattering*

Safronova M S, Porsev S G, Sanner C and Ye J 2018 *Phys. Rev. Lett.* **120** 173001 *Two clock transitions in neutral Yb for the highest sensitivity to variations of the fine-structure constant*

Saha B and Fritzsche S 2006 *Phys. Rev. E***73** 036405 *Be I isoelectronic ions embedded in hot plasma*

Saha B and Fritzsche S 2007 *J. Phys. B***40** 259 *Influence of dense plasma on the low-lying transitions in Be-like ions: relativistic multiconfiguration DiracFock calculation*

Scholz-Marggraf H M, Fritzsche S, Serbo V G, Afanasev A and Surzhykov A 2014 *Phys. Rev.* **A90** 013425 *Absorption of twisted light by hydrogenlike atoms*

Sapirstein 1987 *Phys. Scr.* **36** 801 *Quantumelectrodynamics of manyelectron atoms*

Shabaev V M 1984 *Vestn. Leningrad. Univ. Fiz. Khim.* **N4.15**

Sharma L, Surzhykov A, Inal M K and Fritzsche S 2010 *Phys. Rev.* **A81** 023419 *Polarization transfer in the innershell photoionization of sodiumlike ions*

Simon A,1, Warczak A, ElKafrawy T and Tanis J A 2010 *Phys. Rev. Lett.* **104** 123001 *Radiative double electron capture in collisions of O^{8+} ions with carbon*

Stone N J 2005 *Atomic Data and Nuclear Data Tables* **90** 175 *Table of nuclear magnetic dipole and electric quadrupole moments*

Surzhykov A, Radtke T, Indelicato P and Fritzsche S 2009 *Eur. J. Phys. Spec. Topics* **169** 129 *Photon polarization in the two-photon decay of heavy hydrogenlike ions*

Surzhykov A, Volotka A, Fratini F, Santos J P, Indelicato P, Plunien G, Stoöhlker and Fritzsche S 2008 *Phys. Rev.* **A81** 042510 *Angular correlations in the twophoton decay of heliumlike heavy ions*

Surzhykov A, Jentschura U D, Stöhlker T and Fritzsche S 2006 *Phys. Rev.* **A73** 032716 *Radiative electron capture into high-Z few-electron ions: Alignment of the excited ionic states*

Tchang-Brillet W L 1, Wyart J-F, Meftah A and Mammar S A 2018 *atoms* **6** 52 *Parametric calculations of radiative decay rates for magnetic dipole and electric quadrupole transitions in Tm IV, Yb V, and Er IV*

Tupitsyn I I, Shabaev V M, Lopez-Urrutia J R C, Draganic I, Orts R S and Ullrich J 2003 *Phys. Rev.* **A68** 022511 *Relativistic calculations of isotope*

shifts in highly charged ions

Uchida M and Tonomura A 2010 *Nature* **467** 737 *Generation of electron beams carrying orbital angular momentum*

Verbeeck J, Tian H and Schattschneider P 2010 *Nature* **467** 301 *Production and application of electron vortex beams*

Vlcek J 1989 *J. Phys. D***22** 623 *A collisional-radiative model applicable to argon discharges over a wide range of conditions. I. Formulation and basic data*

Volotka A V, Yerokhin V A, Surzhykov A, Stöhlker T and Fritzsche S 2016 *Phys. Rev.* **A93** 023418 *Many-electron effects on x-ray Rayleigh scattering by highly charged He-like ions*

von der Wense, Seiferle B, Stellmer S, Weitenberg J, Kazakov G, Palffy A and Thirolf P G 2017 *Phys. Rev. Lett.* **119** 132503 *A laser excitation scheme for* ^{229m} *Th*

Yudin V Y, Taichenachev A V and Derevianko A 2014 *Phys. Rev. Lett.* **113** 233003 *Magnetic-dipole transitions in highly charged ions as a basis of ultraprecise optical clocks*

Yutsis A P, Levinson I B und Vanagas V V 1962 *Mathematical apparatus of the theory of angular momentum.* Israel Program for Scientific Translation, Jerusalem 1962

Zaitsevskii A V und Heully J-L 1992 *J. Phys.* **B25** 603 *Rayleigh-Schrödinger QDPT for hermitian intermediate Hamiltonians by the shift technique*

Zambrini R and Barnett S 2006 *Phys. Rev. Lett.* **96** 113901 *Quasi-intrinsic angular momentum and the measurement of its spectrum*

Zarrabian S, Laidig W D und Bartlett R J 1990 *Phys. Rev.* **A41** 4711 *Convergence properties of multireference many-body perturbation theory*

Index